Fermi National Accelerator Laboratory

FERMILAB-Conf-94/419-E

CDF

The Top . . . is it There? A Survey of the CDF and DØ Experiments

A.V. Tollestrup

Fermi National Accelerator Laboratory
P.O. Box 500, Batavia, Illinois 60510

December 1994

Published Proceedings *Frontiers in Particle Physics, Cargese 94*, Institu D'Etudes Scientifiques de Cargese, Cargese, Corsica, August 1-13, 1994

Disclaimer

CDF/PUB/TOP/PUBLIC/2913
FERMILAB-CONF-94/419-E

Published Proceedings Frontiers in Particle Physics - Cargese 94,
Institut D'Etudes Scientifiques de Cargese, Cargese, Corsica,
August 1-13, 1994.

THE TOP ...IS IT THERE? A SURVEY OF THE CDF AND D0 EXPERIMENTS

A. V. Tollestrup
Collider Detector
Fermilab National Accelerator Laboratory
Batavia, IL 60510

I. INTRODUCTION

The Standard Model requires the Top.

Quarks		
u	c	t
d	s	b

Leptons		
e	μ	τ
ν_e	ν_μ	ν_τ

The b was discovered in 1977, and speculation immediately began about whether or not it had a partner. A direct measurement of the weak isospin of the b is possible through the Z decay to $b\bar{b}$ at LEP. The following two diagrams interfere and give a forward-backward asymmetry to the decay.

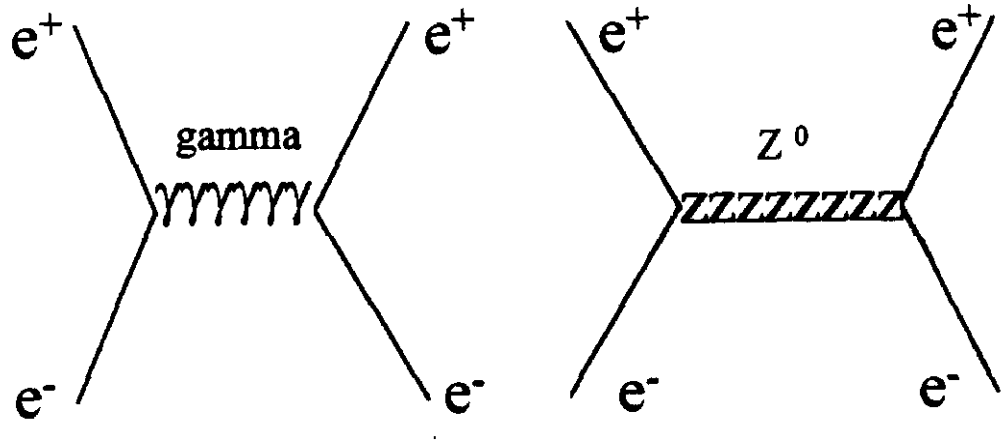

Figure 1. Two diagrams that interfere with each other in Z production .

The asymmetry is proportional to the coupling which is given by:

$$\begin{aligned} t_3 + 0.33 \sin^2\theta_W &= 0.07 \text{ if } t_3 = 0 \\ &= 0.43 \text{ if } t_3 = -1/2 \end{aligned}$$

Direct measurements at LEP have given the value for $t_3 = -0.504^{+0.18}_{-.011}$, indicating that the b is a weak isospin doublet. By definition the object with $t_3 = +1/2$ is the "top."

The mass of the top has been growing with time. The early searchers started at small multiples of the b mass, and a number of guesses were made at formulas that would relate the masses of the quarks and leptons to each other which were then extrapolated to predict the mass of the top. However, as higher energies became available, direct searches gave lower limits for the top mass that increased with time. The most exciting time came in 1983 when UA1 at CERN had evidence for a top with a mass in the range between 30 and 50 GeV, Ref. 1. This created great excitement in the community as it opened up the possibility that TRISTAN could make Toponium. However, it later turned out that the evidence at UA1 was a statistical fluctuation, and the limit for the mass of the top grew even higher.

LEP took up the search and came up with the direct limit of 46 GeV. Later in 1987 CDF set a limit that M_{top} was greater than 62 GeV from a measurement of the width of the W, Ref. 2. If the W can decay into top and b, then the width of the W is wider than if this decay cannot occur as is the case when the mass of the top is greater than the mass of the W. This particular test has an advantage that it would detect nonstandard decays (such as those involving a light Higgs) that a direct search might miss.

Assuming Standard Model top decays, CDF pushed the limit to 91 GeV in 1993, Ref. 3, and early in 1994, D0 increased this limit to 131 GeV, Ref. 4. These searches looked for the Standard Model decays of top to W + b, where the W could be either real or virtual.

Indirect effects from the existence of the top have allowed the LEP experiments to produce a set of mass predictions that have increased with time. The most recent prediction given at the Glasgow Conference was $M_{top} = 178 \pm 11^{+18}_{-19}$ GeV. An easy way to see how the top can show itself through an indirect effect is to look at the following pair of diagrams.

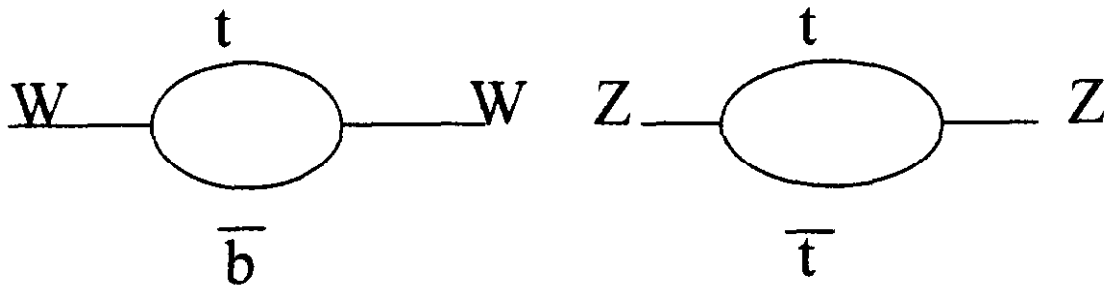

Figure 2. Diagrams that split the W and Z.

The virtual loop for the W contains a t and a $\bar{b}$, whereas the virtual loop for the Z contains a t and $\bar{t}$. The difference caused by these two loops splits the mass of the W and the Z. This splitting of mass is quadratic in the top mass and is logarithmically dependent upon the mass of the Higgs. Eventually a precise measurement of the top mass and the W mass will allow an indirect prediction of the mass of the Higgs. This is one of the simpler cases in which the result from a physical measurement is sensitive to virtual loops involving the top. There are many of these, and the LEP measurements have been analyzed carefully to give the prediction mentioned above. It is thus clear that we are now in the process of searching for an object that has a very high mass.

Dalitz, Ref. 5, shows the predicted lifetime for the top quark to decay as a function of its mass. When the mass is less than the mass of a W plus a b quark, the decay is through a virtual W, and the decay lifetime goes like the inverse mass of the top to the fifth power. When the mass becomes greater than this limit, the lifetime goes like the inverse mass cubed. For masses in the region indicated above, the width is of the order of 1 or more GeV. This makes the lifetime too short for Toponium to be observed and, in addition, the quark does not have time to clothe itself before it decays. Remember that the momentum transfers in a typical hadronization process for a quark are only of the order of 100 MeV, and thus these processes don't compete with the fundamental rapid decay of the top into a boson plus a quark. A very interesting observation in the future will be whether or not there is any non Standard Model interactions between and t and $\bar{t}$. We should be able to answer questions such as this within the next year.

Production and Decay of the Top

Let us now consider production of the top and its various decay channels that are useful for a search. Laenen et al., Ref. 6, have made the next-to-next leading order calculation for the production of the top. This is shown in Fig. 3. At masses

around 100 GeV, the diagrams involving gg collisions comprise about 30 percent of the cross section and $q\bar{q}$ going to $t\bar{t}$ comprise the rest. As M_t increases, the glue contribution decreases to only 7 percent at 200 GeV. The dotted lines shown on the graph reflect the uncertainty expected in the cross section due to structure function errors as well as diagrams that have been neglected. A top mass of 150 GeV has a cross section of about 10 picobarns. The experimental data that I am going to talk about in these lectures covers a running period in 1992-1993 of the Tevatron at Fermilab, and the integrated luminosity was about 20 inverse picobarns. This means that the experiments have to be sensitive to only a few hundred $t\bar{t}$ pairs, and the statistical fluctuations in the various production processes and backgrounds will dominate our discussion.

The search for top production is centered on identifying the products of the $t\bar{t}$ system when it decays. Since the primary decay process is dominated by t going to W + b, we can make the table shown in Fig. 4 for the various decay channels available. Each channel has a weight of 1, and the quarks are shown with their three color states. We see that there are a total of nine ways that a W can decay, and there are 81 ways that we can list for the two W's. The tau, since it decays into 2 neutrinos and a lepton, is not very useful. Hence, we will concentrate on only the electron and the muon. We see from the table that the branching ratio is 4 out of 81 to give us a dilepton mode where the dileptons are e's and μ's in any combination. There are 24 out of 81 combinations where we have a μ or an e plus jets, and there are 36 out of 81 combinations where the W's both decay hadronically.

Let's examine these various channels individually. In the case of the dilepton mode, we also have two neutrinos. Thus, we are looking for two leptons and two b jets plus a large amount of missing transverse energy which is carried away by the neutrinos. If both the b jets could be tagged by their decay, this would be a rather unique signature for this mode. However, we will see that the efficiency for tagging a b is only of the order of 20 to 30 percent, which when coupled with the small branching ratio of this mode makes these events rather rare. It is also obvious that we cannot reconstruct this mode uniquely because of the two neutrinos that are involved in the decays. However, it is true that given a large number of these events, one could obtain an estimate of the mass of the top by studying the momentum distribution of the leptons and the b's.

The next channel that we investigate involves one of the W's decaying hadronically, so that we have two jets from one of the W's plus two b jets, a lepton, and a neutrino. It turns out that this category of event can be reconstructed kinematically and, hence, an estimate of the top mass obtained. Also, the branching ratio of 24 out of 81 is 6 times larger than the dilepton signature. However, we will see that the background for this channel is higher than it is in the dilepton case, and it will require some additional information to separate it from the production of a W plus 4 QCD jets.

Finally, there is the case where both W's decay hadronically, and in this case one is looking at 6 jet events. Although the branching ratio of this channel, 36 out of 81, is high, it has an enormous background from the QCD production of 6 jet events. Kinematics can aid in separating out top decays, but it becomes imperative to also tag the b jets, if one is to study this channel. The b tag reduces the sensitivity of the search, and at present it looks possible but very difficult to identify $t\bar{t}$ production through this channel. Future success will require that the b jets be tagged with a high efficiency.

A summary of the experimental challenge is the following. We have a process with a very small cross section, and we are expecting to find a few events in 10^{12}. In order to establish that the top is really there, we must accomplish the following:

1. Establish a selection criteria for triggering the detector so that these events will be written to tape.
2. Measure the efficiency of the trigger.
3. Measure the efficiency of the offline event reconstruction program.
4. Measure the background:
   (a) Real processes that fake real events.
   (b) Mismeasurements due to detector errors that fake real events.
5. If the above process yields an excess of signal events over background events, then we must show that the events are characteristic of top decay. We must reconstruct the decay and show that it leads to a unique mass, and the ratio between the different channels should be consistent with that which we expect for the decay of the top.

Tevatron and Detectors

For the rest of these lectures, we will be concerned with experiments that have been done at the Tevatron at Fermilab. The Tevatron characteristics are shown in the following table:

TEVATRON CHARACTERISTICS

- Pbar P 900 x 900 GeV
- 6 bunches
- Bunch separation 3.5 micro sec
- Initial luminosity 1.2 x 10^{31}

- Initial lifetime $\sim$ 12 hours increases to $\sim$ 20 hours
- About 2 interactions/crossing
- Beta* $\sim$ 3.5 meters
- Sigma X = Sigma Y = $\sim$ 60 microns
- Length of interaction region sigma Z $\sim$ 26 cm
- Protons/bunch 200 x 10^9 Pbar/bunch 60 x 10^9
- Pbar stacking rate 4 x 10^{10}/hour
- Integrated luminosity $\sim$ 30 pb^{-1} in 1994
  30 pb^{-1} in 1992
  9 pb^{-1} in 1988

Briefly there are 6 bunches of protons and 6 bunches of counter-rotating antiprotons in the machine. The bunches are spaced equally such that there is a collision every three and one-half microseconds at the two intersection regions ...B0 and D0, where large detectors are located. Electrostatic separators generate helical orbits for the bunches so that they only intersect at the detector location. This is necessary because of the large beam-beam turn shift that would result if the bunches crossed at 12 places. The energy is 1.8 TeV in the center of mass, and the initial luminosity of a store is 1.3×10^{31} with an initial lifetime of about 12 hours, and which increases to 20 hours as the luminosity decreases. At peak luminosity, there are about two interactions per crossing. This is achieved in a collision region that has a sigma of about 26 centimeters along the beam direction and has a circular cross section with a rms radius of about 60 microns. The integrated luminosity delivered to each of the experiments that are described here, was about 30 inverse picobarns in 1992. At present a new run is in progress where we have accumulated an additional 30 inverse picobarns, and we hope to have several times this amount of data before the end.

CDF Detector

The CDF Detector is described in detail in Ref. 7 and shown in Fig. 5. The features of it that are important for this discussion are the following:

1. A Silicon Vertex Detector located at few centimeters from the beam centerline which enables the impact parameter of a track to be measured with an accuracy of 15 to 20 microns (Ref. 8).
2. A large 3 meter diameter by 3 meter long central tracking chamber immersed in a 1.4 Tesla magnetic field that allows precise measurement of charged particle momenta.

3. Electromagnetic and hadronic calorimetry. In the central region this calorimeter uses scintillation plastic for a readout; in the forward and backward region, it uses proportional chambers.

4. A muon system that allows the identification and momentum measurement of muons when their transverse energy is over about 2 GeV.

Since we will be discussing the identification and detection of various kinds of particles in the rest of these lectures, we show in Fig. 6, in cartoon form, the technique for identifying electrons, muons, gluons, quarks, and b particles. These techniques are specific for CDF but are also widely used by all large modern particle detectors.

Muons are the easiest. Their momentum is measured in the central magnetic field and the tracking chamber with a precision of $\Delta p/p = 0.001p$. When a muon passes through the calorimeter, it deposits energy only through ionization loss, and hence leaves the signal of a minimum ionizing particle. Finally, it exits the calorimeter which has 5 or more absorption lengths in it, and its position and angle is detected by tracking chambers that surround the detector. The primary identification for the muon then comes from the minimum energy loss in the calorimeter plus the fact that it traversed an amount of absorber that would have removed a hadron through strong interactions, thus removing any track in the backup position detector.

Electrons are identified first of all by having their momentum measured in the central tracking chamber to the same precision as was given for the muons and by their total absorption in the lead absorber of the electromagnetic calorimeter. The criterion for an electron then is that the momentum measured in the magnetic field equals the energy loss in the electromagnetic calorimeter, and the fact that the position of the shower matches the entry point of the track.

Quarks and gluons, of course, are not measured directly as they hadronize and turn into a shower of particles. The size of the cone containing the energy of these particles is measured by its span in rapidity η and azimuth ϕ and is generally equal to a number between 0.7 and 1. At 90 degrees this amounts to an opening angle of between 40 and 50 degrees. A cone of this size does not completely contain the energy of the gluon, and corrections must be made for so-called out of cone losses. An additional correction must be made for the fact that the underlying event structure can also put energy into this cone which is not associated directly with the gluon or the quark under consideration. b-quarks are a special case in that during the hadronization process the quark will emit hadrons but also imbedded in the shower will be a B meson or a B hadron associated with the jet. The lifetime of these particles is generally of the order of 10^{-12} seconds and corresponds to a $c\tau$ of about 500 microns. Thus, if ones sees a shower and finds inside a detached vertex by means of using a silicon vertex detector, this shower can either be associated with the b or a c quark. Since a b quark has a mass of about 5 GeV, whereas the c quark is considerably lighter, the transverse energy of the decay helps distinguish these two

quarks from each other.

Finally, we come to the question of neutrinos. If there is a single neutrino associated with the event, it will reveal itself through the lack of the transverse momentum balance in the event. Since there is no transverse momentum in the initial state, the final state should sum to zero. This includes the momentum of all of the neutrinos plus all the charged particles and the leptons. Since there are errors associated with measuring the momentum of the quarks, there will be some error reflected in the measurement of missing E_T. The accuracy with which this variable can be measured is then determined by the resolution of the calorimetry plus the hermeticity. It is clear that any cracks or undetected energy that escapes the calorimetry will result in the missing E_T. Note also that p_Z^ν is not measured.

This short summary of how various partons are identified is generic in nature, and the accuracy of the identification as well as the accuracy of the measurement depend upon the details of the detector. The numbers given above are typical of the CDF detector.

D0 Detector

A cross section of the D0 Detector is shown in Fig. 7 and described in Ref. 9. The main feature of the detector is the large uniform liquid argon calorimeter for measuring total particle energies. There is not a magnetic field in the central region, but the momentum of muons is measured in magnetized iron in a system that surrounds the liquid calorimeter. The very fined grained high resolution calorimetry provided by the liquid argon allows a better measurement of the missing energy in an event than is available in CDF. On the other hand at present there is not a silicon vertex detector nor a central field for measuring the momentum of the tracks. Thus the techniques used in the two detectors to search for $t\bar{t}$ events tend to be complimentary in nature.

The rest of these lectures will describe first the experiments that have taken place at CDF, and then we will continue on to describe the results from D0.

II. CDF EXPERIMENT

I am assuming that these notes are being read in conjunction with the papers that have been published by CDF and D0. CDF has published a complete paper, Ref. 10, on the experiment with an enormous amount of detail, and I consider that these notes are only a guide through that paper. The same applies to the D0 experiment, although only the notes given in the Glasgow 1994 Conference were available at the time of the School. Ref. 12 gives additional results that are more recent and includes additional information not available at the time of these lectures.

High p_T Dilepton Search

We will now consider the dilepton channel. The first thing we must do is establish some kind of criterion for selecting the events. The variables that we have available are the p_T of the leptons, the missing E_T, and the energy of the jets associated with the event. The distributions of these variables are shown in Fig. 8. The lepton p_T is particularly useful as cuts on this variable can be implemented in a fairly fast fashion at the trigger level. Later in the analysis, considerably more sophisticated cuts can be made in the software analysis package. See Ref. 10 for details on the trigger.

After the events have been collected by either the inclusive electron or muon trigger, the additional cuts are implemented in the software. These cuts are as follows. Both of the leptons must have a p_T greater than 20 GeV and be of opposite charge. At least one of the tracks must have η less than 1.0 and be "isolated." The missing transverse energy E_T must be greater than 25 GeV. In addition, we will want to discuss the two b jets, and the cuts placed on these require that their transverse energies should be greater than 10 GeV, and their $|\eta|$ should be less than 2.4. These cuts were established after extensive work looking at the backgrounds from various processes and at the efficiency for finding top. Fig. 9 shows the number of data events surviving the consecutive requirements.

We will now show the results of this search in Fig. 10 and then come back and discuss the individual components. The rows labelled CDF data are the number of events surviving all of the cuts. In addition, the table shows in itemized fashion the backgrounds from various sources as well as the effect of the missing E_T and two jet cuts. The $e-\mu$ events are displayed separately from the ee and $\mu\mu$ events. The bottom line is that for all channels we observe two events with an expected background of $0.56^{+0.25}_{0.13}$.

Let us now examine these results in detail. First of all, it is necessary when considering the ee and $\mu\mu$ channels to make a cut on the invariant mass in order to eliminate the Z. The two additional jets can come from gluon radiation in the initial state of Z production thus faking the overall event. Therefore, all of the events with an invariant mass of the leptons between 75 and 105 GeV are removed. 80 percent of the dielectron and dimuon events from the $t\bar{t}$ are expected to pass this invariant mass cut. The effect of this cut is shown in Fig. 9 where we see that only 10 percent of the dilepton events are outside of this mass window and that the missing E_T cut removes essentially all of the rest.

Fig. 10 also lists other sources of background. For instance W pair production can lead to dilepton events where the two additional jets come from initial state radiation. This figure also shows the reason for the two-jet cut on the data. It is a cut that reduces the background by a factor of 4 or more, whereas the efficiency for top of 120 GeV is greater than 60 percent and grows with increasing M_T. The same effect of the two-jet cut can be seen in the rest of the channels as well.

A second source of background is $Z \rightarrow \tau\tau$. The missing E_T comes from the neutrinos associated with the tau decay. However, the direction of this missing E_T would be expected to be closely collimated with the lepton direction as the τ is quite high energy. Thus a cut was instituted that increases the missing E_T required in the event to be greater than 50 GeV when the angle of the missing E_T with respect to either of the leptons is less than 20 degrees.

There are two other backgrounds listed in Fig. 10 labelled $b\bar{b}$ and fake. The $b\bar{b}$ production cross section is very large, and the background comes from the two b's decaying into leptons with associated QCD jets. The missing E_T comes from the neutrinos associated with the b decay or from a mismeasurement of the jet energies in the detector. Fakes come from QCD jet events in which the leptons are mimicked by rather rare jets that consist of only a single particle which in turn fakes a lepton. This is not a very probable process, but as the QCD jet cross section is very high a small background is generated. In this case the missing E_T comes from an incorrect measurement of the jet energies. Since an under measurement of a jet energy will lead to a missing E_T parallel in direction to the jet, a cut is made to decrease the probability of this process. If the missing E_T lines up within 20 degrees of the jet, the cut is increased from 25 GeV to 50 GeV. Fig. 11 is a a plot of the missing E_T versus the angle between the missing E_T and the closest lepton or the jet. Fig. 11a is for the $e-\mu$ case, and Fig. 11b is for the dielectron or dimuon data after the invariant mass cut. Fig. 11c shows the result that would be expected in the 160 GeV top Monte Carlo.

Fig. 12 shows a study carried out using a Monte Carlo for simulating top events and displays the efficiency of the various cuts versus the mass of the top. We note that the efficiency of the two-jet cut increases as the mass increases because of the higher energy given to the b jets for high mass top. The geometrical and kinematical acceptance also increases with energy as the events from high mass top tend to become more centrally located in the detector. The lepton I.D. efficiency falls with increasing mass because the events become more collimated and the chance increases of the leptons being covered up by other particles in the decay. Finally, we note that requiring two jets for top masses above 100 GeV is rather efficient.

As the mass of the top increases, it becomes easier to kinematically identify the products from the decay. Therefore, it is expedient to place a lower limit on what the top mass can be. D0 has set a limit of 130 GeV (Ref. 4), but for self-consistency of the analysis, CDF has used the dilepton events to set a lower limit on the mass of the top. This was done by simply looking at the dilepton themselves with the two jet requirement removed. This is necessary because if the mass is close to the W mass, the b jets have very low energy, and the efficiency for finding them is low. Thus, to set a limit one looks for simple $e-\mu$ events with a missing E_T cut greater than 25 GeV and compares this with the production expected for $t\bar{t}$. Fig. 13 shows the upper limit at the 95 percent confidence level on $\sigma_{t\bar{t}}$ for the combined 1988-1989 and

1992-1993 runs. The number obtained is that the top mass is greater than 118 GeV with a 95 percent confidence level. For the rest of the experiment, the mass search concentrated on masses greater than 120 GeV.

Lepton Plus Jet Search

We will now consider the channel where only one of the W's decays leptonically, and the other one goes through the hadronic mode. Thus, the handles for this mode will be two b jets, two hadronic jets in the W, a missing E_T, and a lepton from the other W decay. This is shown schematically in Fig. 14. For a heavy top, the jets and leptons will be in the central region of the detector, and the event will be rather spherical in nature. There is a major background to this process; it is shown cartoon style in the same figure. It involves a W produced with initial state radiation in the form of four additional jets. The QCD radiation from the initial state tends to be along the forward and backward direction. However, since this is a strong QCD process, there is a probability that the tail of it can generate a W with high p_T jets that are in the central region of the detector. This will be a major background with which we must contend, and we will spend a considerable amount of time discussing it.

To select events for this mode, we use the following cuts: The electron has an E_T of greater than 20 GeV, muon p_T of greater than 20 GeV, missing E_T greater than 20 GeV, three or more jets with an E_T of greater than 15 GeV, and an η less than 2.0. The jet E_T is not corrected for detector effects and hence will tend to be associated with a parton whose energy is 20 GeV or more. The missing E_T is corrected for the muon only. Recall that the electron and muon modes are equal and together account for about 30 percent of the $t\bar{t}$ decays.

When we apply these cuts on the event sample, we find the results given in Fig. 15. The events are categorized by whether they are associated with an electron or a muon and then listed in terms of the number of jets associated with the event. The final sample of three of more jets contains 52 events total, and it is this set of events that we use for the top search. To get an idea of the efficiency of the cuts that we have made, Fig. 16 shows the spectrum of missing E_T expected for 120 GeV or 180 GeV top production. The lower part of the figure shows the jet multiplicity expected for these same mass tops. The cut on missing E_T greater than 20 GeV is seen to be highly efficient. The efficiency of the jet multiplicity cut is more dependent upon the mass of the top. The cut on the number of jets has been made at 3 or more, and approximately 75 percent of the $t\bar{t}$ events with a top mass of 160 GeV will pass this cut whereas less than one-half percent of all of the W events are retained. Cutting on Njet = 4 is not only less efficient, but also makes the cut highly sensitive to the top mass. The reason an intrinsic four-jet event can turn into less than four jets, is because some of the jets fall outside of the η cut or are such a low energy that they do not pass the E_T cut. In the 52 remaining events, one would expect to find a small

number of $t\bar{t}$ events. It is thus clear that we require additional means for identifying the top and separating it out the W plus QCD jet production. We will discuss the techniques for doing this next.

Separating Top Candidates from Background

There are several ways to obtain the increased rejection that we need in order to find the $t\bar{t}$ signal in the W plus jet background. Since there are two b jets, it is possible to try to identify the b decays in the event. There are two ways of doing this. Since the $c\tau$ for a b is almost 500 microns, one can search for a secondary vertex. This technique requires a silicon vertex detector that can identify tracks coming within a few tens of microns of the primary vertex. A second technique is to look for the associated soft electron or muon accompanying a semileptonic decay. A generic B has a branching ratio of about 20 percent for semileptonic decay into an electron or muon. In this case one looks for either a muon or an electron in close association with a jet, and the cuts are designed to enhance the sensitivity of the measurement to the higher transverse mass of the b as compared to other quarks.

There are other techniques for discriminating between W plus QCD jets and $t\bar{t}$ production. These methods rely on the fact that for a heavy top the decay products will have a much more nearly spherical distribution in space than for the QCD production. For instance, the momentum distribution of the jets can be studied, and it is found that this provides a discriminant. Two variables are useful for this study. The first is the aplanarity of the event which measures it sphericity, and the second is the sum of the total transverse energy in the event which for a high mass intermediate state should increase as the mass increases. One can also examine the kinematics of the events and test whether the distribution in energy of the jets resemble that expected for $t\bar{t}$ production. In this case the Monte Carlo program called VECBOS is used to mimic the W plus QCD jet production, and ISAJET is used to simulate the $t\bar{t}$ production. The ultimate test, of course, is to reconstruct the mass of each event and look for a peak in the distribution corresponding to the top mass. We will investigate all of these avenues in turn.

It is worth pointing out, however, that these approaches are somewhat complimentary in nature, and that final identification of the top will rely on a combination of all of them. For instance, a set of events could have b's associated with them and yet not be $t\bar{t}$ production. Also a set of events could give a peak in the mass distribution and yet not have the kinematics of the individual events correspond with $t\bar{t}$ production. It is also not known what the correlations are among the various kinematic discriminants. Some studies are being done of the correlations and will be used in studying the larger data set from the present run.

Tagging with the SVX

A schematic diagram of the SVX (Ref. 8) is shown in Fig. 17. The beam pipe for CDF is made of beryllium and has a radius of 1.9 centimeters. Just outside of this beam pipe is a four layer silicon microstrip vertex detector called the SVX. Since the interaction region has a length of about 50 centimeters, it is necessary to have a fairly long detector if it is to have a high efficiency. The SVX has a total length of 51 centimeters, but it is split into two sections at Z = 0. The microstrips are etched on 300 micron thick silicon wafers that are about 9 centimeters long. Three of these wafers have their microstrips connected in series in order to form the half-module. The flat silicon planes are configured in the form of a duodecagon around the axis of the beam. There are four layers located at 3.0, 4.2, 6.8, and 7.9 centimeters radius. The three innermost wafers have the strips etched with a 60 micron pitch, and the outer layer has the pitch reduced to 55 microns. There is no Z readout, and thus this detector gives an rϕ view of the event, and the impact resolution in that plane at high momentum is measured to be 17 microns. The 1992-1993 run was the first time that a silicon detector had been operated in a hadron collider, and as a result it suffered a certain amount of radiation damage, resulting in some deterioration of the signal to noise ratio during the run. This detector has since been replaced with a radiation hard version of the electronics. Fig. 17 shows a cartoon of an event with a secondary decay vertex separated from the primary vertex and indicates how such a decay vertex can be reconstructed. The primary vertex is reconstructed in the same manner as the decay vertex and indeed the resolution of the SVX is high enough so that the distribution of the interactions in the rϕ plane can be investigated. The beams have a radius of about 60 microns. Recall that the impact parameter resolution is of the order of 17 microns, and the decay distance $c\tau$ for a B is typically 450 microns.

A drawing of the SVX is shown in Fig. 18. It fits inside of a drift chamber, the VTX, that reconstructs the event in the rz plane. Both of these chambers fit inside of the CTC which has three-dimensional track reconstruction. The challenge of the tracking programs lies in attaching the tracks measured by the CTC which starts at a radius of about 27 centimeters to the measurements made in the SVX where the last plane is at 7.9 centimeters, and then associating these tracks with tracks in the VTX that give the Z position of the interaction.

In order to select the events, it is necessary to place some cuts on the significance of the tracks that are to be tested for association with a possible secondary vertex. The tracks must be associated with jets that have an E_T greater than or equal to 15 GeV and an η less than 2.0. An SVX track is said to be associated with the jet if the opening angle between the track direction and the jet direction is less than 35 degrees. The tracks must have a p_T greater than 2 GeV and must have an impact parameter significance of D/σ_D greater than 3. This sample of tracks is used to search for a secondary vertex as described in Ref. 10. If one is found, a cut is made on L_{XY}/σ_{XY} greater than 3. Fig. 19 shows the result of applying the jet vertex tagging algorithm

to a sample of inclusive electron events. These events are heavily populated by b production. The histogram shows a Monte Carlo fit to the data using the world average b lifetime. It should also be noticed that there are a few events located at negative $c\tau$ that are due to tracking errors of one kind or another. Studies have shown that this type of background should be symmetric about zero, and this fact is used to estimate the number of erroneous events on the positive side of the origin. The p_T spectrum and the L_{XY} distribution expected for top production are shown in Fig. 20.

The results of applying the SVX tagging algorithms to the W plus jet sample is shown in Fig. 21. The observed number of tagged events as a function of the number of jets is shown in the last line. Of the 52 W plus three or more jets, six have observed tags. We must now consider two questions: First, what is the efficiency for tagging events, and, second, what is the background that one would expect in the tagged sample?

To measure the efficiency of tagging, it would be nice if we could place the SVX in a beam of b's and measure directly the efficiency for tagging the secondary vertex. This, of course, is not possible, but we can come close to that by performing the following experiment. We take a large sample of inclusive electron events selected by requiring an electron to be in the central region of the detector and have that a p_T greater than 10 GeV. It is known that this sample is rich in b decays. If we knew the fraction of b's in the sample of, then we could count events observed with the SVX and directly determine the efficiency for finding a secondary vertex. The fraction of semileptonic b's has been measured to be about 37 percent. This is determined by two methods. The first involves looking for an associated low p_T muon near the electron direction. A Monte Carlo is used to estimate how often the cascade decay of the b should give an observable μ. This method gives the fraction of b's in the inclusive electron sample $f_b = 37 \pm 8\%$. However, there is an alternative way that this fraction can be checked. This approach relies on kinematically reconstructing $D^0 \rightarrow K\pi$ decays. This directly tags the D associated with the semileptonic b decay and gives a number that is consistent with the previous described measurement.

Using these measured efficiencies and a Monte Carlo to describe the $t\bar{t}$ production and decay, a number for the efficiency for tagging a b in $t\bar{t}$ production can be obtained. Fig. 22 shows the efficiency for tagging one of the b's as a function of the top mass. The expected number of events obtained from using the theoretical cross section is also shown.

Next we must worry about the background associated with the tagging operation. This background can come from a number of sources which are listed in Fig. 21. The important components of this background come from the following considerations. First, in the W plus QCD jet production it is possible for one of the gluons to split into a $b\bar{b}$ pair. This would give an event with two real b's in it plus the W. Then, there is the possibility that the tag is an artifact of the tracking. This type of mistake is called a mistag. There are a few other small sources of background that are also

listed.

In order to understand mistags a model for the SVX must be constructed that accurately predicts these mistakes in a variety of situations. The jets from W plus N jets can occur over a wide range of E_T, and with a large variation in the number of tracks associated with them. Thus we need a model for the SVX that accurately predicts it's behavior as a function of these variables. The model was constructed after studying a sample of 67,000 events that passed the 50 GeV jet trigger. These events containing 137,000 jets with E_T greater than 15 GeV were designated as generic jets in that they were not necessarily enriched in heavy flavor. The tagging rate, both positive and negative, was studied as a function of the jet E_T and the track multiplicity. The negative tag rate refers to the rate for a jet to produce a negative L_{XY}. For instance, jets with an E_T between about 20 and 120 GeV have a positive tag rate that varies between 2 and 3 percent and a negative tag rate of about 1 percent. Both rates are a function of the track multiplicity in the jet which can vary from a minimum of 2 to up to greater than 10 in the sample that was used. These empirical measurements were then used to construct a Monte Carlo model for the SVX that could predict both a negative and positive tagging rate for a generic jet. This model was checked against other samples obtained by means of different triggers. The agreement between the predictions and the measurements was excellent. See Ref. 10 for a complete description.

To predict the number of the background events in W plus N jet, we will make the assumption that the tagging rate for W plus N jet is the same as it would be for generic jets. This assumption will be an overestimate because the generic jets contain some direct $b\bar{b}$ production in addition to gluon splitting whereas W production only contains gluon splitting. Thus the model that we have constructed gives a conservative estimate of the b content in W plus N jets and is called method 1.

A second approach is possible. The mistag rate should be correct as it comes from a prediction of the negative L_{XY} tags. It is possible to use theory to directly calculate the expected $Wb\bar{b}$ cross section. Combining these two numbers should give the background actually expected. It has the weakness of having to rely on theory for a calculation of an important contribution to the background. We call this method 2.

The first line of Fig. 21 assumes that the generic jets model the b content accurately, and this conservative number has been used in order to estimate the background. A comparison of method 1 and 2 is shown in Lines 8 and 9. Thus, of the 6 tagged events, we conservatively predict a background of 2.3 $\pm$ .29. A summary of these results is shown in Fig. 23 for the $c\tau$ distribution of all of the W plus jet sample. There are four negative tags, but predominately the tags are consistent with b production. The predicted tags are shown as a histogram and compare well with the measurements. The shaded region show the tags for events with three or more jets. Fig. 24 shows this data in yet another form. It plots the number of events versus

the number of jets, both for the tag and untagged data as well as the background from method 1 and method 2.

Tagging the b with Soft Leptons

As mentioned earlier, we can tag the b's by looking for their semileptonic decay: $b \rightarrow e\nu X$ or $b \rightarrow \mu\nu X$. Calculations indicate that there is about .8 of an e or μ for each $t\bar{t}$ event. As before we have two questions that have to be answered. One is the efficiency for tagging an event which gives us the signal, and the second is the mistag rate which gives the background.

The probability of finding the e or the μ depends upon the momentum spectrum in the decay. Fig. 25 shows the P_T spectrum of the leptons from b decays as well as the lepton spectrum from c decays that are the secondary of b decays. The hardness of the spectrum, of course, depends upon the mass of the top, and that has been chosen to be 160 GeV for Fig. 25. It is necessary to make a low momentum cut on either the electron or the muon in order to eliminate a large amount of background that would come in from extraneous processes. In the case of the muon this low momentum cut must be higher than 2 GeV because that is the energy required for a muon to traverse the hadron calorimeter and be detected in the chambers just to the rear. A study of the electron backgrounds indicated that this was also a sensible place to make the cut for electrons. The efficiency of these cuts is seen to be very high.

The background in both cases is associated with the probability that a track will fake a lepton. For instance, a muon can be faked by a pion decay in flight or an electron can be faked by a pion giving a big interaction in the electromagnetic calorimeter. To calculate the background then requires a detailed study of these probabilities which can depend on the track momentum as well as a number of other cuts that are made in the calorimetry. Details of these are given in Ref. 10. Fig. 26 and 27 show the tag rate per track for electrons and muons in generic jets. It is seen that this tag rate in both cases is less than 1 percent. The background then for the tagging algorithm consists of folding this information about the fake track tagging rate into the distribution of tracks expected from the jets that are being studied. Again, as in the case of the SVX, a number of independent sources of jets were examined to see how well the predicted and observed number of tracks agreed with each other. Fig. 28 shows a summary of this information. And it can be seen that the predicted numbers agree quite well with those actually observed. The deviation between and predicted numbers and the observed numbers is used to estimate the systematic error on this procedure.

Fig. 29 shows a summary of the backgrounds as well as the tagging rate for SLT events. Again, as in the case of the SVX, we assume that a generic jet has the same b content as the W + jets and again, we understand that this is a conservative

assumption as it is probably an overestimate of the $Wb\bar{b}$ contribution. The summary is given in the bottom line where we observe that the 52 W plus more than three jets events have seven tags and an estimated background 3.1 $\pm$ 0.3 events.

Statistical Significance of the Counting Experiments

We are now in a position to evaluate the statistical significance of the results from the counting experiments. We have three channels each showing an excess. The numbers are shown in Fig. 30. The bottom line gives the observed number of events in each channel and just above, is the expected background. For comparison, the first four lines of the table give the number of events predicted from using the theoretical value of the cross section for four different top masses. If we treat the channels independently, we can calculate the probability that the estimated background has fluctuated up to a number greater than or equal to the number of events seen. We find P_{DIL} is equal to 12 percent, P_{SVX} is equal to 3.2 percent, and P_{SLT} is equal to 3.8 percent. However, one can make a stronger statement by calculating a combined probability for the three results. Recall that there are two dilepton tags (one event has both an SLT and SVX tag). There are 6 SVX tags and 7 SLT tags. However, 3 of the SVX events overlap 3 of the SLT events. The question of how to combine this data was investigated at length, and the following ansatz was finally used. Instead of using tagged events, the number of tags in the sample was taken as the variable except in the dilepton case, where events were used. Thus, there are 15 "counts;" the 2 dilepton events, the 6 SVX tags, and the 7 SLT tags. This procedure gives extra weight to the double-tagged events which are more likely to be real than false and, therefore, have a considerably smaller background than single tagged events. However, there are still correlations among the experiments that must be properly understood in order to calculate correctly the combined probability. A Monte Carlo program was used which generated many samples of the 52 events with the background such as W + $b\bar{b}$, etc. fluctuating around their mean value. The procedure is described in great length in Ref. 10 and leads to the result that $P_{combined}$ is equal to 0.26 percent which, if it were a Gaussian probability, would be a 2.8 σ excess.

Assuming that these excess events come from $t\bar{t}$ production, one can calculate the cross section as a function of M_T. The dependence on M_T enters because the acceptance of the experiment is slightly dependent upon the top mass. The results are shown in Fig. 31. The next task is to estimate the mass from the kinematics of the events.

Checks on the Counting Experiments

Before we study the behavior of the kinematic variables, we will describe briefly some of the checks that are made on the counting experiment. An obvious place to test the validity of the procedure would be to study the corresponding situation

in Z + jets. In this case, no top signal is expected, however, the smaller number of events in which the Z is identified through its e^+e^- decay mode will make these checks statistically rather limited. In order to compare W + jets with Z + jets, we subtract the top signal from the W + jet sample. This is possible because we know the efficiency for tagging a top event, and we also know from Monte Carlo studies the population of the top events in the W + N JETs sample. It is true that there is a small variation of tagging efficiency with mass, but this variation is less than 10 percent for the SVX and less than 5 percent for the SLT over a top mass range from 120 to 180 GeV. Fig. 32 then shows the corrected number of W + QCD jets that are observed. Notice that the contribution from the top is so large that it completely accounts for all of the events observed in W + four or more jets. To see if this is reasonable, we compare these numbers with a VECBOS calculation in Fig. 33, and there seems to be a deficit in the W + four jet events. However, the uncertainty on the VECBOS predictions due to the choice of the Q^2 scale dependence makes the uncertainties hard to quantify.

The numbers from Fig. 33 are shown in Fig. 34 along with the experimental numbers from a study of Z + N jets. The last column shows the ratio between the W and the Z columns. Again, in the case of three of more jets, there seems to be a deficit of events in the W + N jet case, but the statistics is unfortunately rather limited. An additional feature of the Z events is that there are two b-tagged Z events with greater than or equal to 3 jets where only .64 is expected. The resolution of these questions will have to await additional experimental data.

The Analysis of the Event Structure

So far we have been considering the search for the top as a counting experiment, that is to say, was there an excess number of W + 3 or more jets in the data, or was there an excess of dilepton events. The question of whether the kinematics of the event describes a $t\bar{t}$ production and decay has arisen only indirectly in calculating the detector acceptance. However, it is clear that a study of the event variables may be able to distinguish between QCD processes and $t\bar{t}$ production. We investigate that question now.

Fig. 35 shows a lego plot of E_{t2} versus E_{t3} for W + 3 or more jets where the VECBOS calculation has been used for the QCD background and ISAJET has been used for the $t\bar{t}$ case. A top mass of 170 GeV has been assumed. This figure graphically illustrates the fact that a heavy mass top tends to populate the central regions of the detector with rather high jets. The fourth jet would also show this effect. However, in the interest of maximizing the signal and minimizing the systematic errors at low jet energy, we initially exclude consideration of the fourth jet.

Fig. 36 shows the $\cos\theta^*_{max}$ predicted by Herwig for top production, and by VECBOS for W + 3 jet events. The upper figure shows the inclusive distribution, and the

lower figure shows the distribution after applying a rapidity cut to the jets which requires them to be in the central region of the detector. $\cos\theta^*_{max}$ is the maximum $\cos\theta$ of the three jets. The curves have been normalized to the same area for comparison. If one cuts on $|\cos\theta^*_{max}|$ then the region greater than 0.7 will contain an enhanced background. The number of top events in the two samples should be about equal, but in the latter sample the background should be three times higher. The region of large $\cos\theta$ is called the background region, and the region less than 0.7 is called the signal region in the following discussion.

Since we will be comparing top decay with W + QCD jets, it is imperative that we have the good model for the QCD process. The model used here is VECBOS. However, in using VECBOS, it is necessary to define the Q^2 scale for α_s. The VECBOS program allows generation of W events with N = 0, 1, 2, 3, and 4 partons. We require the p_T of the parton to be greater than 10 GeV, and the η of the parton to be less than 3.5 as well as the ΔR separation of 2 partons to be greater than .4 in order to avoid infrared divergences. The partons have been fragmented using Herwig as well as Field-Feynman. The results are not sensitive to this feature. However, they are somewhat sensitive to the Q^2 scale that is chosen. In this study $Q^2 = M_W^2$ has been used as it yields the hardest distribution for the jet partons. Two checks of this model are possible. The E_T distribution for the jets in the W + 2 or more jets sample can be studied as well as the complementary reaction with the Z. In both cases, reasonable agreement with the model is found.

To display this data, we define an absolute likelihood as follows:

$$aL = \left(\frac{1}{\sigma}\frac{d\sigma}{dE_{T1}}\right) \times \left(\frac{1}{\sigma}\frac{d\sigma}{dE_{T2}}\right)$$

E_{T1} and E_{T2} are the energies of the highest two jets in the W + 2 or more jet sample. The distributions in E_{T1} and E_{T2} are shown in Fig. 37, and the distribution in absolute likelihood as defined above, is shown in the lower histogram. It is seen that the agreement between the model and the experimental data is quite good, although the data may be slightly softer than the model.

We now proceed to the W + 3 or more jet events, and we now expect both QCD background plus real top to be present. As described above, we can enhance the signal by making a cut $|\cos\theta^*_{max}| < 0.7$. The distributions expected from $t\bar{t}$ events and from VECBOS plus 3 or more jet events in shown in Fig. 38. The curves have been normalized to unity for reasons that will become apparent shortly. The top curves have been drawn for 170 GeV top, and it is apparent that the E_{T1} and E_{T2} and E_{T3} spectra are considerably harder than would be expected for the QCD events. The experimental data are shown in Fig. 39.

We now need a way to test whether an event is more like the QCD case or more like the top case in its characteristics. We define an absolute likelihood in analogy with the 2-jet case but use E_{T2} and E_{T3}. We note that given an event with an E_{T2}

and a E_{T3}, we could use either of the distributions shown in Fig. 38 to calculate an absolute likelihood. That is, we could use the QCD distribution to measure a likelihood that it is similar to a QCD event or we could use the distribution from the top Monte Carlo to measure the probability that it resembles the top. A convenient way to display this data then is to define a relative likelihood by the following formula. This relative likelihood is the ratio between the absolute likelihood that the event is a top and the absolute likelihood that it is a QCD event.

$$rL = aL^{top}/aL^{QCD}$$

The normalized histograms of Fig. 38 are used for calculating this ratio.

Large values of relative likelihood will indicate a top-like candidate. And small values of relative likelihood will indicate a QCD-like event. Note that this whole process is sensitive to the parent distributions which involve the Q^2 scale for VECBOS and also the mass used for the top in the $t\bar{t}$ distributions. The dependence on the mass assumed for the top is shown in Fig. 40.

The distributions predicted by a Monte Carlo calculation of rL are shown in Fig. 41a for the signal region and 41c from the control region. The solid curve is from top production and the dotted from the VECBOS Monte Carlo. The curves have all been normalized to unity.

The distribution of the data in the two regions is displayed in Fig. 41b and Fig. 41c. The data is shown as a solid line and the VECBOS predictions as crosses. The VECBOS points have been normalized to the region $\ell n(rL) < 0$. It is seen that there is an indication of a top-like signal in the data.

We have one more test of the nature of these events in that we can look at the b-tags in the SVX and SLT. There are 14 events in the signal sample, and four of these events have an SVX tag. The distribution of the tagged events is shown in Fig. 42. The shaded region is an estimation of the tags that would be expected from background processes. The method for estimating this background is similar to that described in the SVX and SLT search. There is one event in the background region, and three events in the top region where the expected background is $0.58^{+.12}_{-.09}$. The probability that the observed number of tags is due to a statistical fluctuation of the background is 0.4 percent. Four of the 14 events include a soft lepton tag, and the expected background in this case is $1.2 \pm .3$ events with a probability of the background fluctuating up to 4 or more events being 4 percent. In the control sample there is one SVX tag and one soft lepton tag, and the expected number of tags is of the order of 2.

Thus, within the limited statistics that are available, the kinematic structure shows a top-like signal. In the future when a large sample of events is available, this will become an important technique for demonstrating that the events have the distributions in E_{T2} and E_{T3} corresponding to that expected for a top. We now

proceed to the reconstruction of mass and note that it would be possible to have events reconstruct to a top mass without having the distribution of the kinematic variables fit the $t\bar{t}$ hypothesis. Thus, the event structure analysis gives independent evidence as to the nature of the events.

Mass Reconstruction

If it is assumed that the excess of b-tagged events described in the preceding sections comes from $t\bar{t}$ production, then it should be possible to determine the mass of the top directly by reconstruction. In order to do this, it is necessary to have access to all four jets. For this reason, we will change the cuts slightly to increase the acceptance for a fourth jet which will now be included if it has an uncorrected E_T greater than 8 GeV and an η less than 2.4. Monte Carlo studies show that for 170 GeV mass, 60 percent of the events having three jets will also have a fourth jet passing the standard criteria, while 86 percent will have a fourth jet passing passing these relaxed criteria. Of the 10 b-tagged events, 7 pass the relaxed criterion for having a fourth jet.

For the purposes of making a constrained fit, we assume that the production and decay process goes through the following steps.

1. $\bar{p}p \rightarrow t_1 + t_2 + x$
2. $t_1 \rightarrow b_1 + W_1$
3. $t_2 \rightarrow b_2 + W_2$
4. $W_1 \rightarrow \ell + \nu$
5. $W_2 \rightarrow j_1 + j_2$

This is a five vertex system in which we make measurements of the jet energies, the lepton energy, and the missing E_T. It is assumed that the initial state transverse momentum is zero. The overall kinematic fit has two degrees of freedom. There are 20 equations and 18 unknowns. However, the association between the jets and the partons is not unique. If both of the b jets were correctly tagged, there would still be multiple solutions. First, there are two solutions for the p_Z for the neutrino, and there would be an additional two combinations in the association of the b with the correct top. However, we only have one b-jet tag, and hence there are 12 different configurations that we must choose between. If none of the b jets are tagged, then there are 24 possible configurations. To chose among the different configurations, we calculate χ^2 and demand that $\chi^2 < 10$. We will discuss the efficiency of this method shortly. The calculation is also complicated by the possibility that one of the jets may come from initial state radiation and is not even associated with the t or $\bar{t}$ decay.

The outline of the solution above requires that we know the parton momenta. However, the detector measures jet energies. In order to do the reconstruction, we need to relate the jet energy to the parton energy. Furthermore, in order to calculate a χ^2, we need to estimate the error on the parton energy that arises because of uncertainties in the jet measurement. It should be remembered that the major uncertainties in this process come from the jet measurements as the lepton is measured quite accurately.

Fig. 43 illustrates the problem of associating parton energy with jet energy. A large sample of Monte Carlo events was generated with Herwig using a top mass of 170 GeV. The jets generated by this process can be associated with the b jet or with light quark jets coming the W decay. In addition the b jets can be categorized as generic b jets or as b jets that decay semileptonically with an electron or with a muon. The jets from Herwig have been run through the CDF detector simulation, and the horizontal axis is the difference between the parton energy and the reconstructed jet energy using the standard calorimetry codes. Fig. 43a shows the spread in reconstructed energies versus the E_T of the jet. The spread is reasonably Gaussian and is determined by the statistical processes that take place in the calorimetry. Fig. 43b shows generic b jets, and it can be seen that the neutrino is making a non Gaussian tail due to the fact that it has taken away a fair amount of energy from the jet. Fig. 43c and 43d further elucidates this feature for the case of semileptonic decays involving an electron and a muon. Since the electron is well measured by the calorimeter, this skewing in c is less than that in d where the muon only deposits a minimum amount of energy calorimetrically.

As a result of this study, a new correction code for jets was generated. This algorithm attempted to relate directly the parton energy to the observed jet energy, and by studying the deviations shown in Fig. 43, the uncertainty in the parton energy from the jet measurement was evaluated. Fig. 44 shows an interesting example of the effect of this correction. The top plot shows the mass of the W calculated using jets with only standard corrections, and the bottom plot shows the mass using the new algorithm. The horizontal axis is the momentum of the W. Note, that in the future, when one has a large sample of $t\bar{t}$ decays to study, it will be possible for the first time to study the accuracy of reconstruction of events using calorimetric data. The check on the process will come from measuring how well the W mass can be resolved.

A number of systematic effects in this model were studied. One of the most important tests verified that the reconstructed top mass coincided with the input mass for the top that was used in the Monte Carlo generator over the range between 120 and 200 GeV. The jet energy scale of the calorimeter is also an important number in determining the mass. Fortunately, uncertainty in the scale of 10 percent results in a top mass uncertainty of the order of 5 percent because the lepton energy is very well measured, and also because there are additional constraints on the W mass in the fitting procedure.

Fig. 45 shows a reconstructed top mass distribution for Monte Carlo generated events with $M_{top} = 170$ GeV. The full histogram corresponds to the best fit obtained by the program when requiring that one of the b jets is a b in the fit. The dashed histogram refers to the fit with a correct assignment for each jet. The χ^2 assignments of the jets only lead to a correct assignment in 31 percent of the time, and the long tail on the mass distribution is due to an incorrect assignment of the jets to the partons. It is interesting to note that even if no b tagging is used, one still obtains a peak at the correct mass but with somewhat worse tails. Picking the event with the best χ^2 is fairly effective at generating the correct mass.

W plus multijets were generated by VECBOS and studied, and it is found that 83 percent of the events that pass our selection criterion can be fit with the $t\bar{t}$ hypothesis. The mass spectrum from these events is shown in Fig. 46, and peaks at about 140 GeV.

We now consider the sample of 7 tagged events and estimate the background in this sample to be $1.4^{+2}_{-1.1}$ events. This estimate corresponds essentially to method 2, since in this case we are not doing a counting experiment, we will not use the most conservative estimate for the background but rather our best estimate of what it should be. A likelihood function is constructed which includes the number of background events and the number of signal events, the sum of which is constrained to be 7. The likelihood fit is shown in Fig. 47 and has a minimum at 174 GeV. The best estimate for the background fraction is $0.16^{0.16}_{-0.14}$ compared with the estimated value of .20. If one imposes the constraint that the number of top events is 0, the hypothesis that W + jet background spectrum fits the observed spectrum is 2.3 standard deviations away from the top + background hypothesis. Fig. 48 shows the top mass distribution as a solid histogram on the expected background of 1.4 events. The dashed histogram represents the sum of 5.6 top events and 1.4 background events as calculated from Monte Carlos.

The systematic errors on the mass measurement are given in Fig. 49. They come from the absolute energy scale of the calorimeter, the uncertainty due to gluon radiation effects being modelled correctly in the Monte Carlo, and an uncertainty in the shape of this background that is modelled by using VECBOS. Using a different scale for Q^2 and different fragmentations can change the shape of the background slightly. These uncertainties combined in a quadrature manner yield the final value for the top mass $M_{top} = 174 \pm 10^{+13}_{-12}\,GeV/c^2$. Using the acceptance for the top mass of 174 GeV gives a $\sigma t\bar{t}(174) = 13.9^{+6.1}_{-4.8}$ pb.

Summary of the Collider Detector Experiment

In summary, the CDF experiment has some strong evidence for the top, but there are some observations that do not support this conclusion.

In support of the hypothesis, we observe two dilepton events with a background of

0.56. In addition we observe 6 lepton + jet events with b tagging information from the SVX on a expected background of 2.3, and 7 events on a background of 3.1 using the soft lepton from the semileptonic b decay to identify the b. The background has been estimated in a conservative manner from the data. In addition, one of the dilepton candidates is tagged by both b tagging techniques. This, together with the observed excess of lepton + jet events, gives evidence for both $Wb\bar{b}$ and $WWb\bar{b}$ production as would be expected in $t\bar{t}$ decays. There is evidence in the lepton + jet events that the kinematics of the decays are consistent with the $t\bar{t}$ hypothesis, and in fact a kinematic reconstruction of the events yields a mass of 174 GeV. This mass also agrees with the mass inferred in precision electroweak measurements.

On the other hand some features of the data do not support this hypothesis. Z + multijet events have been studied, and 2 tagged events are seen in the Z + 3 or more jets where only 0.64 would be expected. In addition, the $t\bar{t}$ cross section that we find is large enough so that it absorbs all of the rate for W + multijet production that should be seen in the W + 4 jet events. It is imperative to have more data to answer some of the questions that have been raised by this analysis. At present the machine is running again, and there is already additional data equal to the amount presented in this analysis.

III. SEARCH FOR THE TOP QUARK AT THE D0 DETECTOR

We now discuss the results found by the D0 Collaboration. The most complete reference at this point is the report from the Glasgow Conference, Ref. 11. And, as in the case of the CDF experiment, this report should be consulted, along with these lecture notes. An additional paper is now available, Ref. 12, which includes additional results from this experiment which were not available at the time of these lectures.

A cross section of the D0 detector is shown in Fig. 7. The main feature of the detector is the large uniform liquid Argon calorimeter for measuring total particle energies. There is not a magnetic field in the central region, but the momentum of muons is measured in magnetized iron in a system that surrounds the liquid calorimeter. The very fine grained, high resolution calorimetry provided by the liquid Argon allows a better measurement of the missing E_T in an event than is available in CDF. On the other hand, at present there is not silicon vertex detector. Thus, the techniques used in the two detectors to search for $t\bar{t}$ events tend to be complimentary in nature.

Dilepton Search

The dilepton analysis is reported in Ref. 4 and was updated at Glasgow. It requires the presence of 2 high p_T leptons, a large missing E_T, and 2 jets with E_T jet greater than 15 GeV. The results are shown in Fig. 50, along with the expected

top signal and backgrounds. Fig. 51 shows these events plotted in the E_T, p_T plane for the data before the final cuts requiring 2 jets. The Monte Carlo prediction for a top mass equal to 170 GeV is also shown. There is one event observed in this data, and a likelihood analysis of the kinematics would indicate a value for the mass in the vicinity of 150 GeV.

Search in Electron + Jet Mode

We have already studied in detail the difficulty of isolating $t\bar{t}$ events from W + QCD events in the mode of lepton plus missing E_T plus jets. Some additional discrimination is needed in the W + 4 jets in order to isolate the top production. The D0 experiment has two techniques for dealing with this. The first is use the kinematic differences between the $t\bar{t}$ production and the W + QCD jets to isolate the top events. They also have developed a way to search for a soft secondary muon which would identify a b jet in the event. This is similar to the muon SLT search described in the CDF experiment. We will first of all consider the kinematic technique.

The two variables that are chosen are the aplanarity A of the event which is defined to be 1.5 times the smallest eigenvalue of the normalized momentum tensor constructed in the overall $p\bar{p}$ frame from jets with η less than 2. The second variable called H_T is defined as the sum of the scalar transverse momentum of all final state jets. Large A and large H_T correspond to decay of high mass states. The cuts placed on the events to select them are as follows: Either the electron E_T^e is greater than 20 GeV and $|\eta_e| < 2$ or $p_T^\mu > 15$ GeV and η_μ is less than 1.7. Missing E_T must be greater than 25 GeV for the electronic mode and greater than 20 GeV for the muonic mode. And finally there must be least four jets with E_T greater than 15 GeV in the region of $|\eta| < 2$. Furthermore events with a soft muon are eliminated to keep this search statistically independent of the one that we will describe shortly. Fig. 52 displays a Monte Carlo study of how these variables distinguish events. The upper left hand plot shows A versus H_T for QCD multijets, and the right-hand side shows W + jets. A $t\bar{t}$ Monte Carlo is shown in the lower left-hand corner, and data from the experiment is shown in the lower right.

The event distributions shown in Fig. 52 can be used to directly estimate the fraction of events for each of the two processes which fall in each of the four quadrants of the A – HT space. Using these fractions, one can then fit the data in the lower right-hand corner directly to obtain the background and the signal. There are a total of four events in the signal region, and the background is estimated to be 1.7 $\pm$ 0.8 $\pm$ 0.4 events.

A second method of obtaining the background after the topological cuts is to study the behavior of the background W + QCD jets as a function of the number of jets. This information is then used to predict the QCD background in the lepton + four jet category. Once this number is obtained the cuts shown in Fig. 52b give the fraction of these events that will wind up in the signal region.

Fig. 53 summarizes the result of the study. The top curve shows the number of W + jet events versus the inclusive number of jets for E_T greater than 15 GeV and E_T greater than 25 GeV. The open symbols are the data, and the filled symbols show the prediction of the Monte Carlo, and the lines are fit to the data for the interval between 1 and 3 jets. A similar study carried out for the case of QCD multijets is shown in Fig. 53b. In this case, the selection of the sample is made from multijets, where one of the jets fakes an electron, and where there is also a missing E_T that is less than 25 GeV. This sample should contain no signal from the top. The slope is similar to the slope shown in Fig. 53a, and again the scaling hypothesis seems to work rather well. Therefore, the extrapolation of the curves to N = 4 jets is considered a reliable way to estimate the background. The number of predicted background events is then decreased by the fraction that would fall in the signal region of the AH_T space. The background predicted by this technique is $1.8 \pm 0.8 \pm 0.4$, agreeing well with the direct fitting procedure described above.

Muon Tagging

The muon discrimination in the D0 detector is very good, and hence they can use this to look for a secondary muon associated with a b jet in order to tag it. This search is performed on the e + multijet sample. The results of this search are presented in Fig. 50 along with the other channels. The bottom line gives the data for the various channels, and the line just above the estimated background. The overall search finds 7 events on an expected background of $3.2 \pm .1$. The probability that the background alone could fluctuate and give the 7 events < 7.2 percent or about 1.5 standard deviations in a Gaussian approximation. If this result is combined with the acceptance of the detector which varies with top mass, then the D0 results can be presented as shown in Fig. 54. The CDF result is shown as a cross. See Ref. 12 for more complete D0 results.

IV. SUMMARY AND CONCLUSIONS

It is still early to make a comparison in detail of the two experiments. However, Fig. 55 shows the acceptances and the background rate of the two detectors in the various channels as reported at the Glasgow Conference. It is seen that the acceptance of the two experiments is comparable. The major difference comes in the way that lepton + jet events are treated. In the case of CDF, these events are analyzed with the SVX and with the SLT technique to identify b jets. The advantage of a secondary vertex detector is that it enables the systematics of the tagging process to be investigated in much greater detail. The topology is then used as an independent check of the likelihood that the events are top. D0 uses the topology to select the events except in the case where they use a secondary muon tag. Shortly D0 will have the soft muon tag working for the muon + jet events.

Within the next year or so, there should be several times the amount of data available that has been presented in these lectures. An identification of the top will have decays seen in all the channels. One would hope to see lepton + jet events and dilepton events, where both of the b jets are tagged although this will be rare. The properties of the B may even give more information that will help associate it with the correct W. However, it is clear at this point that the dilepton events themselves present a very strong case for a new class of events. As a group they are remarkable! Fig. 56 is a histogram of the sum E_T of the jets in the CDF dilepton events. The upper figure displays the data of the 8 $e\mu$ events from Fig. 9. The lower figure shows the histogram from a Monte Carlo study of WW events compared to that expected for top production. It serves as an example of how $t\bar{t}$ production compares to a typical background. In Fig. 57, I show a different plot of the dilepton events. The vertical axis in the missing E_T and the horizontal axis is the jet sum E_T as in Fig. 56. I have included the D0 event as reported at Glagow and Ref. 4, as well as an additional CDF event from early in the 1994 run. Although one cannot conclude from this meager sample that the events are top, it is clear that they are unique events!

The future is exciting. Shortly there will be enough new data available to answer all of the unanswered questions raised in these lectures. We will be able to actually study how accurately jet spectroscopy is able to measure the mass of the top. There will be internal consistency checks within the reconstruction due to the hadronic decay of one of the W's. The study of the interaction between the t and $\bar{t}$ could lead to exciting new physics. There will be information from the spin correlations that will help check our understanding of the production and decay. Finally, combining an accurate measurement of the top mass with the precision measurement of the W that will be available from CDF and D0 will give the first solid prediction for the mass of the elusive Higgs. There is still some fun left!

I would like to thank my many colleagues in both CDF and D0 for help in assembling this information for these notes, especially Carol Picciolo for transcribing these notes.

REFERENCES

1. G. Arnison et al., UA1 Collaboration, Associated Production of an Isolated, Large Transverse Momentum Lepton (Electron or Muon), and Two Jets at the CERN $\bar{p}p$ Collider, *Phys. Lett.* 147b, 493 (1984).

2. F. Abe et al., The CDF Collaboration, Top-Quark Search in the Electron + Jets Channel in Proton-Antiproton Sollicions at $\sqrt{s} = 1.8$ TeV," *Phys. Rev. D* 43, 664 (1991).

3. F. Abe et al., The CDF Collaboration, Lower Limit on the Top-Quark Mass from Events with Two Leptons in $p\bar{p}$ Collisions at $\sqrt{s} = 1.8$ TeV," *Phys. Rev. Lett.* 68:447 (1992).

4. S. Abachi et al., D0 Collaboration, Search for the Top Quark in $\bar{p}p$ Collisions at $\sqrt{s}$ = 1.8 TeV, *Phys. Rev. Lett.* 72:2138 (1994).

5. R. H. Dalitz et al., Where is the Top?, *Int. J. of Modern Phys.* 9A:635 (1994).

6. E. Laenen, J. Smith, W. Van Neerven, Top Quark Production Cross Section, *Phys. Lett.* 321B:254 (1994).

7. F. Abe et al., The CDF Collaboration, The CDF Detector: An Overview, *Nucl. Instrum. Methods Phys. Rev., Sect. A* 271:387 (1988).

8. D. Amidei et al., The Silicon Vertex Detector of the Collider Detector at Fermilab, Nucl. Instrum. Methods Sect. A 350:73 (1994).

9. S. Abachi et al., D0 Collaboration, The D0 Detector, *Nucl. Instrum. Methods A* 338:185 (1994).

10. F. Abe et al., The CDF Collaboration, Evidence for Top Quark Production in $\bar{p}p$ Collisions at $\sqrt{s}$ = 1.8 TeV," *Phys. Rev. D* 50:2966 (1994).

11. 27th International Conference on High Energy Physics, University of Glasgow, Glasgow, Scotland, July 20-27, 1994. See contributions by:

    (a) P. Grannis

    (b) S. Protopopescu

    (c) S. J. Wimpenny

    (d) R. Raja

12. S. Abachi et al., D0 Collaboration, Search for High Mass Top Quark in $p\bar{p}$ Collisions at $\sqrt{s}$ = 1.8 TeV, submitted to *Phys. Rev. Lett.* November 1994. FERMILAB-PUB-94/354-E.

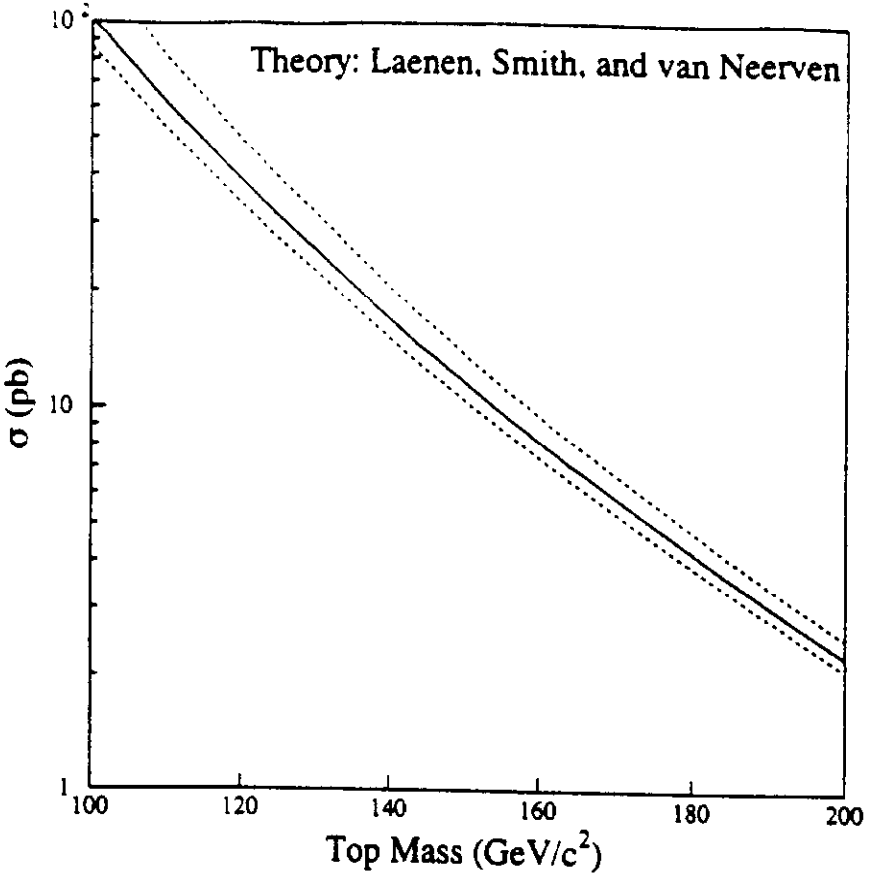

Figure 3: Top cross section according to ref 6. The dotted lines are the quoted estimates of the theoritical uncertainty.

STANDARD MODEL TOP DECAY

$\bar{p}p \rightarrow t\bar{t} \rightarrow W^+ b \; W^- \bar{b}$

		W^+								
		$\bar{e}$ ν	$\bar{\mu}$ ν	$\bar{\tau}$ ν	u $\bar{d}$	u $\bar{d}$	u $\bar{d}$	c $\bar{s}$	c $\bar{s}$	c $\bar{s}$
W^-	$e\bar{\nu}$	1	1	1	1	1	1	1	1	1
	$\mu\bar{\nu}$	1	1	1	1	1	1	1	1	1
	$\tau\bar{\nu}$	1	1	1	1	1	1	1	1	1
	$\bar{u}$ d	1	1	1	1	1	1	1	1	1
	$\bar{u}$ d	1	1	1	1	1	1	1	1	1
	$\bar{u}$ d	1	1	1	1	1	1	1	1	1
	$\bar{c}$ s	1	1	1	1	1	1	1	1	1
	$\bar{c}$ s	1	1	1	1	1	1	1	1	1
	$\bar{c}$ s	1	1	1	1	1	1	1	1	1

Figure 4: Different decay channels for the two W's

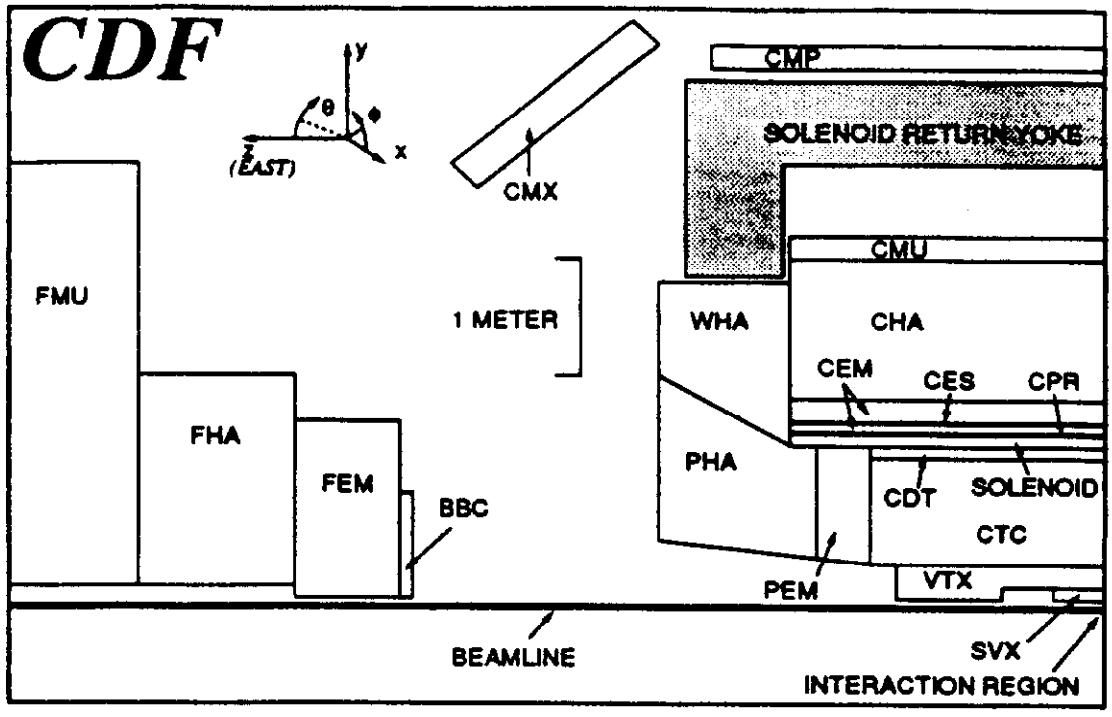

A side-view cross section of the CDF detector. The detector is forward-backward symmetric about the interaction region, which is at the lower-right corner of the figure. See text for detector component definitions.

System	η Range	Energy Resolution	Thickness
CEM	$\lvert\eta\rvert < 1.1$	$13.7\%/\sqrt{E_T} \oplus 2\%$	18 X_0
PEM	$1.1 < \lvert\eta\rvert < 2.4$	$22\%/\sqrt{E} \oplus 2\%$	18-21 X_0
FEM	$2.2 < \lvert\eta\rvert < 4.2$	$26\%/\sqrt{E} \oplus 2\%$	25 X_0
CHA	$\lvert\eta\rvert < 0.9$	$50\%/\sqrt{E_T} \oplus 3\%$	4.5 λ_0
WHA	$0.7 < \lvert\eta\rvert < 1.3$	$75\%/\sqrt{E} \oplus 4\%$	4.5 λ_0
PHA	$1.3 < \lvert\eta\rvert < 2.4$	$106\%/\sqrt{E} \oplus 6\%$	5.7 λ_0
FHA	$2.4 < \lvert\eta\rvert < 4.2$	$137\%/\sqrt{E} \oplus 3\%$	7.7 λ_0

Summary of CDF calorimeter properties. The symbol $\oplus$ signifies that the constant term is added in quadrature in the resolution. Energy resolutions for the electromagnetic calorimeters are for incident electrons and photons, and for the hadronic calorimeters are for incident isolated pions. Energy is given in GeV. Thicknesses are given in radiation lengths (X_0) and interaction lengths (λ_0) for the electromagnetic and hadronic calorimeters, respectively.

Fig. 5

PARTON ID SCHEMES

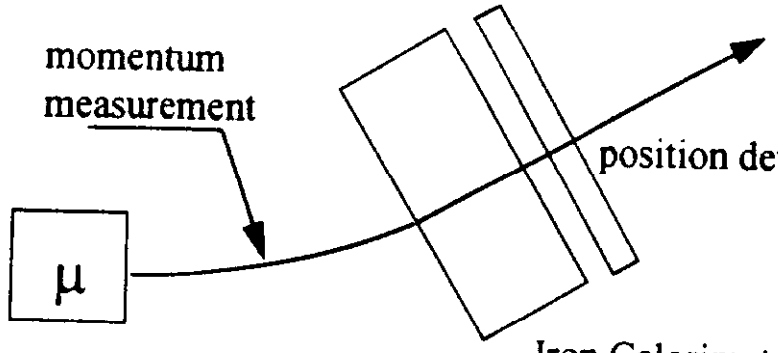

Iron Calorimeter measures dE/dX

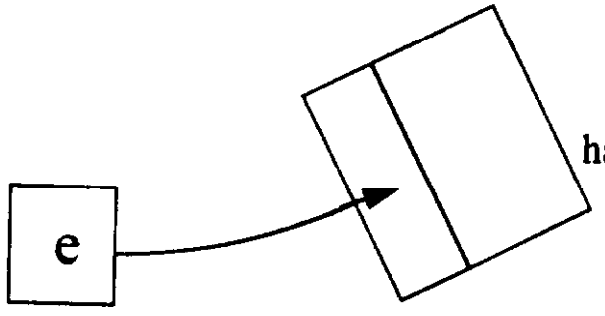

EM calorimeter. E matches P

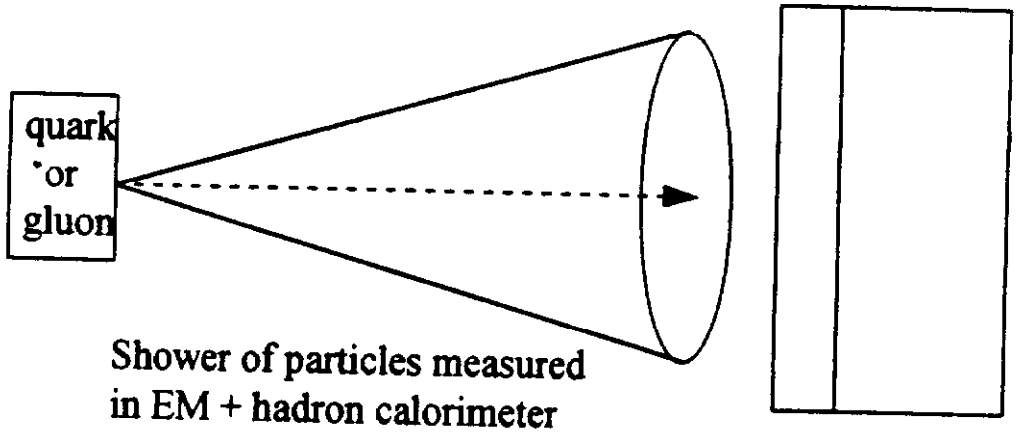

Shower of particles measured
in EM + hadron calorimeter

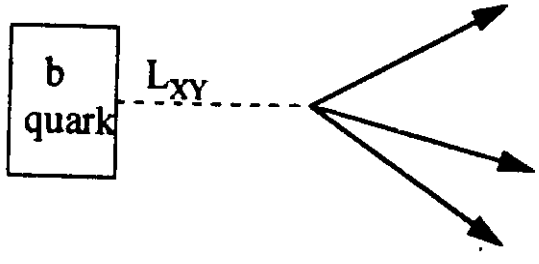

Secondary decay vertex
or a secondary lepton from
the b decay.

Fig. 6

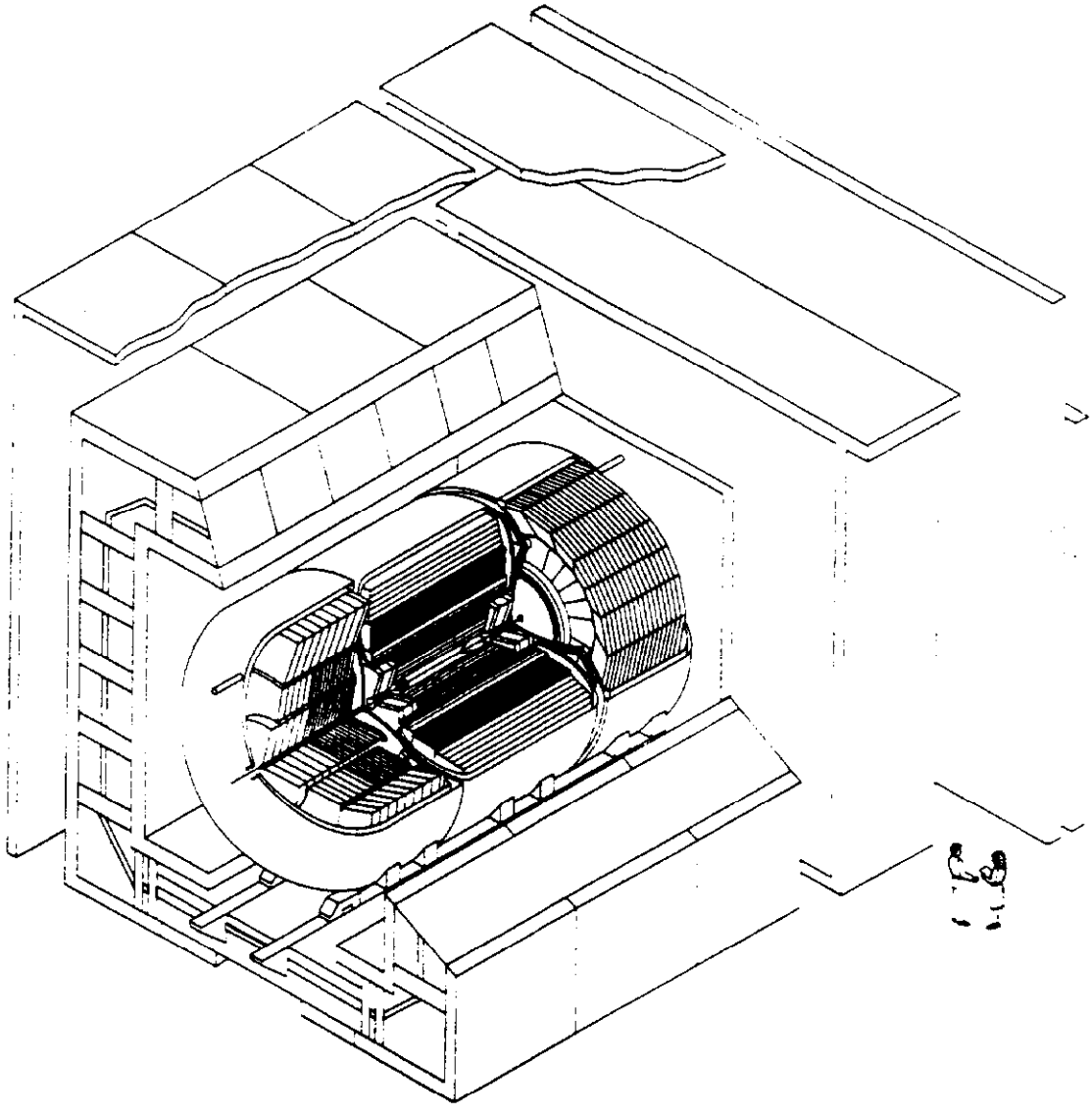

DØ Detector

TRACKING

	Vertex Chamber	Central Drift Chamber	Forward Drift Chamber
Resolution in $r\phi$	60 μm	180 μm	200 μm

CALORIMETRY

Coverage $|\eta| < 4$ $(\vartheta > 2°)$ Granularity $\delta\eta \times \delta\vartheta = 0.1° \times 0.1°$

Electron Energy Resolution = $15\%/E^{.5}$ Hadron Energy Resolution = $50\%/E^{.5}$

MUON SYSTEM

Coverage $|\eta| < 3.3$ $(\vartheta > 5°)$

Resolution $\delta P/P = [0.04 + (0.01P)^2]$

Figure 7: D0 Detector

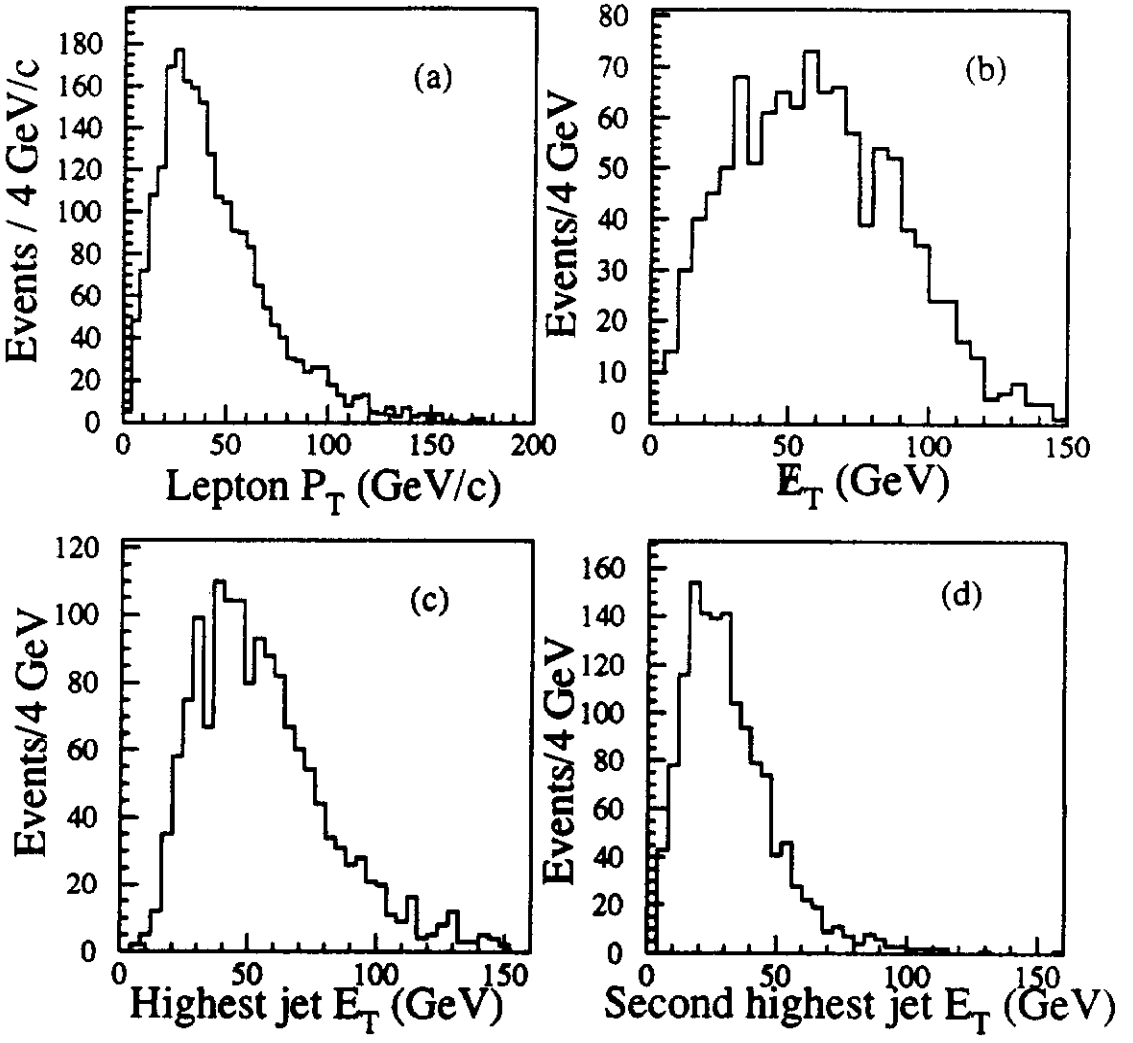

Figure 8. Monte Carlo distributions for M_{top}=160 GeV/c^2. a) Lepton P_T spectrum from $t \rightarrow W \rightarrow \ell$. b) $\not\!\!E_T$ for events with two leptons with $P_T > 20$ GeV/c. c) Leading-jet E_T for dilepton events. d) Next-to-leading jet E_T for dilepton events.

Cut	$e\mu$	ee	$\mu\mu$
P_T	8	702	588
Opposite-Charge	6	695	583
Isolation	5	685	571
Invariant Mass	5	58	62
$\not\!\!E_T$ magnitude	2	0	1
$\not\!\!E_T$ direction	2	0	0
Two-jet	2	0	0

Number of data events surviving consecutive requirements.

Fig. 9

		Without $\not\!\!E_T$ and two-jet cuts	Without two-jet cut	All cuts
$e\mu$	WW	1.1	0.74	0.10±0.04
	$Z \to \tau\tau$	3.7	0.22	0.07±0.02
	$b\bar{b}$	1.2	0.10	0.04±0.03
	Fake	1.2	0.19	0.03±0.03
	Total background	7.2	1.25	0.24±0.06
	CDF data	5	2	2
$ee, \mu\mu$	WW	0.6	0.43	0.06±0.02
	$Z \to \tau\tau$	3.0*	0.20	0.06±0.02
	$b\bar{b}$	1.6	0.12	0.05±0.03
	Fake	1.7	0.25	0.04±0.03
	Drell-Yan	113	0.28	$0.10^{+0.23}_{-0.08}$
	Total background	120	1.28	$0.31^{+0.24}_{-0.10}$
	CDF data	120	0	0

Number of background events expected in 19.3 pb^{-1} and the number of events observed in the data.

Fig. 10

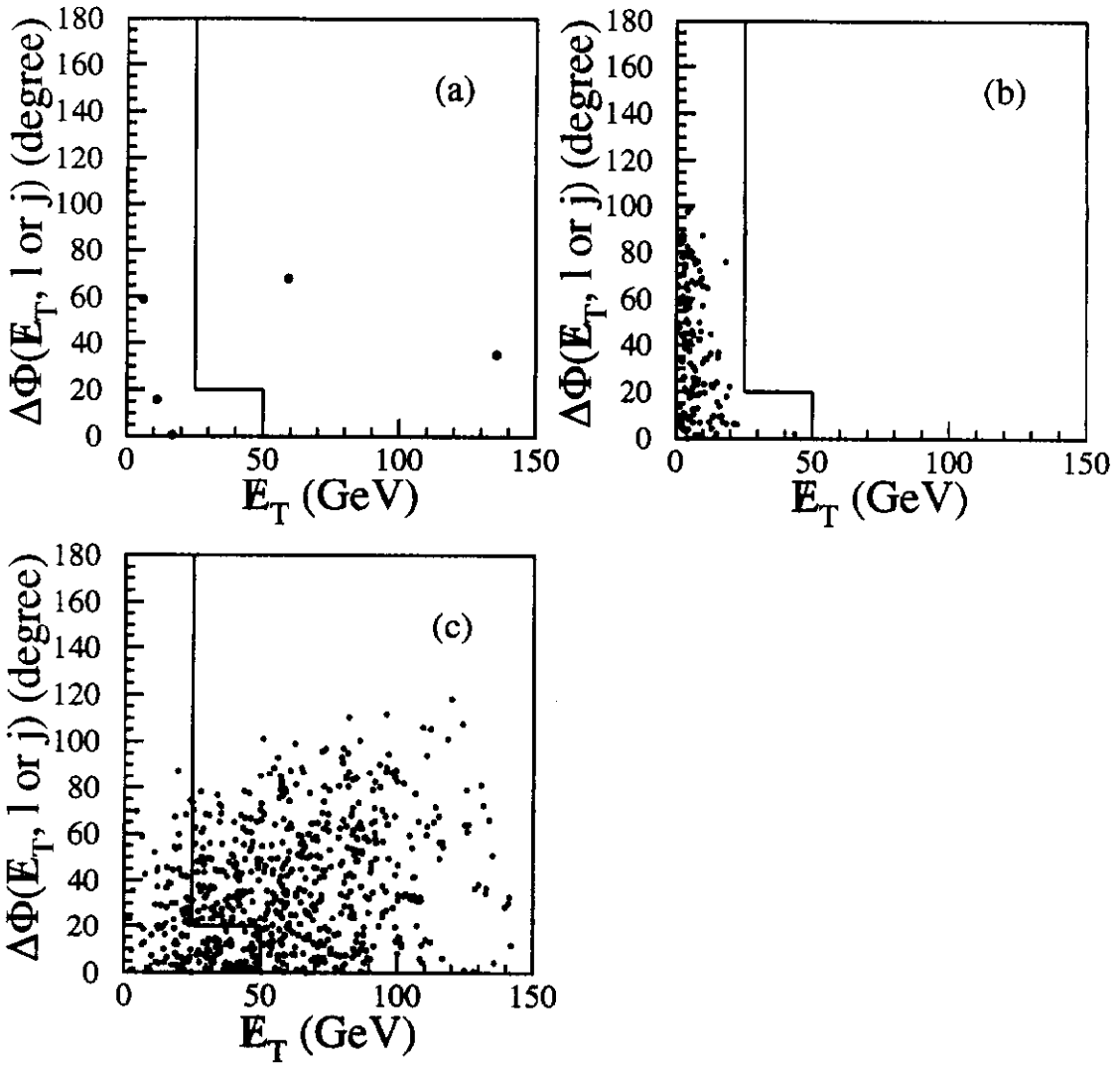

Figure11 Distributions of the azimuthal angle between $\not\!\!E_T$ and the closest lepton or jet versus $\not\!\!E_T$. a) $e\mu$ data. b) Dielectron and dimuon data after the invariant mass cut. c) Monte Carlo events for M_{top}=160 GeV/c^2 (unnormalized). Events in the region to the left of the boundary in the figures are rejected by the $\not\!\!E_T$ cuts.

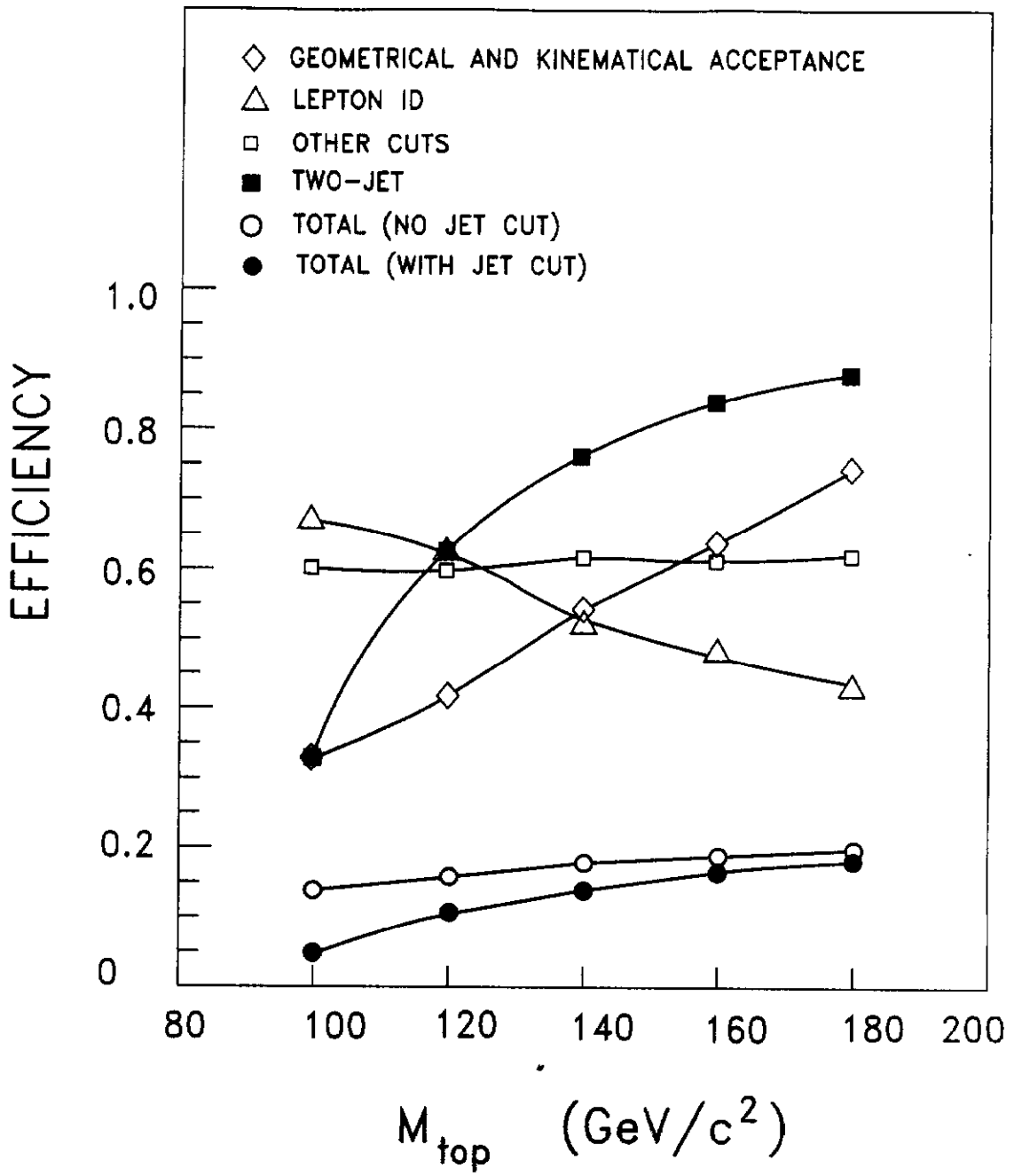

Figure 12. Efficiencies of the dilepton selection as a function of M_{top}. 'Other cuts' corresponds to the combined efficiency for the isolation, topology (opposite-charge, mass, $\not\!\!E_T$) and trigger requirements.

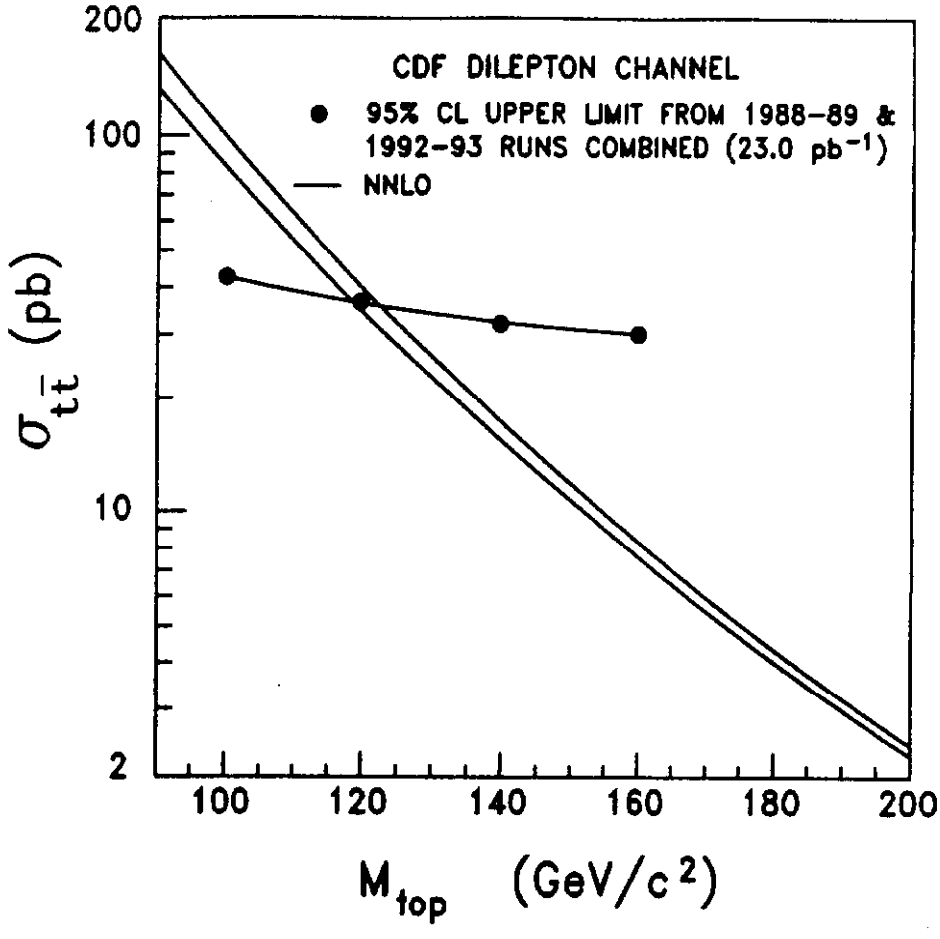

Figure 13: The upper limit at the 95%-C.L. on $\sigma_{t\bar{t}}$, overlaid with the theoretical lower bound and central value of a next to next to leading order (NNLO) calculation from Ref. [10]

T TBAR PRODUCTION AND DECAY

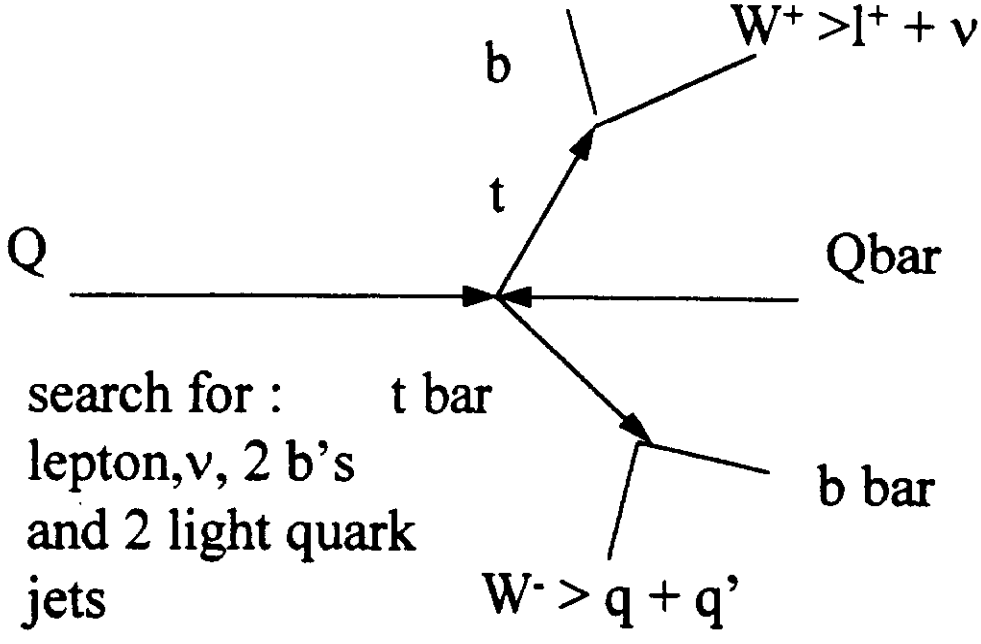

LEPTON PLUS JETS BACKGROUND

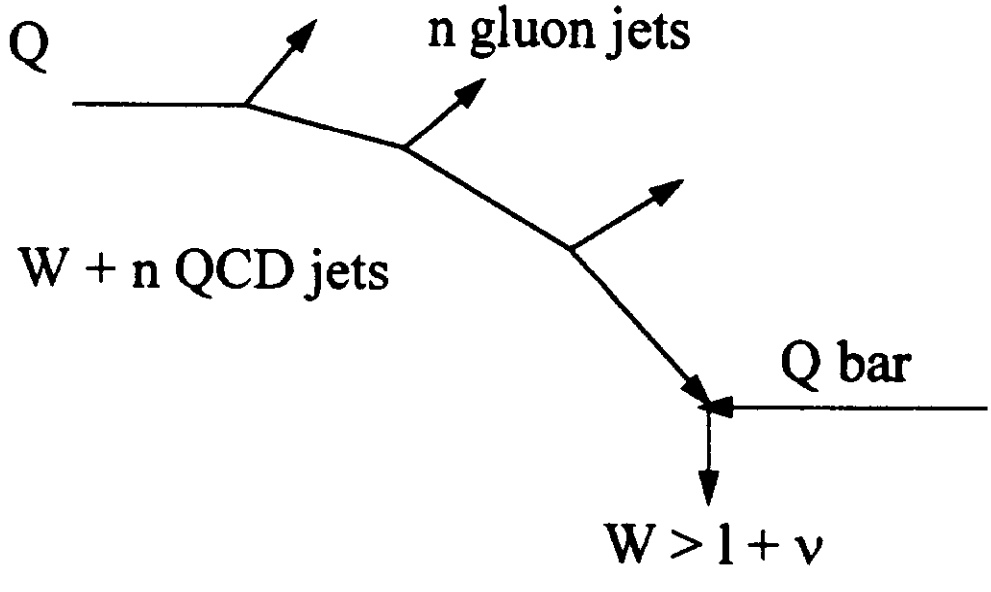

Fig. 14

Selection Criteria	Electrons	Muons
Good Lepton	28,522	17,994
Lepton Isolation Requirement	20,420	11,901
Z Removal	18,700	11,310
$\not\!\!E_T > 20$ GeV	13,657	8,724
Good Quality Run	12,797	8,272
Trigger Requirement	11,949	7,024

Fig.15. The number of events passing various consecutive selection criteria in data. The good lepton requirement includes all quality selection, fiducial requirements, E_T cuts, and conversion removal.

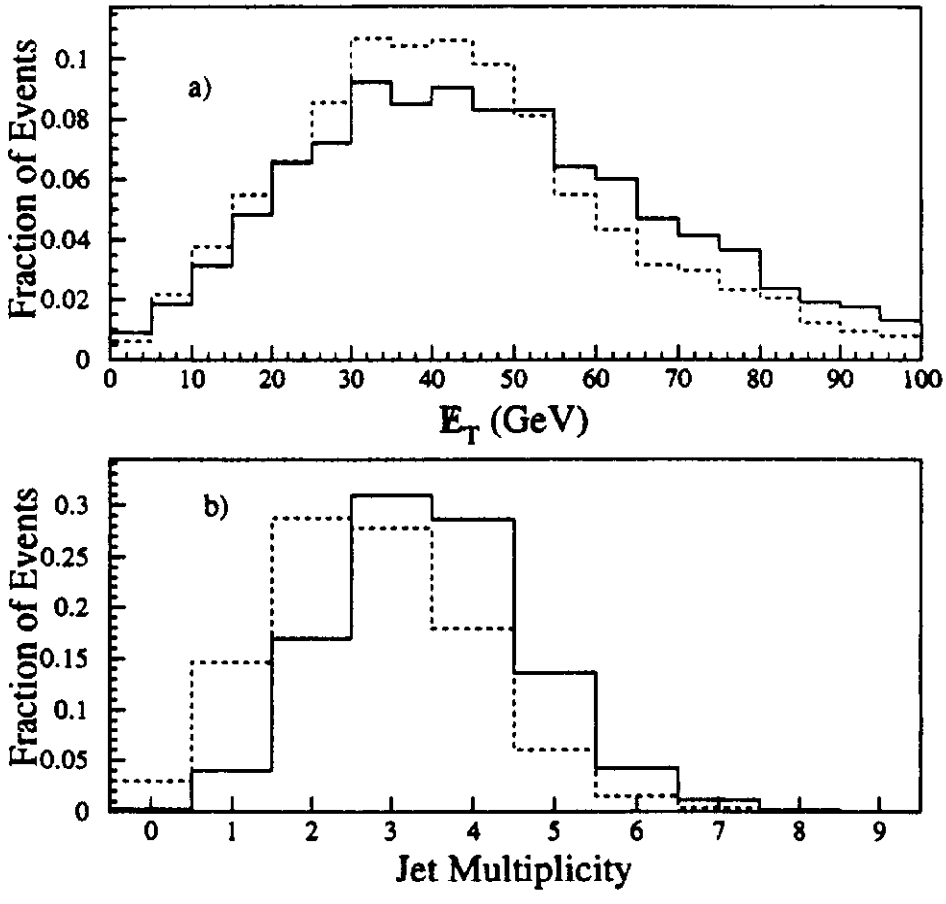

Fig.16.The $t\bar{t}$ Monte Carlo distribution of a) $\not\!\!E_T$ for events with a 20 GeV electron passing electron identification cuts, and b) the expected jet multiplicity distribution for events passing the W selection criteria. In both plots the dashed line is for M_{top} = 120 GeV/c^2 and the solid histogram is for M_{top} =180 GeV/c^2.

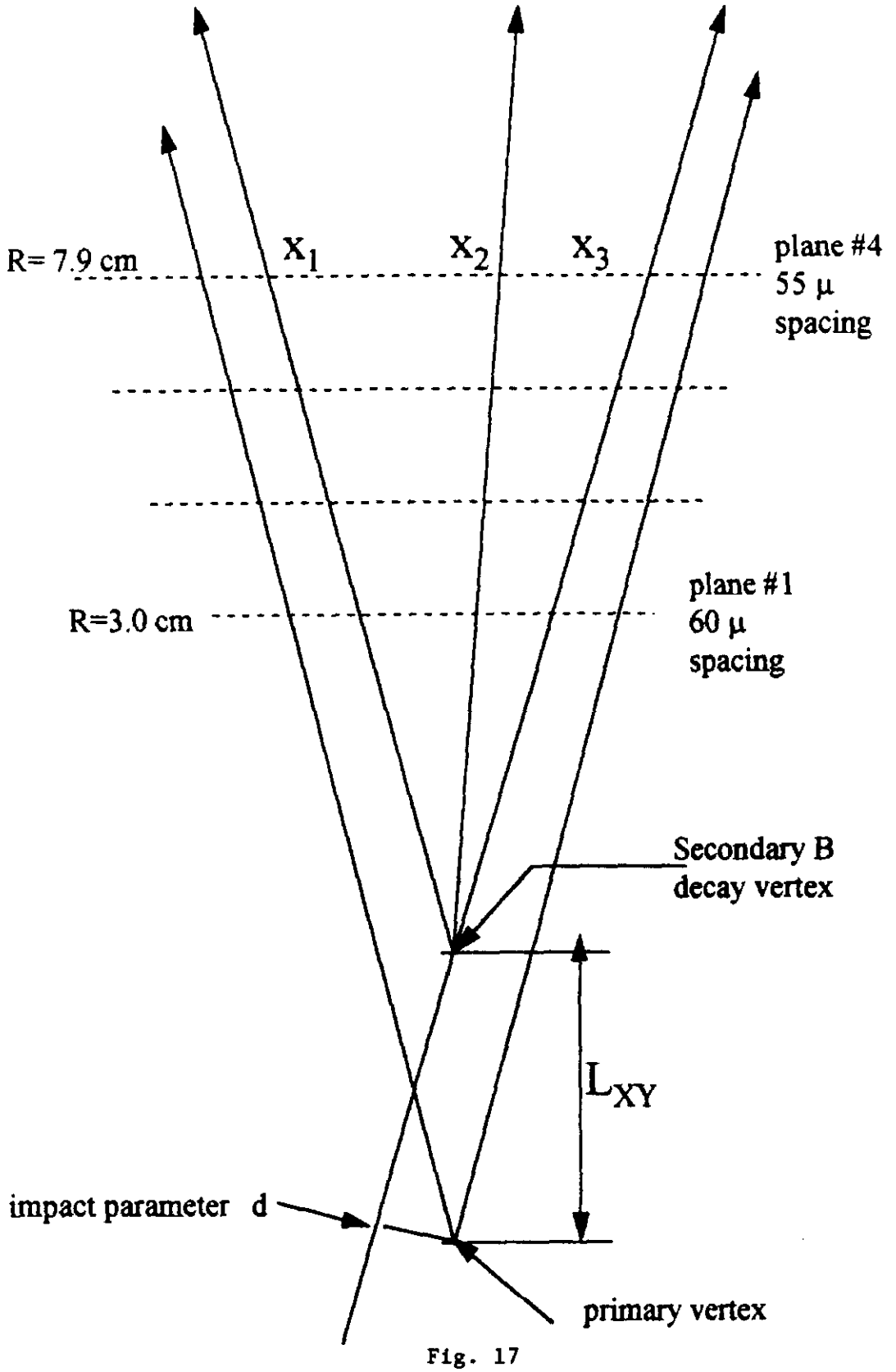
R= 7.9 cm
X_1
X_2
X_3
plane #4
55 μ
spacing
plane #1
60 μ
spacing
R=3.0 cm
Secondary B
decay vertex
L_{XY}
impact parameter d
primary vertex

Fig. 17

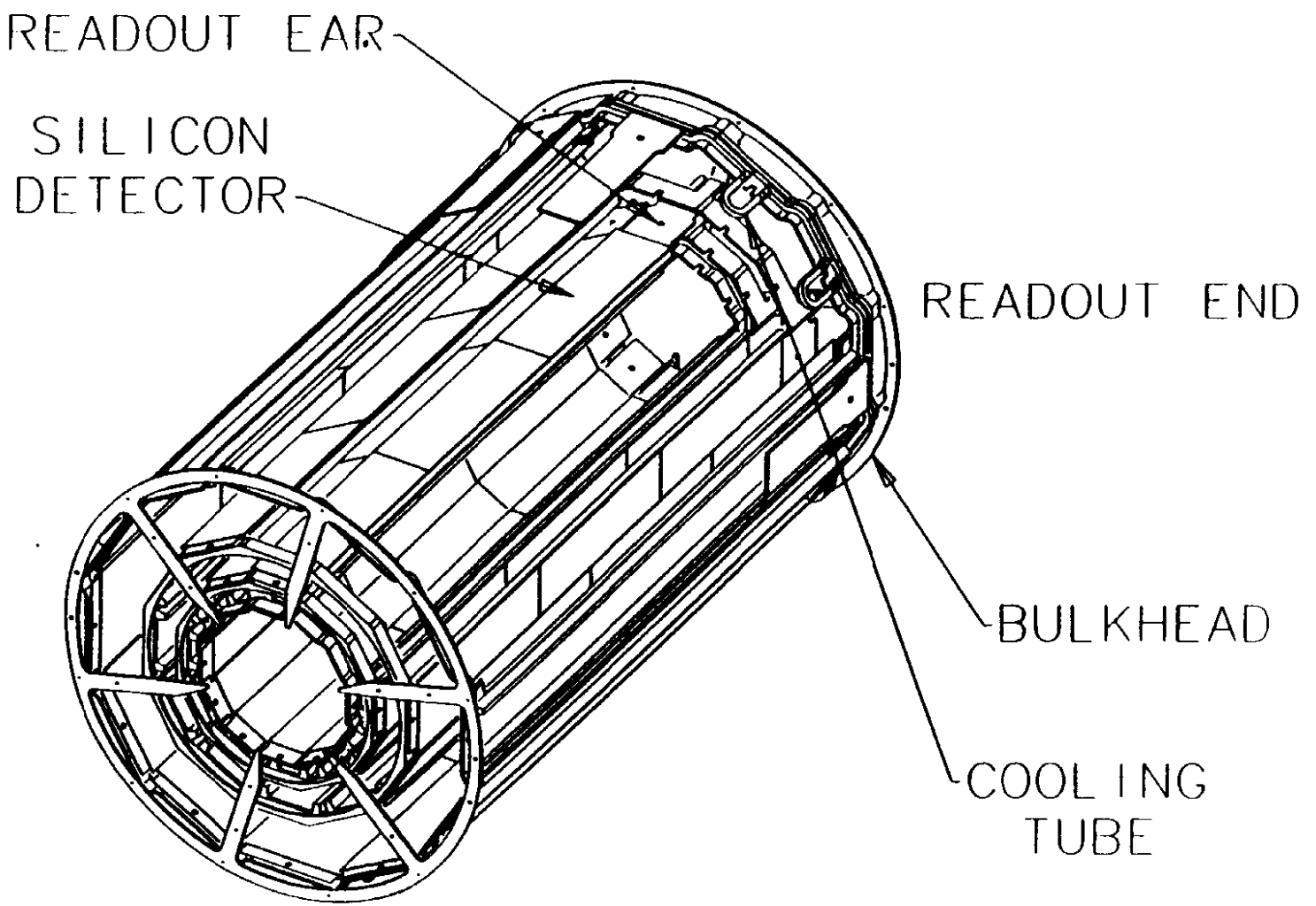
READOUT EAR
SILICON
DETECTOR
READOUT END
BULKHEAD
COOLING
TUBE

Fig. 18

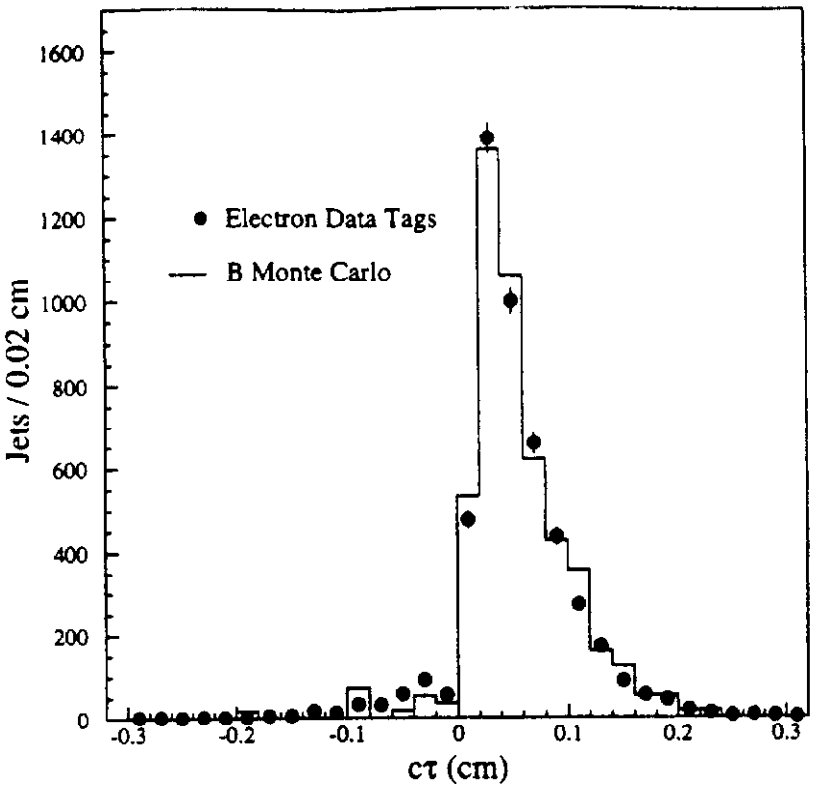

Fig. 19. The $c\tau_{l\beta}$ distribution for jets with a secondary vertex in the inclusive electron data (points with errors) compared to Monte Carlo simulation (histogram) with the world average B lifetime.

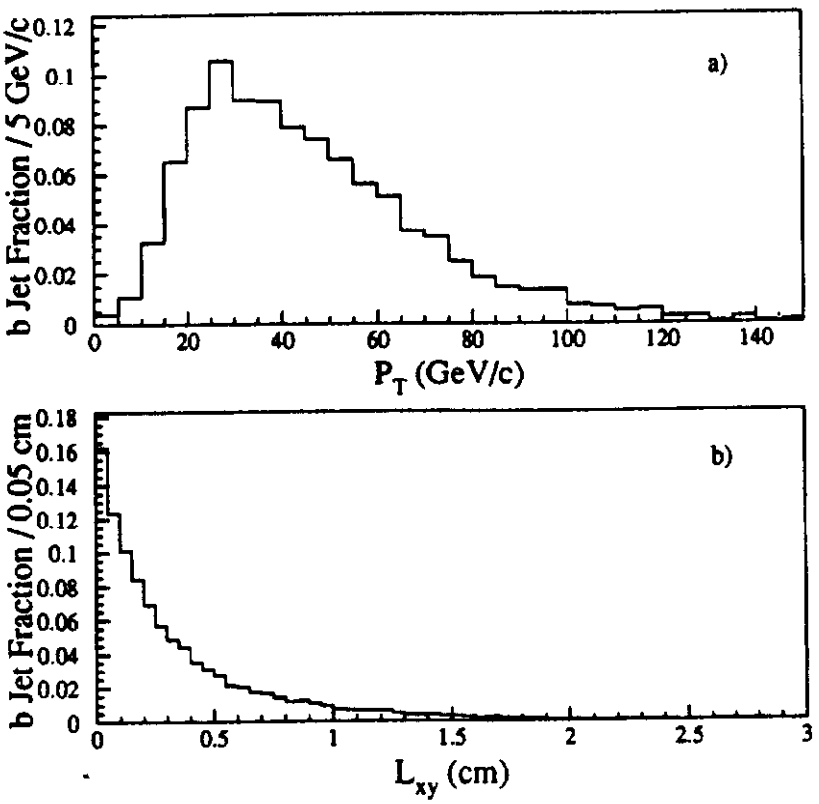

Fig. 20 a) The P_T spectrum for b hadrons from $t\bar{t}$ Monte Carlo events with M_{top} of 160 GeV/c^2. b) The transverse decay length distribution for the b hadrons, before detector resolution effects, in the same sample.

	Source	$W+1$ Jet	$W+2$ Jets	$W+\geq 3$ Jets
(1)	$Wb\bar{b}$, $Wc\bar{c}$ + Mistags, Method 1	12.7 ± 1.7	4.86 ± 0.63	1.99 ± 0.26
(2)	$Wb\bar{b}$, $Wc\bar{c}$ only, Method 2	2.7 ± 2.2	1.05 ± 0.85	0.37 ± 0.31
(3)	Mistags only, Method 2	4.8 ± 2.5	1.85 ± 0.98	0.76 ± 0.43
(4)	$Wb\bar{b}$, $Wc\bar{c}$ + Mistags, Method 2	7.5 ± 3.3	2.90 ± 1.30	1.13 ± 0.53
(5)	Wc	2.4 ± 0.8	0.66 ± 0.27	0.14 ± 0.07
(6)	$Z \rightarrow \tau\bar{\tau}$, WW, WZ	0.20 ± 0.10	0.19 ± 0.09	0.08 ± 0.04
(7)	Non-W, including $b\bar{b}$	0.50 ± 0.30	0.59 ± 0.44	0.09 ± 0.09
(8)	Total Method 1	15.8 ± 2.1	6.3 ± 0.8	2.30 ± 0.29
(9)	Total Method 2	10.6 ± 3.7	4.3 ± 1.4	1.44 ± 0.54
(10)	Events Before Tagging	1713	281	52
(11)	Observed Tagged Events	8	8	6

Summary of Background and Observed Tags

Fig. 21

M_{top} GeV/c^2	ϵ_{tag}	Expected # of Events
120	0.20 ± 0.05	7.7 ± 2.5
140	0.22 ± 0.06	4.8 ± 1.7
160	0.22 ± 0.06	2.7 ± 0.9
180	0.22 ± 0.06	1.4 ± 0.4

Fig. 22. Summary of SVX tagging efficiency (defined as the efficiency of tagging at least one jet in a $t\bar{t}$ event with three or more jets) and the expected number of SVX b-tagged $t\bar{t}$ events in the data sample.

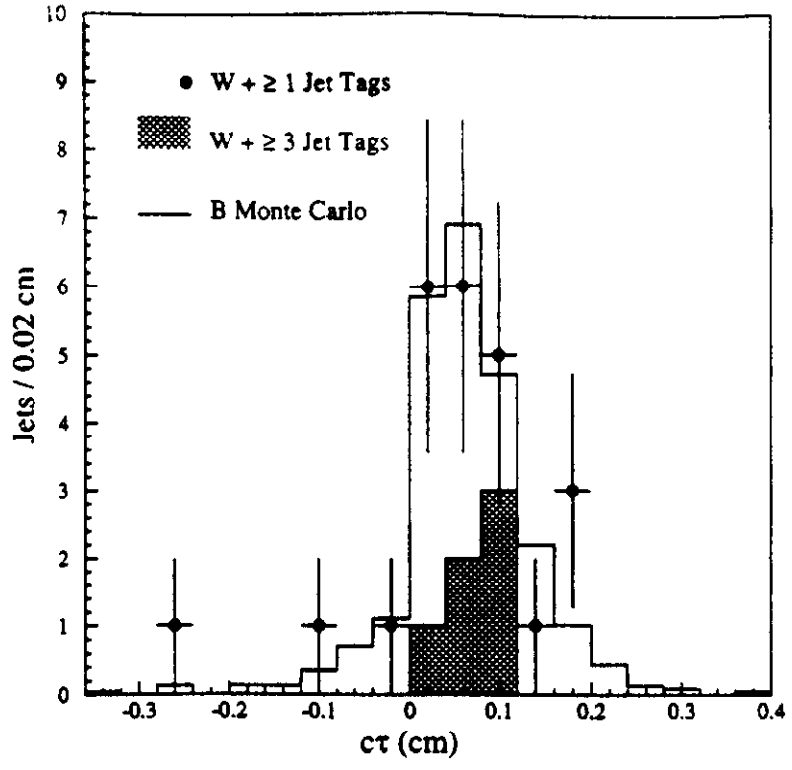

Fig.23 The $c\tau_{eff}$ distribution for jets with a secondary vertex in the W+*jets* data (points with errors) compared to b quark jets from Monte Carlo $t\bar{t}$ events (histogram normalized to data). The shaded histogram is the $W + \geq 3$ jets tags in the data. A W+2 jet event with a $c\tau_{eff}$ = 1.2 cm and a W+1 jet event with a $c\tau_{eff}$ = −0.41 cm are not shown.

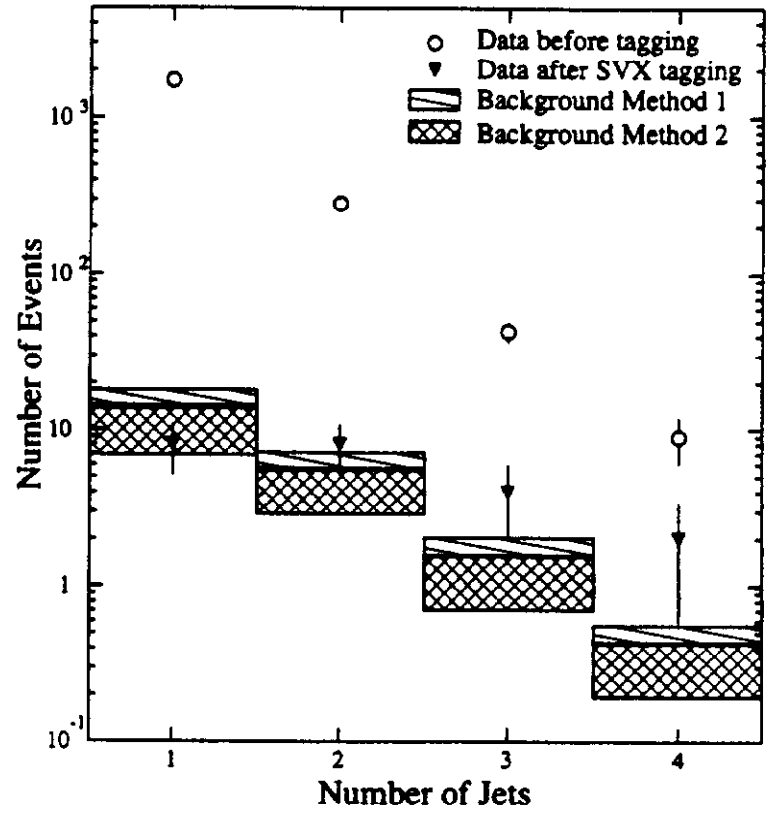

Fig.24 The W+jets distribution observed in the data. The open circles are before SVX tagging and the solid triangles are after SVX tagging. The cross-hatched boxes are the two after tagging background estimates. See text for description.

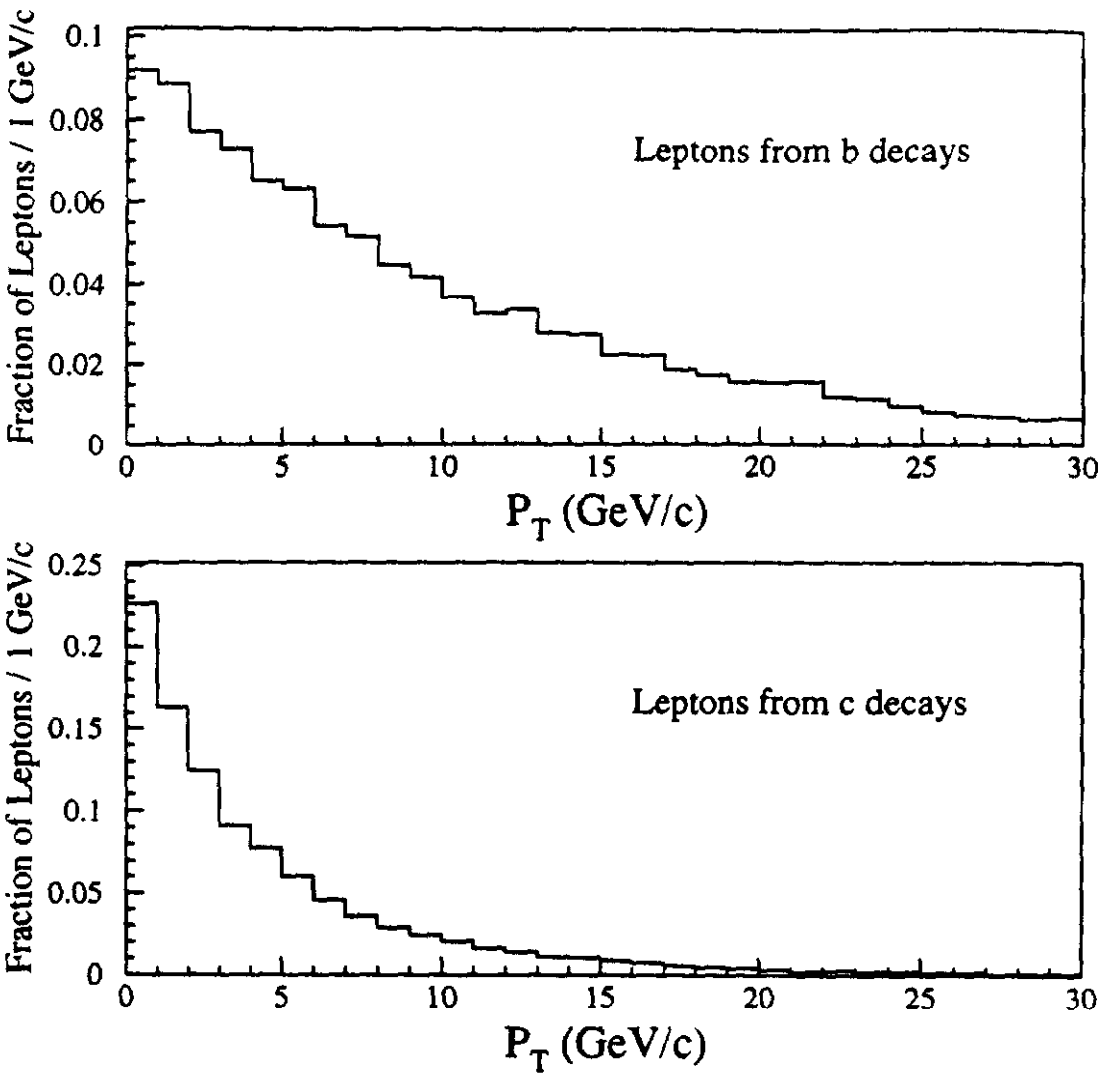

Fig. 25. P_T spectra of leptons from the decay of *b* and *c* quarks in top Monte Carlo events (M_{top}=160 GeV/c^2).

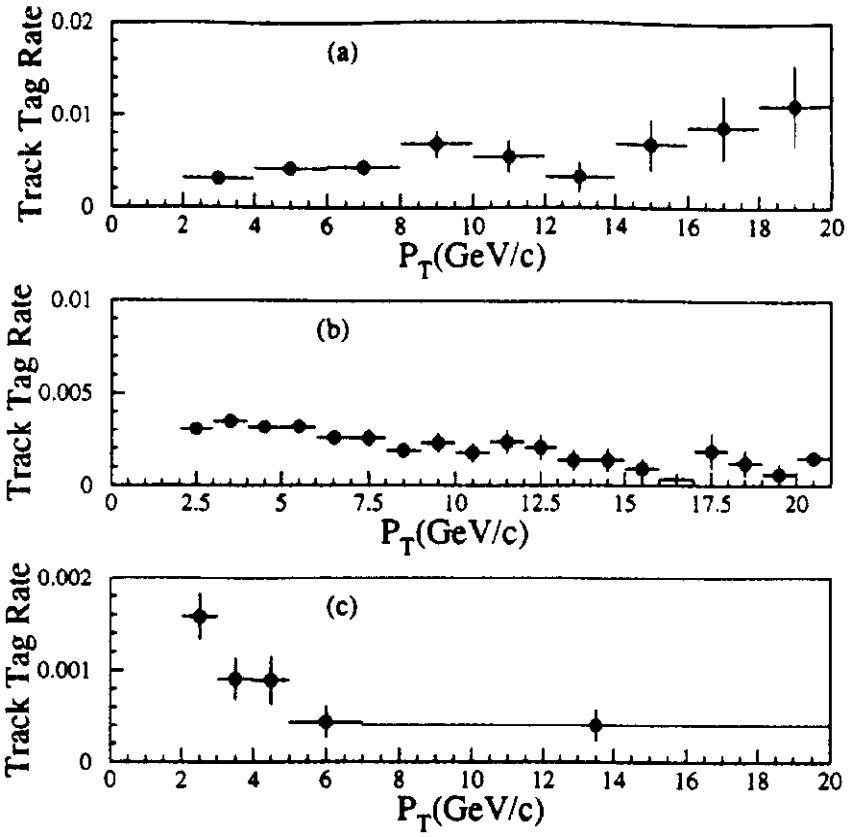

Fig. 26 Track-tag rates for the electron search for tracks satisfying (a) $\frac{\sum p}{p} < 0.2$, where $\sum p$ is the scalar sum of the momenta of all other tracks within a cone of 0.2, and p is the momentum of the track. (b) $0.2 < \frac{\sum p}{p} < 5$. (c) $\frac{\sum p}{p} > 5$.

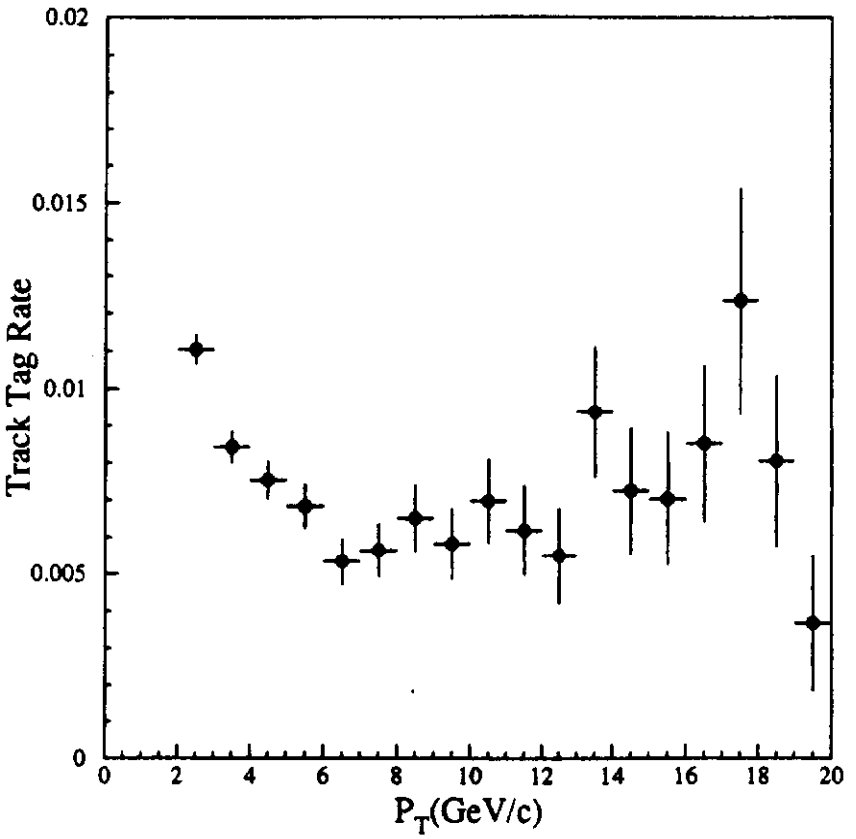

Fig. 27 Track-tag rate for muons in generic jets.

Sample	Number of Electrons		Number of Muons	
	Predicted	Observed	Predicted	Observed
100 GeV jet trigger	598	531	487	471
70 GeV jet trigger	621	631	511	546
50 GeV jet trigger	502	531	374	375
20 GeV jet trigger	757	785	556	557
16 GeV photon sample	30	37	129	128
Six jet sample	65	60	143	144
$\sum E_T$	259	203	762	682
Minimum Bias	25	21	50	47
Z + jets	1.4	2	2.7	4

Fig. 28. A comparison of the observed number of lepton candidates in different samples with the prediction from the track-tag rate parametrizations. The track-tag rate parametrizations were obtained from a mixture of the 20, 50, 70, and 100 GeV inclusive-jet triggers. A trigger bias is present in the muon yields for the inclusive-jet triggers because the energies of jets containing hadrons that do not interact in the calorimeter are measured systematically low. For this reason, only tracks well separated from a trigger-jet are considered in the muon analysis. The statistical uncertainties on the predictions are negligible.

Source		W + 1 Jet	W + 2 Jets	W + $\geq$ 3 Jets
Fakes+$Wb\bar{b}$+$Wc\bar{c}$	e tags	9.9 ± 1.5	2.9 ± 0.4	0.88 ± 0.13
	μ tags	19.2 ± 1.9	5.9 ± 0.6	1.82 ± 0.18
	e + μ tags	$\mathbf{29.1 \pm 2.9}$	$\mathbf{8.8 \pm 0.9}$	$\mathbf{2.70 \pm 0.27}$
$b\bar{b}$	e tags	0.8 ± 0.6	0.14 ± 0.10	0.03 ± 0.02
	μ tags	0.9 ± 0.6	0.14 ± 0.10	0.03 ± 0.02
	e + μ tags	$\mathbf{1.7 \pm 1.2}$	$\mathbf{0.28 \pm 0.20}$	$\mathbf{0.05 \pm 0.03}$
Diboson	e tags	0.25 ± 0.12	0.11 ± 0.06	0.03 ± 0.02
	μ tags	0.28 ± 0.13	0.03 ± 0.02	0.01 ± 0.01
	e + μ tags	$\mathbf{0.53 \pm 0.25}$	$\mathbf{0.14 \pm 0.08}$	$\mathbf{0.04 \pm 0.03}$
$Z \rightarrow \tau\tau$	e tags	0.37 ± 0.13	0.11 ± 0.05	0.08 ± 0.03
	μ tags	0.30 ± 0.11	0.07 ± 0.04	0.06 ± 0.03
	e + μ tags	$\mathbf{0.67 \pm 0.24}$	$\mathbf{0.18 \pm 0.09}$	$\mathbf{0.14 \pm 0.06}$
Drell-Yan	e tags	0.15 ± 0.10	0.03 ± 0.03	0.03 ± 0.03
	μ tags	0.15 ± 0.10	0.03 ± 0.03	0.03 ± 0.03
	e + μ tags	$\mathbf{0.30 \pm 0.20}$	$\mathbf{0.05 \pm 0.05}$	$\mathbf{0.05 \pm 0.05}$
$W + c$	e tags	0.4 ± 0.1	0.10 ± 0.03	0.02 ± 0.01
	μ tags	1.4 ± 0.5	0.32 ± 0.08	0.06 ± 0.02
	e + μ tags	$\mathbf{1.8 \pm 0.6}$	$\mathbf{0.42 \pm 0.11}$	$\mathbf{0.08 \pm 0.03}$
Total	e tags	11.9 ± 1.6	3.4 ± 0.4	1.1 ± 0.2
	μ tags	22.2 ± 2.1	6.5 ± 0.6	2.0 ± 0.2
	e + μ tags	$\mathbf{34.1 \pm 3.3}$	$\mathbf{9.9 \pm 1.0}$	$\mathbf{3.1 \pm 0.3}$
Events Before Tagging		1713	281	52
Events After Tagging	e tags	17	2	4
	μ tags	16	10	3
	e + μ tags	**33**	**12**	**7**

Fig. 29. Summary of SLT backgrounds as a function of jet multiplicity.

Channel:	SVX	SLT	Dilepton
Expected # events M_{top} = 120 GeV/c^2	7.7 ± 2.5	6.3 ± 1.3	3.7 ± 0.6
Expected # events M_{top} = 140 GeV/c^2	4.8 ± 1.7	3.5 ± 0.7	2.2 ± 0.2
Expected # events M_{top} = 160 GeV/c^2	2.7 ± 0.9	1.9 ± 0.3	1.3 ± 0.1
Expected # events M_{top} = 180 GeV/c^2	1.4 ± 0.4	1.1 ± 0.2	0.68 ± 0.06
Expected Bkg.	2.3 ± 0.3	3.1 ± 0.3	$0.56^{+0.25}_{-0.13}$
Observed Events	6	7	2

Fig. 30 Numbers of $t\bar{t}$ events expected, assuming the theoretical production cross sections shown in Table 32, and the numbers of candidate events observed with expected backgrounds.

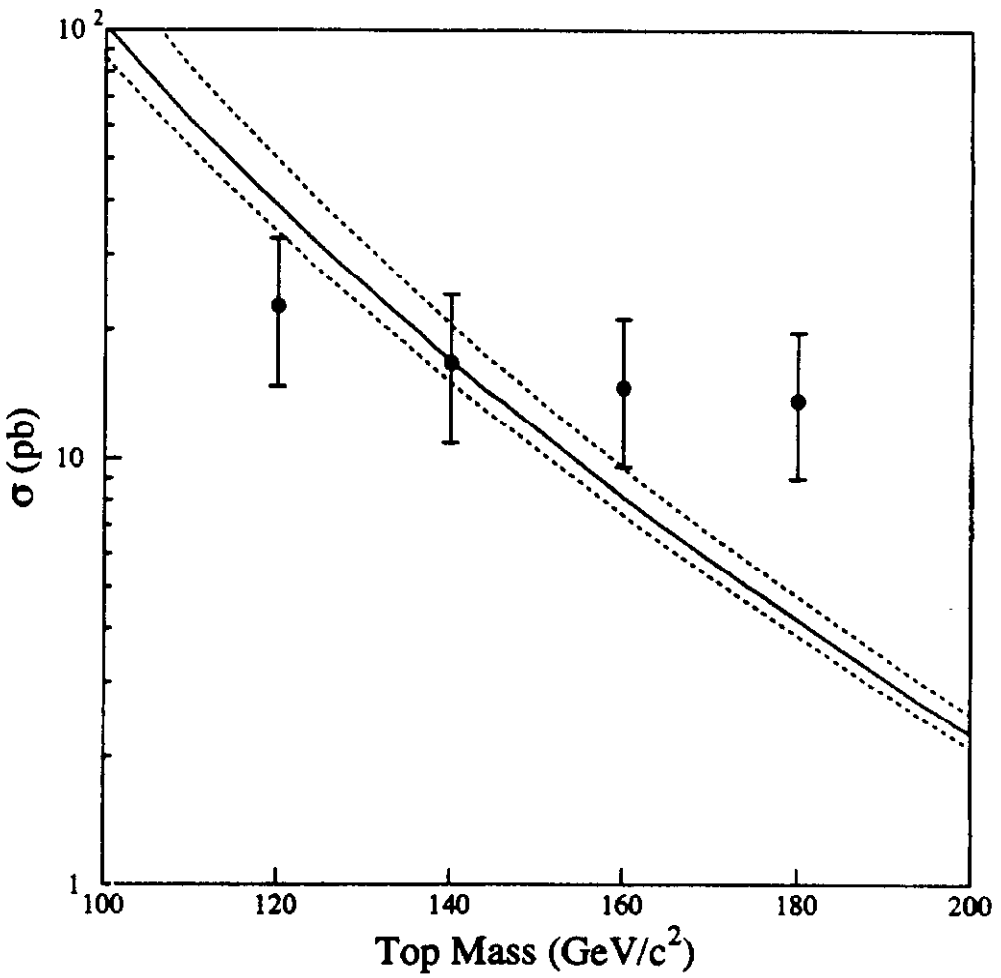

Fig. 31. Combined $t\bar{t}$ production cross section vs. M_{top} from data (points) and theory [10]. The dashed lines are estimates of the theoretical uncertainty quoted in Reference [10].

Jet Multiplicity	Data	Top	Other backgrounds	QCD W + jets
1 Jet	1713	$1.1^{+0.5}_{-0.4}$	284 ± 89	1428 ± 98
2 Jets	281	$5.0^{+2.3}_{-1.7}$	54 ± 15	222 ± 23
3 Jets	43	$10.0^{+4.8}_{-3.1}$	8.9 ± 2.5	$24.1^{+8.0}_{-8.5}$
$\geq$ 3 Jets	52	$21.6^{+9.8}_{-7.6}$	10.8 ± 3.1	$19.6^{+10.9}_{-12.6}$
$\geq$ 4 Jets	9	$11.6^{+5.6}_{-4.5}$	1.9 ± 0.6	$0^{+3.5}_{-0.0}$

Fig. 32. Number of events in the data, number of expected top events, assuming the top cross section measurement from Section 7.1, and number of background events. The number of QCD W+ jets events is obtained by subtracting from the data the top and non-W background contributions. For W+ 4 or more jets, this subtraction yields the unphysical value $-4.5^{+5.4}_{-6.4}$. The value $0^{+3.5}_{-0.0}$ given in the Table is obtained by imposing the constraint that the number of QCD W+ 4 or more jets should be ≥ 0.

Jet Multiplicity	QCD W + jets	VECBOS ($Q^2 = < P_T >^2$)
1 Jet	1428 ± 98	$1571 \pm 82^{+267}_{-204} \pm 55$
2 Jets	222 ± 23	$267 \pm 20^{+77}_{-53} \pm 9$
3 Jets	$24.1^{+8.0}_{-8.5}$	$39 \pm 3^{+11}_{-9} \pm 2$
$\geq$ 4 Jets	$0^{+3.5}_{-0.0}$	$7 \pm 1^{+3}_{-2} \pm 0.2$

Fig. 33. Comparison of QCD W+jet yields from Table 36 with expectations from the VECBOS Monte Carlo. The first uncertainty on the VECBOS prediction is due to Monte Carlo statistics, the second to the jet energy scale and lepton identification efficiency uncertainties, and the third to the uncertainty on the luminosity normalization. The additional uncertainty related to the choice of the Q^2 scale in the VECBOS Monte Carlo program is discussed in the text. The VECBOS predictions include the $W \rightarrow \tau\nu$ contribution.

Jet Multiplicity	W + jets	Z + jets	R_{wz}
1 Jet	1428 ± 98	176	8.1 ± 0.9
2 Jets	222 ± 23	21	10.6 ± 2.6
3 Jets	$24.1^{+8.0}_{-8.5}$	3	$8.0^{+4.3}_{-4.7}$
$\geq$ 3 Jets	$19.6^{+10.9}_{-12.6}$	5	$3.9^{+2.4}_{-2.6}$
$\geq$ 4 Jets	$0^{+3.5}_{-0.0}$	2	$0^{+1.5}_{-0.0}$

Fig. 34. W+ jets and Z+ jets event rates from Tables 36 and 26 as a function of jet multiplicity. R_{wz} is the ratio of the number of W and Z events.

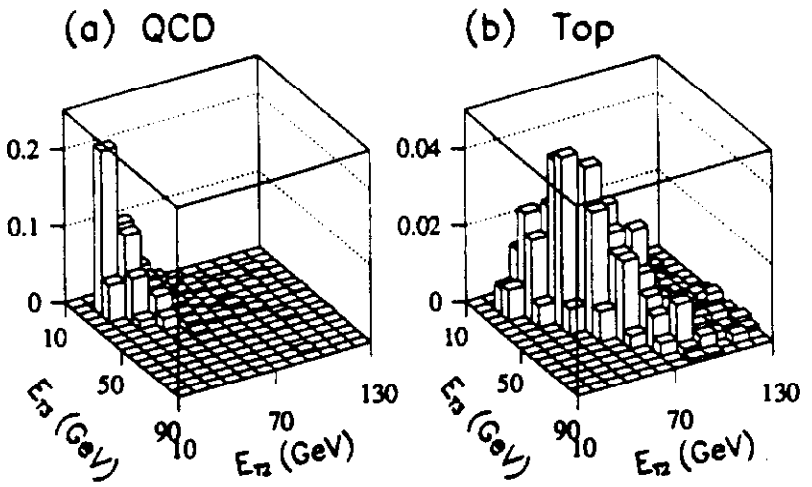

Fig. 35 $d\sigma^2 / dE_{T2}dE_{T3}$ for (a) QCD $W + 3$ jet and (b) top (M_{top} = 170 GeV/c^2) Monte Carlo events. The vertical scale is in arbitrary units.

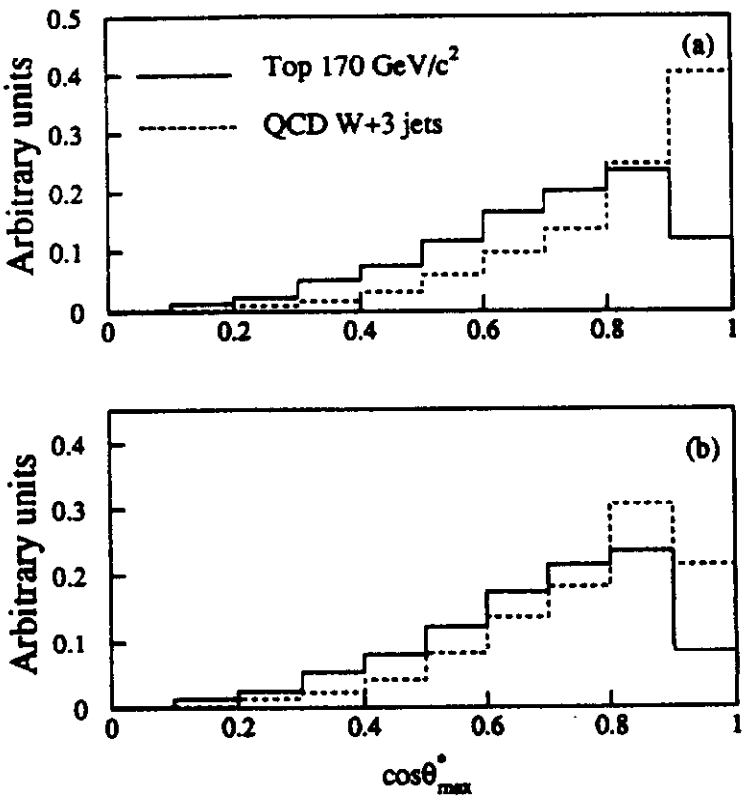

Fig. 36 $Cos\theta^*_{max}$ for HERWIG top (M_{top}=170 GeV/c^2) and VECBOS $W + 3$ jet events. (a) inclusive distribution, (b) after applying a cut on $|\eta(\text{jets})| < 2$. The distributions are normalised to unit area.

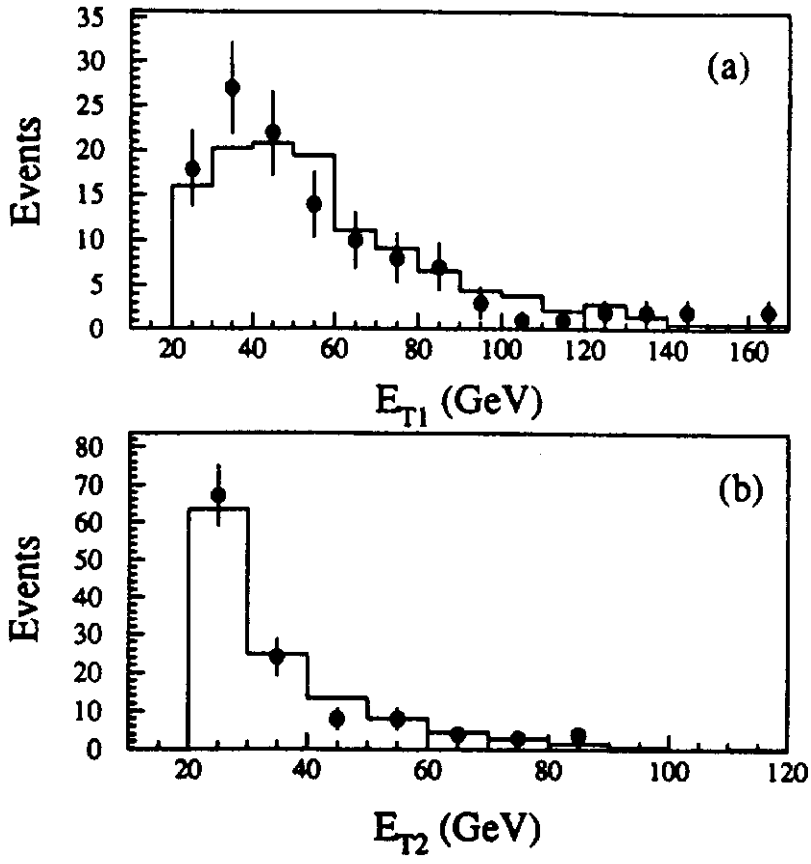

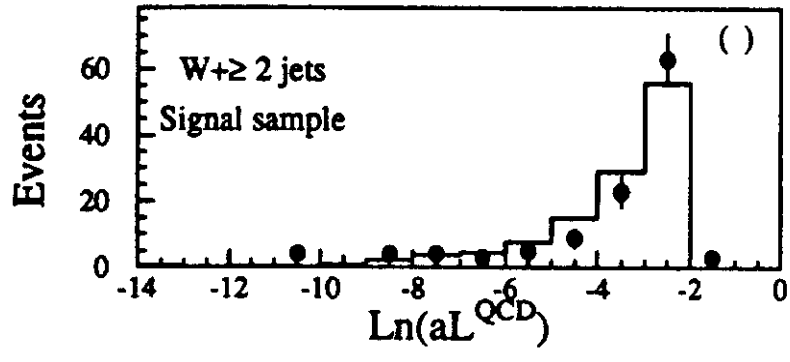

Figure 37: E_T distributions for W + 23 or more jets data (points) and the VECBOS predictions for W + 2 jets (histogram). (a) leading jet, (b) second jet. (c) shows the Ln (aL^{QCD}) for Signal sample.

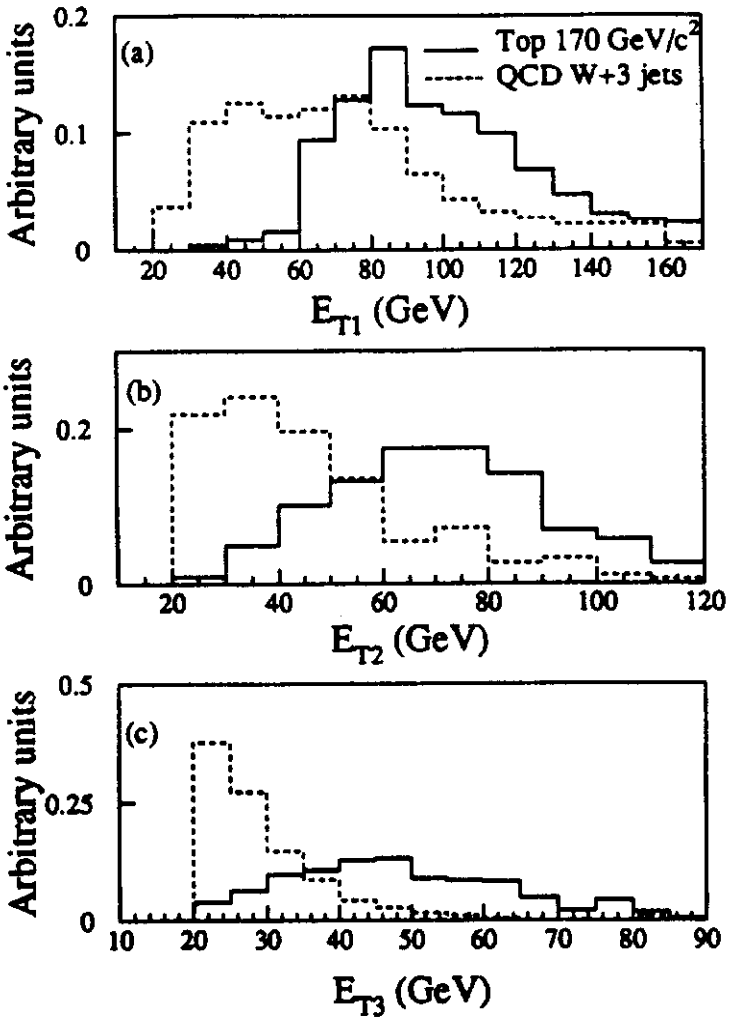

Fig. 38 **Jet energy distributions for HERWIG top (solid line) and VECBOS W + 3 jet events (dashed line) passing the signal sample selection cuts. Each distribution is normalised to unit area.**

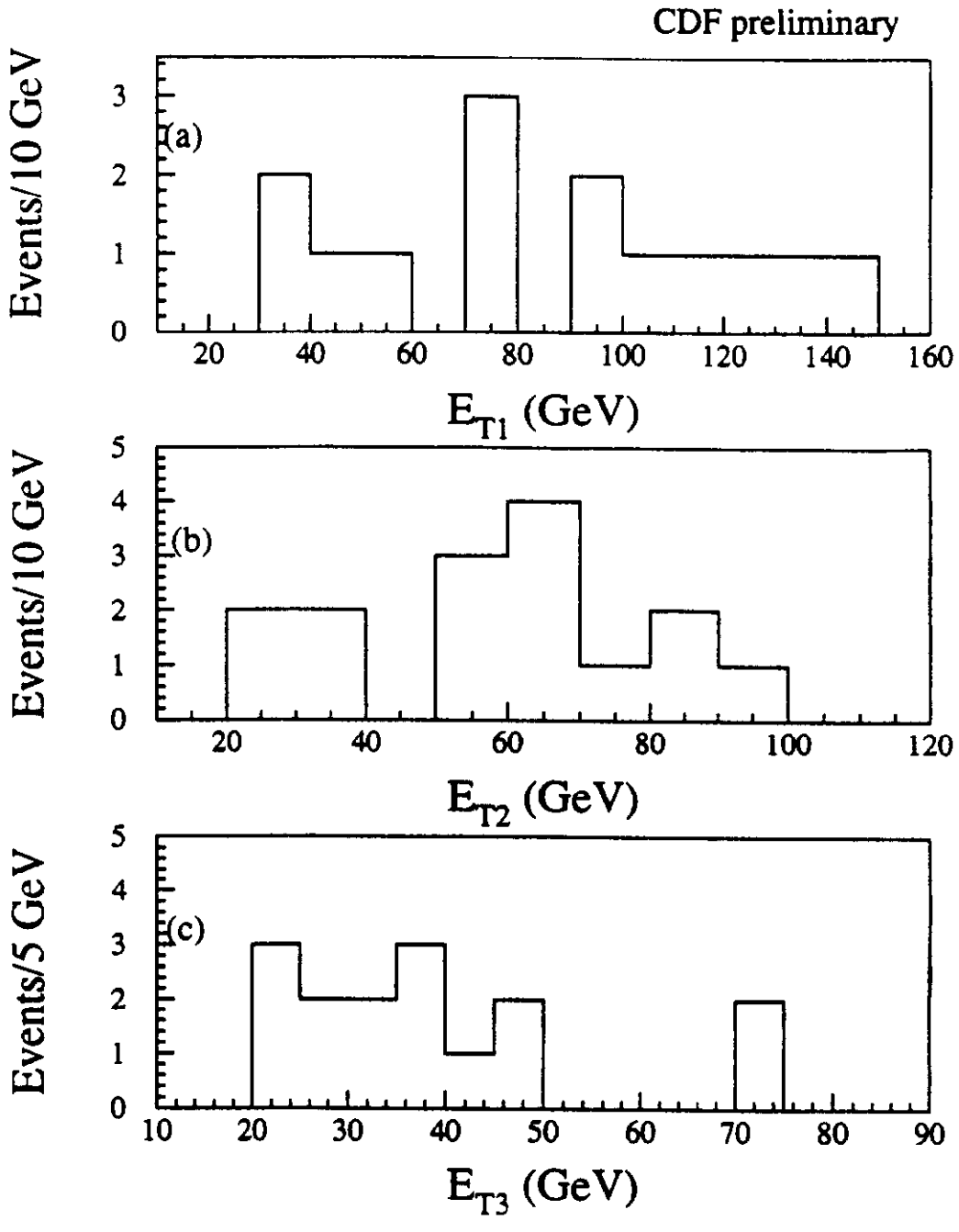

Fig. 39 **Jet energy distributions for the three leading jets in the 14 events passing the signal sample selection cuts. There is one overflow in E_{T1} at E_{T1} = 224 GeV.**

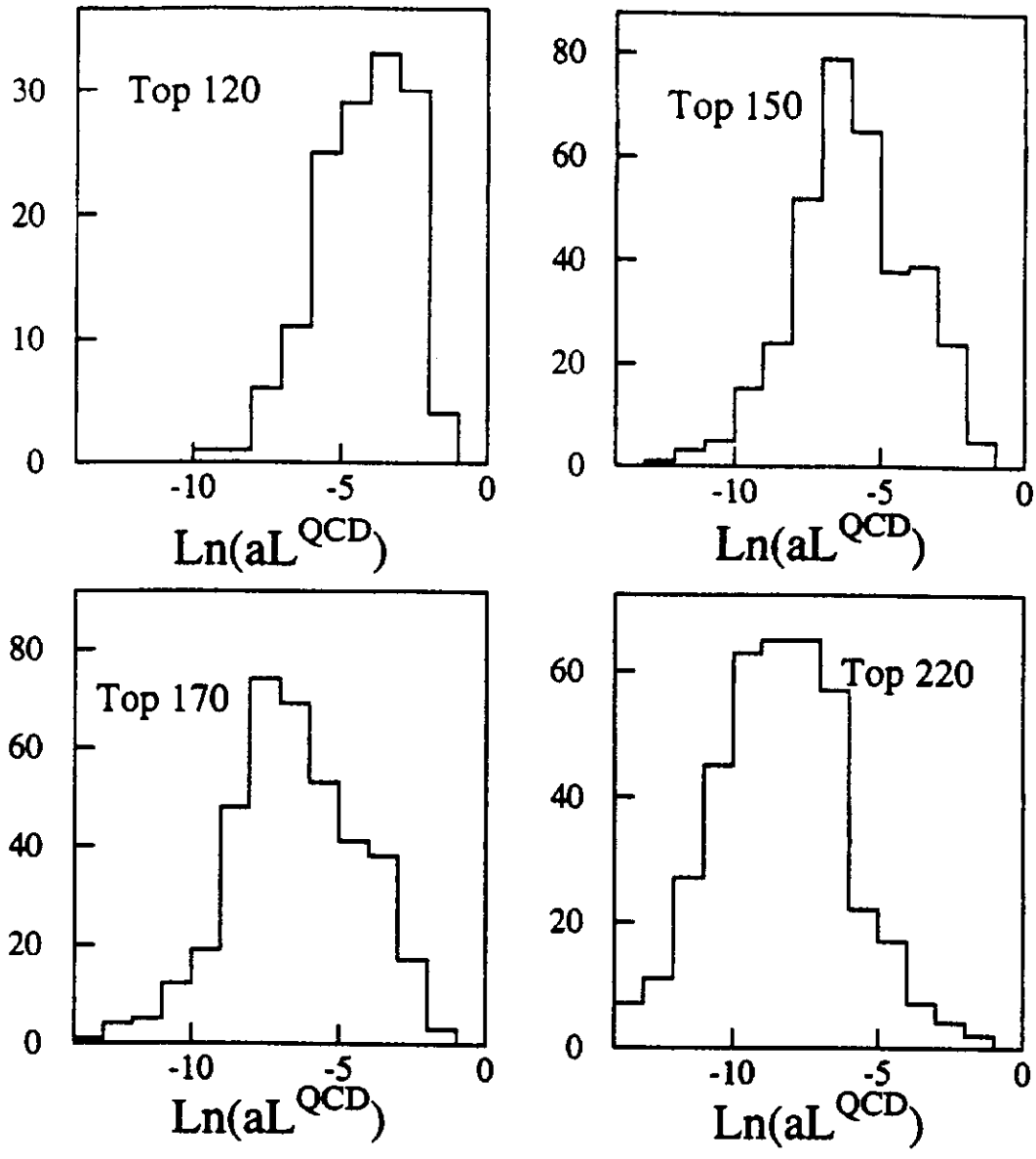

Figure 40: This figure shows the expected distributions of aL^{QCD} for different sets of Monte Carlo t tbar events where the top mass is varied from 130 GeV to 220 GeV.

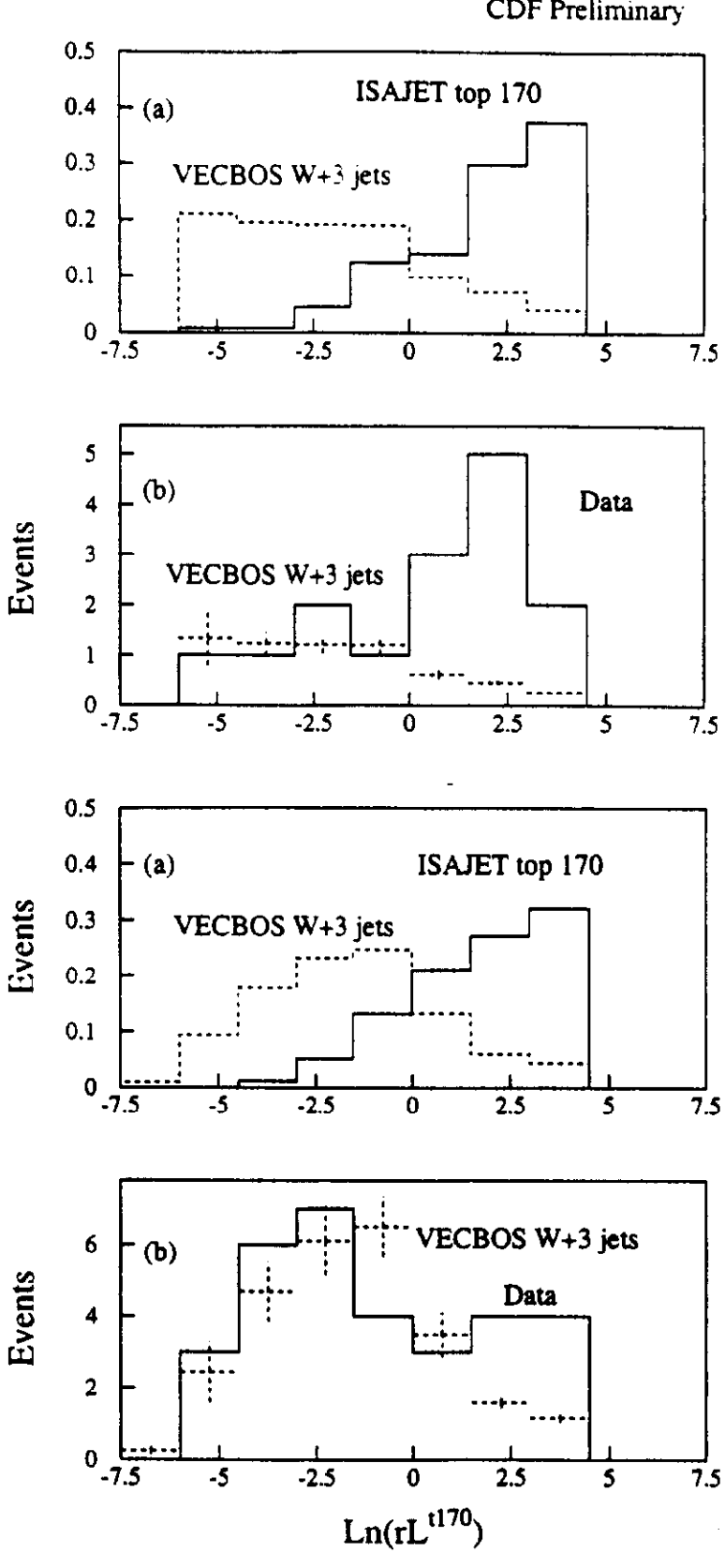

Figure 41: Ln(rL^{t170}) for QCD VECBOS, top Isajet and data events for W plus 3 or more jets. (a) and (c) have had their histograms normalized to 1.0. (a) and (b) are for events in the signal and (c) and (d) are for events in the control region. For (b) and (d) VECBOS MC has been normalised to the data for ln(rL) < 0.

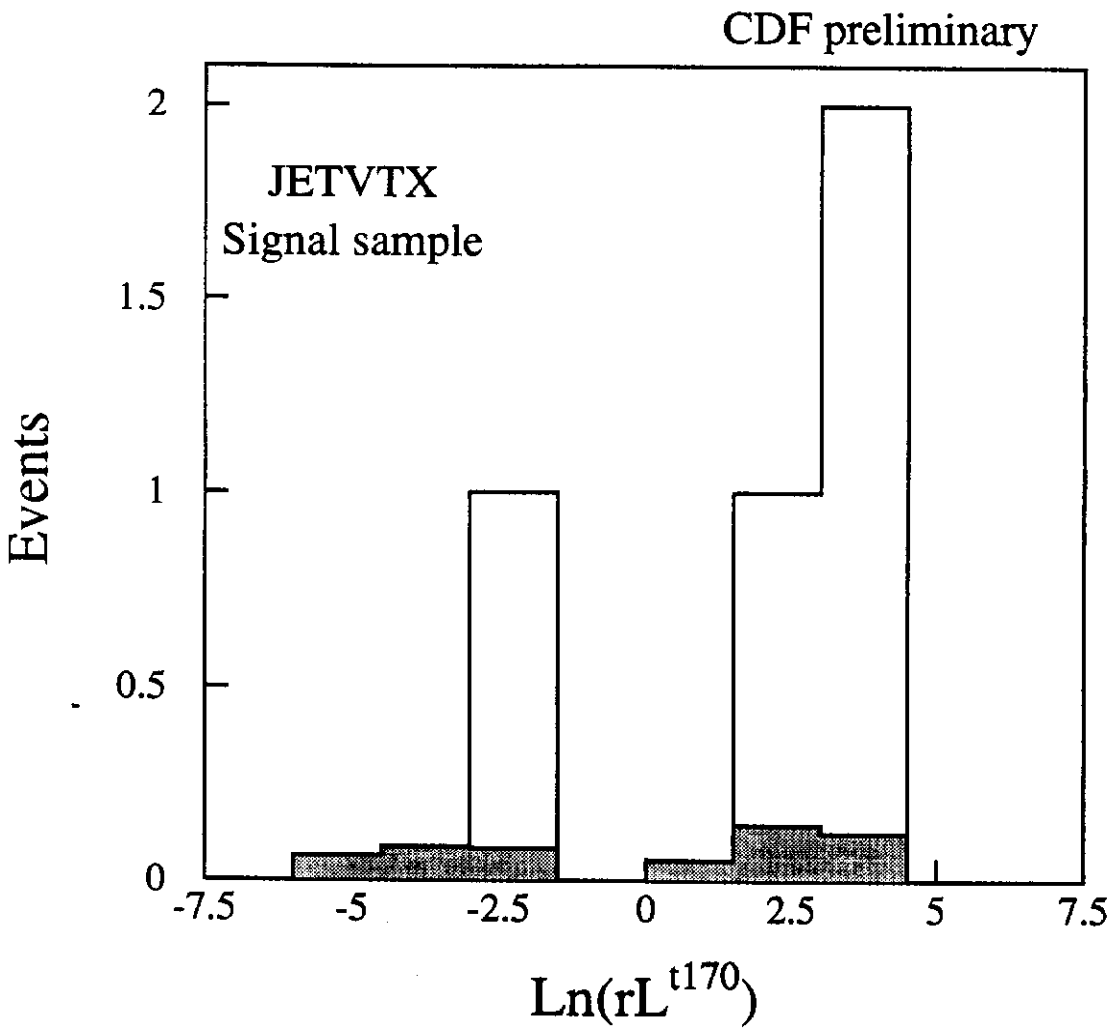

Figure 42: Distribution in ln(rL) of the 4 events of the signal sample tagged by the JETVTX algorithm. The expected fakes are shown as a shaded histogram.

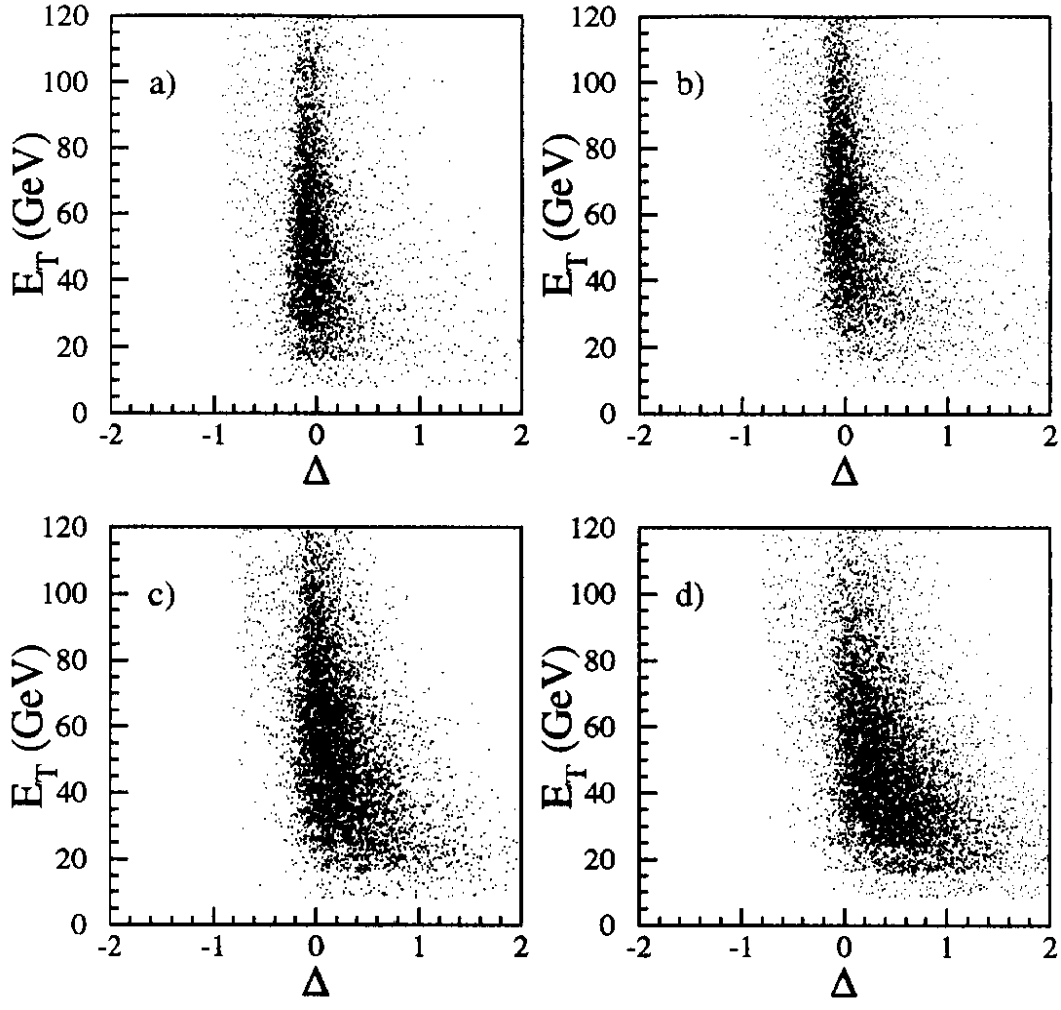

Fig. 43. Scatter plots of jet E_T corrected with standard jet corrections vs. Δ for the four jet types: a) light quarks b) generic b jets c) $b \rightarrow e\nu$ X jets d) $b \rightarrow \mu\nu$X . $\Delta = (P_T(\text{parton}) - E_T(\text{jet}))/E_T(\text{jet})$. The Monte Carlo events have been generated with HERWIG at $M_{top} = 170$ GeV/c^2.

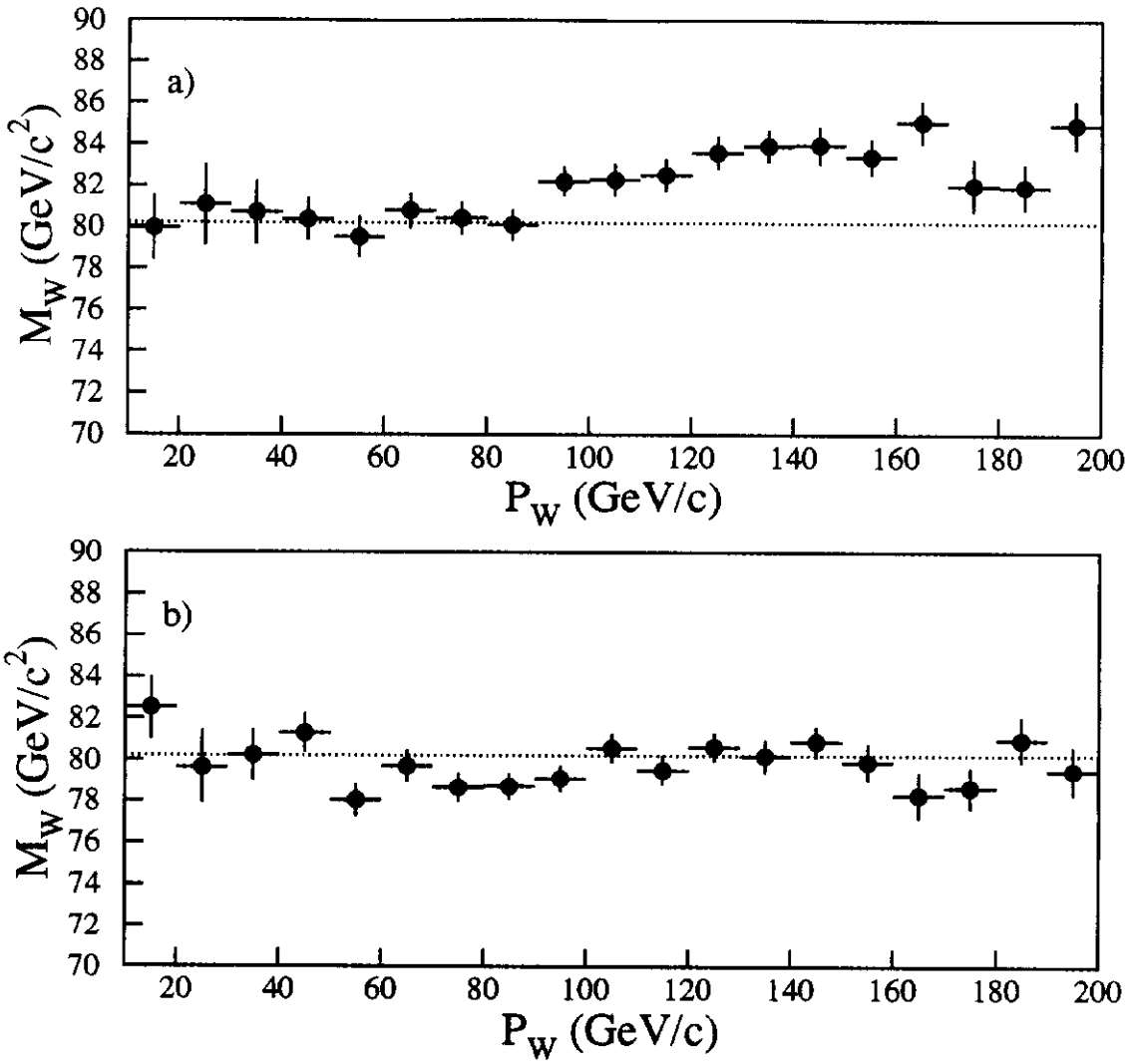

Fig. 44. Mass of the W calculated using the 4-momenta of the jets as a function of the W momentum. The jet momenta are corrected with standard jet corrections (top plot) and with the jet corrections used in the mass analysis (bottom plot). The events plotted are generated with HERWIG at $M_{top} = 170$ GeV/c^2.

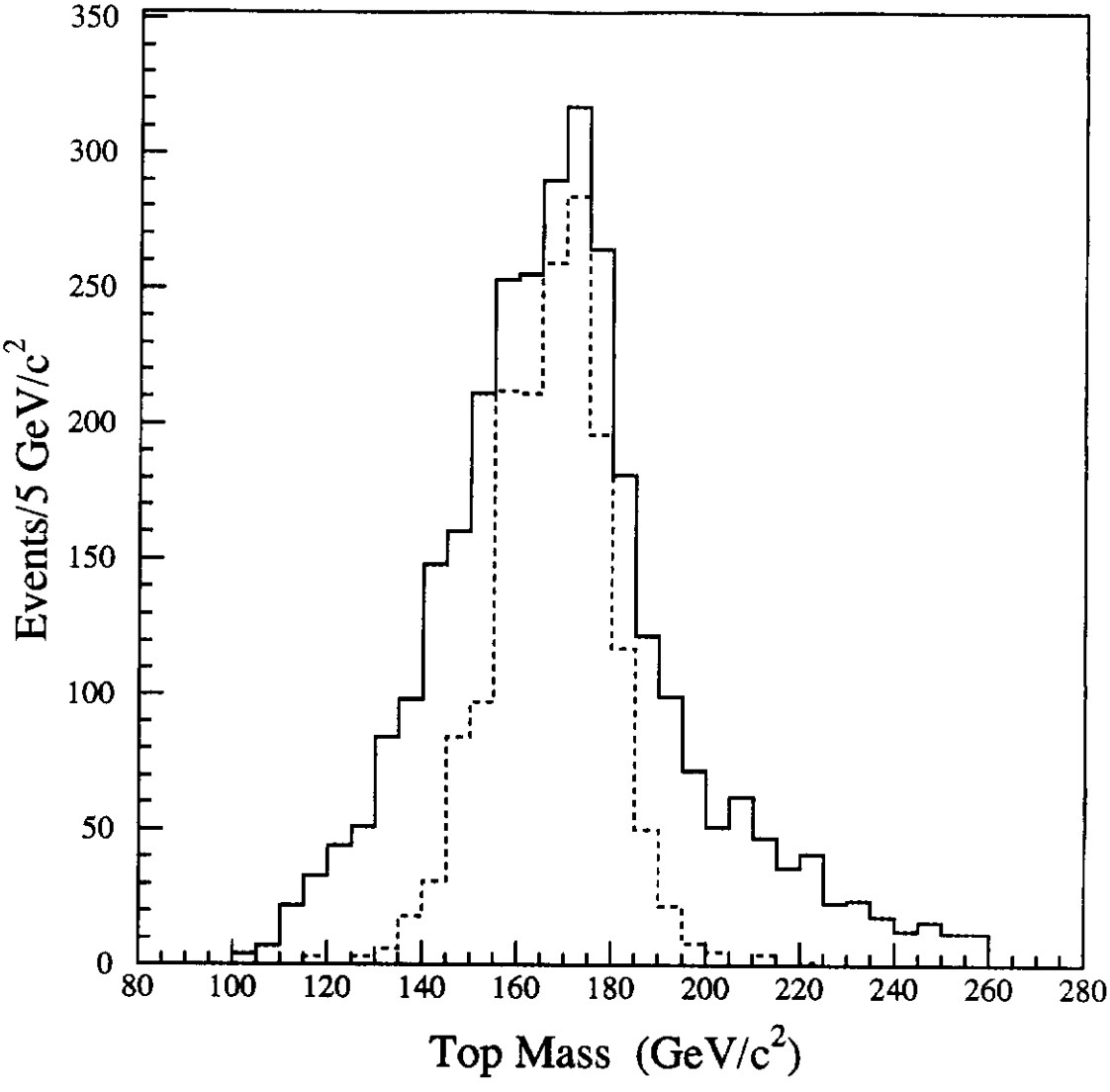

Fig. 45. Reconstructed top mass distribution for Monte Carlo events generated with $M_{top} = 170$ GeV/c^2. The full histogram corresponds to the best fit obtained by the fitting program when requiring that one of the b jets is a b in the fit. The dashed histogram refers to the fit with the correct assignment for each of the jets.

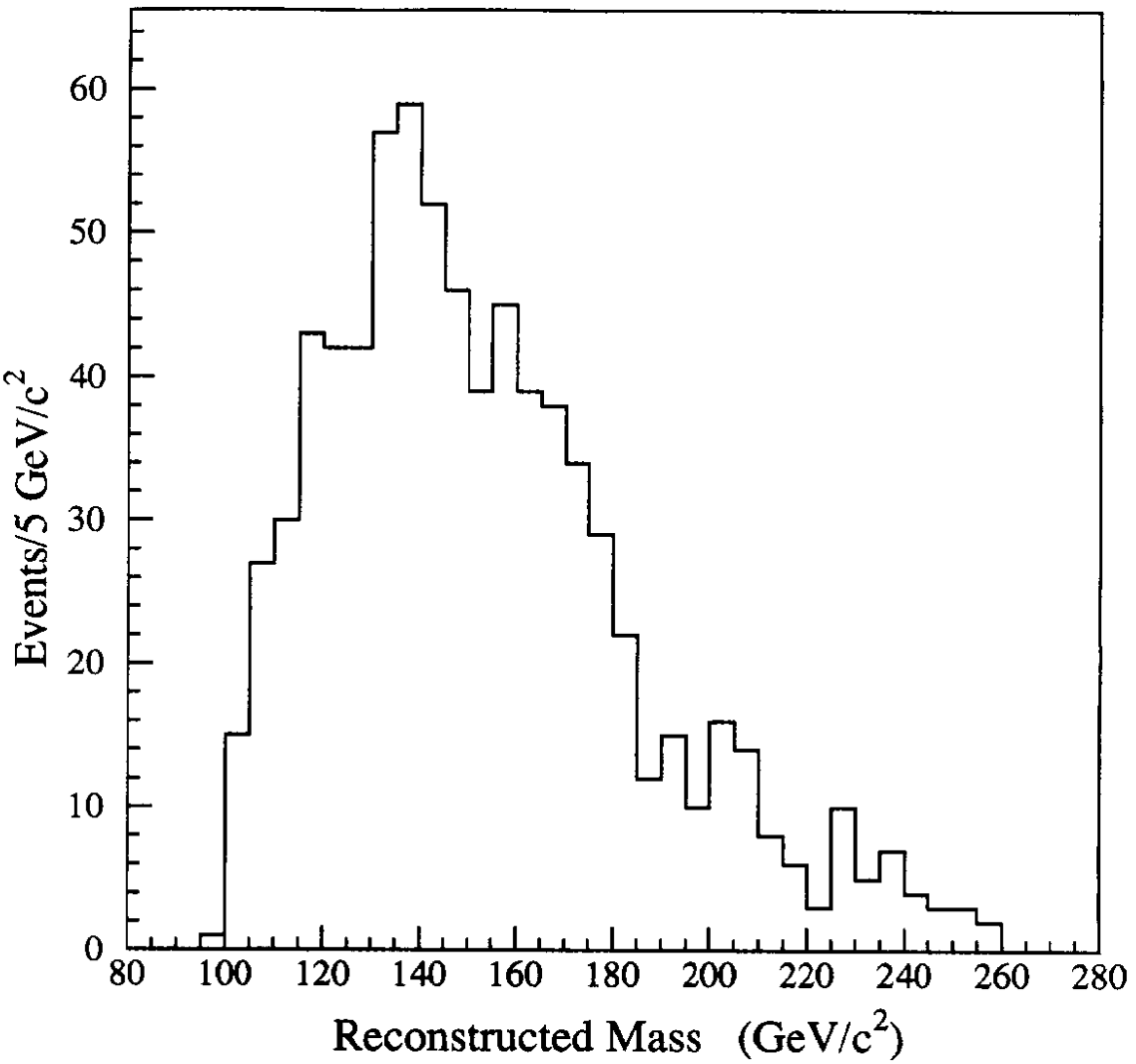

Fig. 46. Reconstructed mass distribution for W + multijet Monte Carlo events.

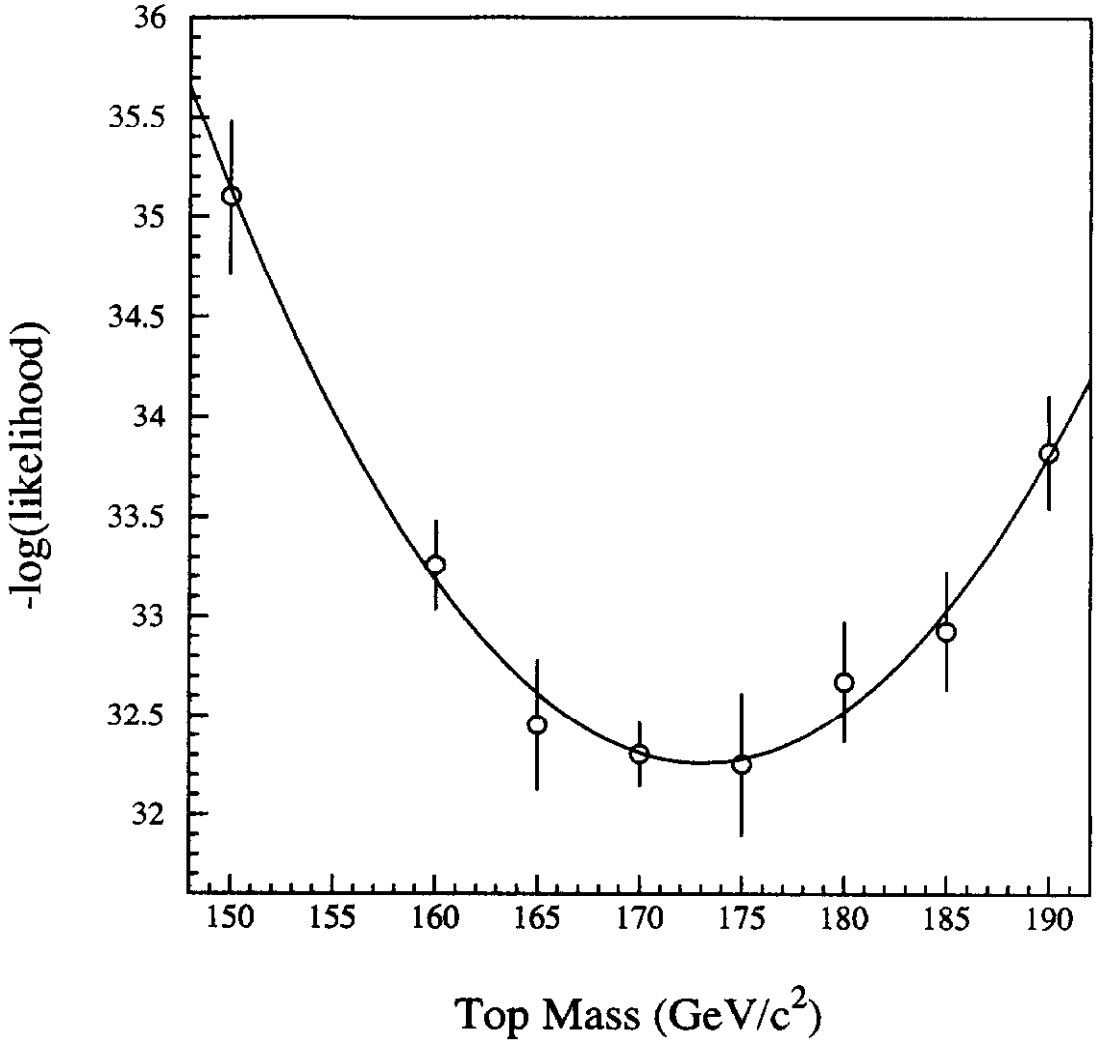

Fig. 47. Likelihood fit of the top mass.

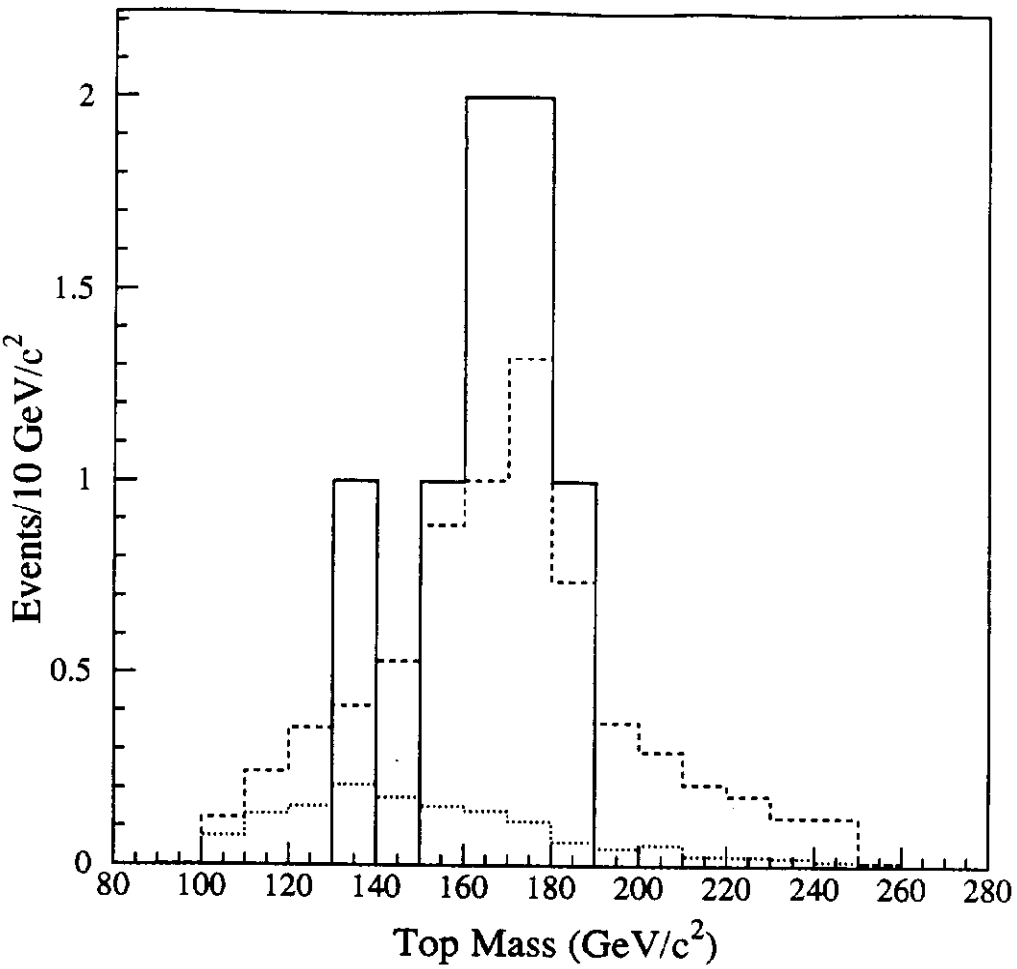

Fig. 48. Top mass distribution for the data (solid histogram) and the background of 1.4 events (dots) obtained from the $W+$ multijets VECBOS events. The dashed histogram represents the sum of 5.6 $t\bar{t}$ Monte Carlo events (from the M_{top}=175 GeV/c^2 distribution) plus 1.4 background events.

	Systematic uncertainties	(%)
a.	Jet Energy Scale (detector effects)	1.8
b.	Gluon radiation effects on parton energy	4.4
c.	Different backgrounds	$^{+5.3}_{-4.4}$
d.	Effects due to tagging algorithms	1.4
e.	Different likelihood fits	1.1

Fig. 49. Systematic uncertainties in the top mass measurement

m_t [GeV/c^2]		$e\mu$	ee	$\mu\mu$	e + jets	μ + jets	e + jets(μ)	ALL
	$\varepsilon \times B(\%)$	$.32 \pm .06$	$.18 \pm .02$	$.11 \pm .02$	1.2 ± 0.3	$.8 \pm 0.2$	0.6 ± 0.2	
140	$\langle N \rangle$	$.72 \pm .16$	$.41 \pm .07$	$.24 \pm .05$	2.8 ± 0.7	1.3 ± 0.4	1.3 ± 0.4	6.7 ± 1.2
	$\varepsilon \times B(\%)$	$.36 \pm .07$	$.20 \pm .03$	$.11 \pm .01$	1.6 ± 0.4	1.1 ± 0.3	0.9 ± 0.2	
160	$\langle N \rangle$	$.40 \pm .09$	$.22 \pm .04$	$.12 \pm .02$	1.8 ± 0.5	0.9 ± 0.3	1.0 ± 0.2	4.4 ± 0.7
	$\varepsilon \times B(\%)$	$.41 \pm .07$	$.21 \pm .03$	$.11 \pm .01$	1.7 ± 0.4	1.2 ± 0.3	1.1 ± 0.2	
180	$\langle N \rangle$	$.23 \pm .05$	$.12 \pm .02$	$.06 \pm .01$	1.0 ± 0.2	0.5 ± 0.2	0.6 ± 0.2	2.5 ± 0.4
Background		$.27 \pm .09$	$.16 \pm .07$	$.33 \pm .06$	1.2 ± 0.7	0.6 ± 0.5	0.6 ± 0.2	3.2 ± 1.1
$\int \mathcal{L}dt$ [pb^{-1}]		13.5 ± 1.6	13.5 ± 1.6	9.8 ± 1.2	13.5 ± 1.6	9.8 ± 1.2	13.5 ± 1.6	
Data		1	0	0	2	2	2	7

TABLE

Fig. 50. **Efficiency × branching fraction ($\varepsilon \times B$), expected number of events ($\langle N \rangle$) for signal and background sources for the observed integrated luminosity ($\int \mathcal{L}dt$), and number of events observed in the data.**

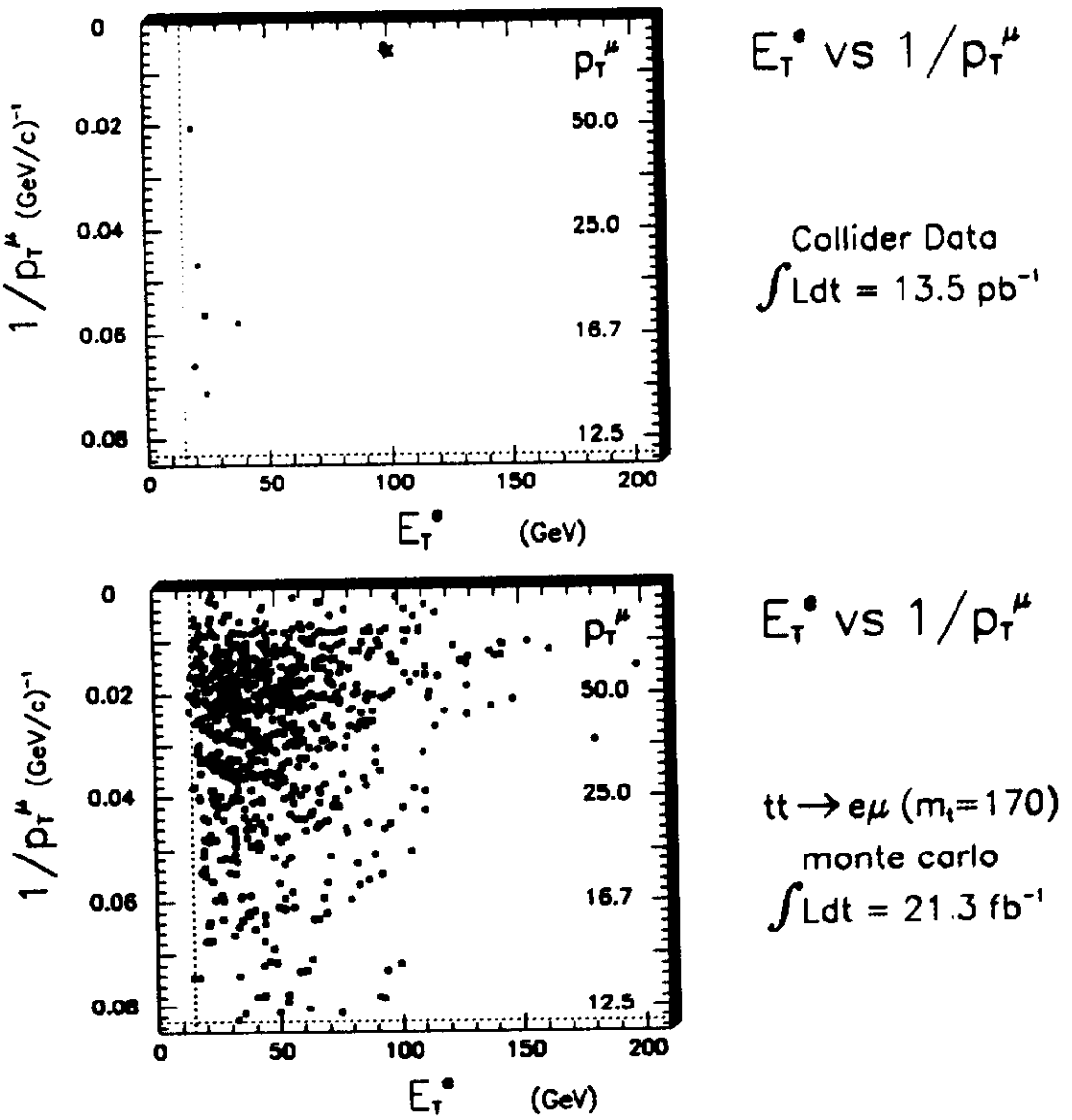

Figure 51: Distribution of events in E_T^e and $1/p_T^\mu$ for the data (before application of the final cut requiring two jets) and for Monte Carlo t tbar events with M_T = 170 GeV/c^2. The Monte Carlo corresponds to about 1600 times the luminosity shown for the data.

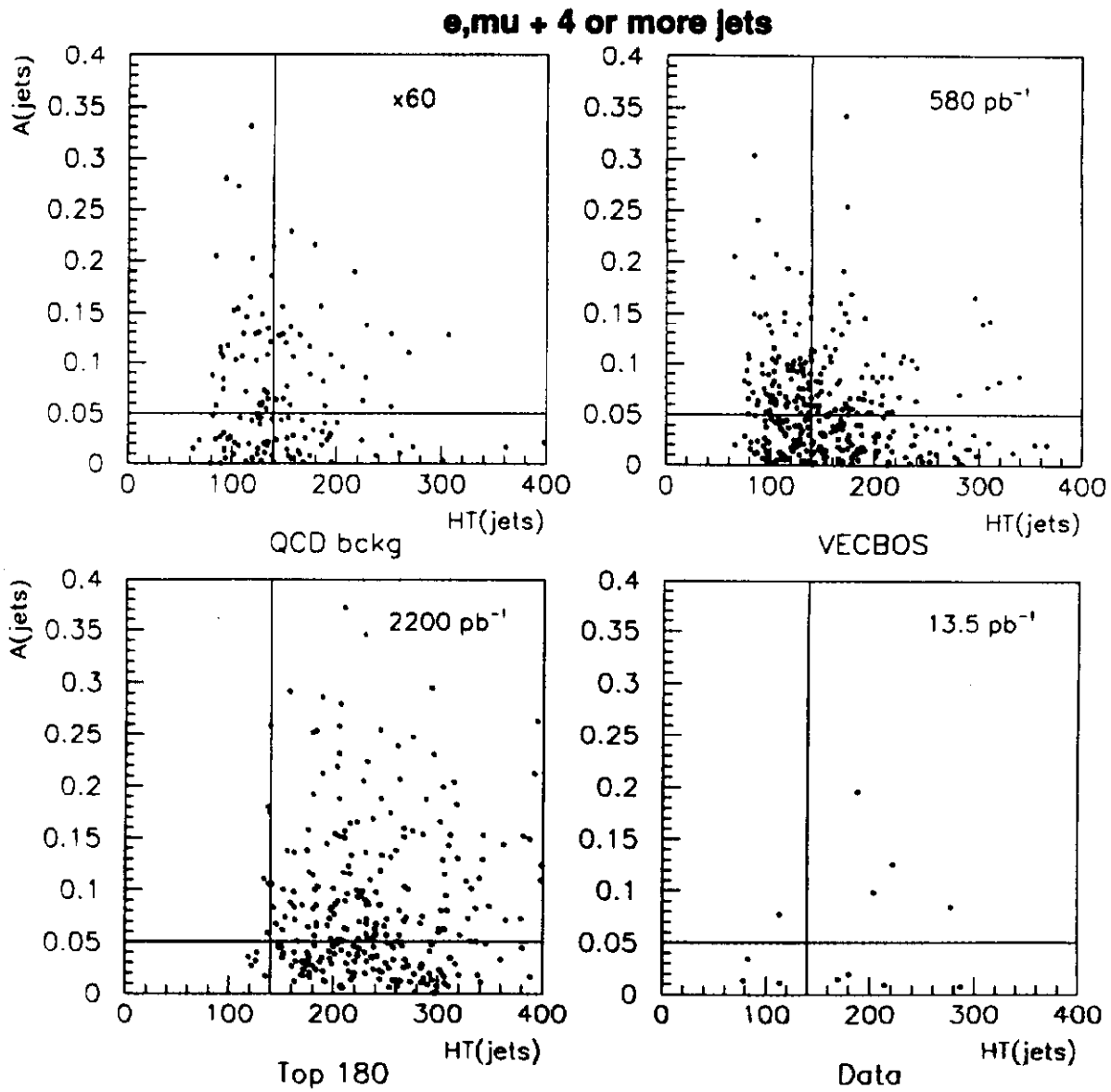

Figure 52: Event distributions vs aplanarity and H_T for QCD multijets (upper left), W + jets (upper right), a t tbar Monte Carlo with M_T= 180 GeV/c^2 (bottom left) and for data (lower right).

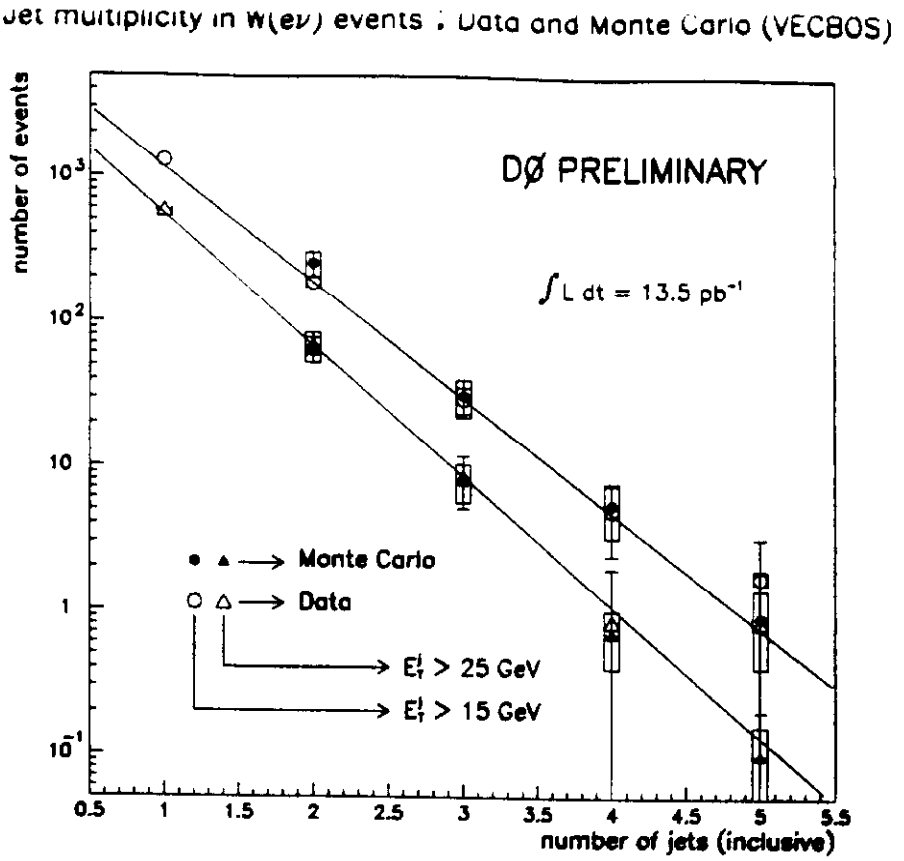

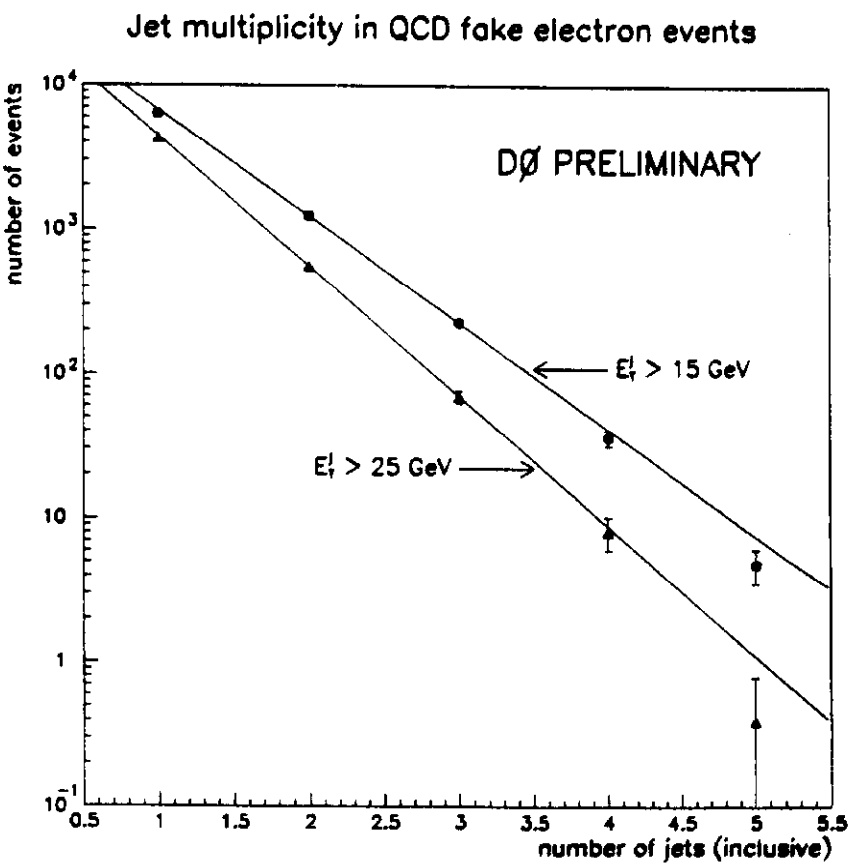

Figure 53: (a) Number of W + jets events (W > e,nu) vs. the inclusive number of jets for E_T > 15 GeV (upper points) abd E_T > 25 GeV (lower points). The open symbols denote data and the solid show the Monte Carlo. The lines are fits to the data for $1<N_{jet}<3$. (b) Number of multijet events for E_T 15 GeV (upper points) and E_T > 25 GeV (lower points). The filled symbols denote data and the lines are fits to the data for $1< N_{jet} < 4$.

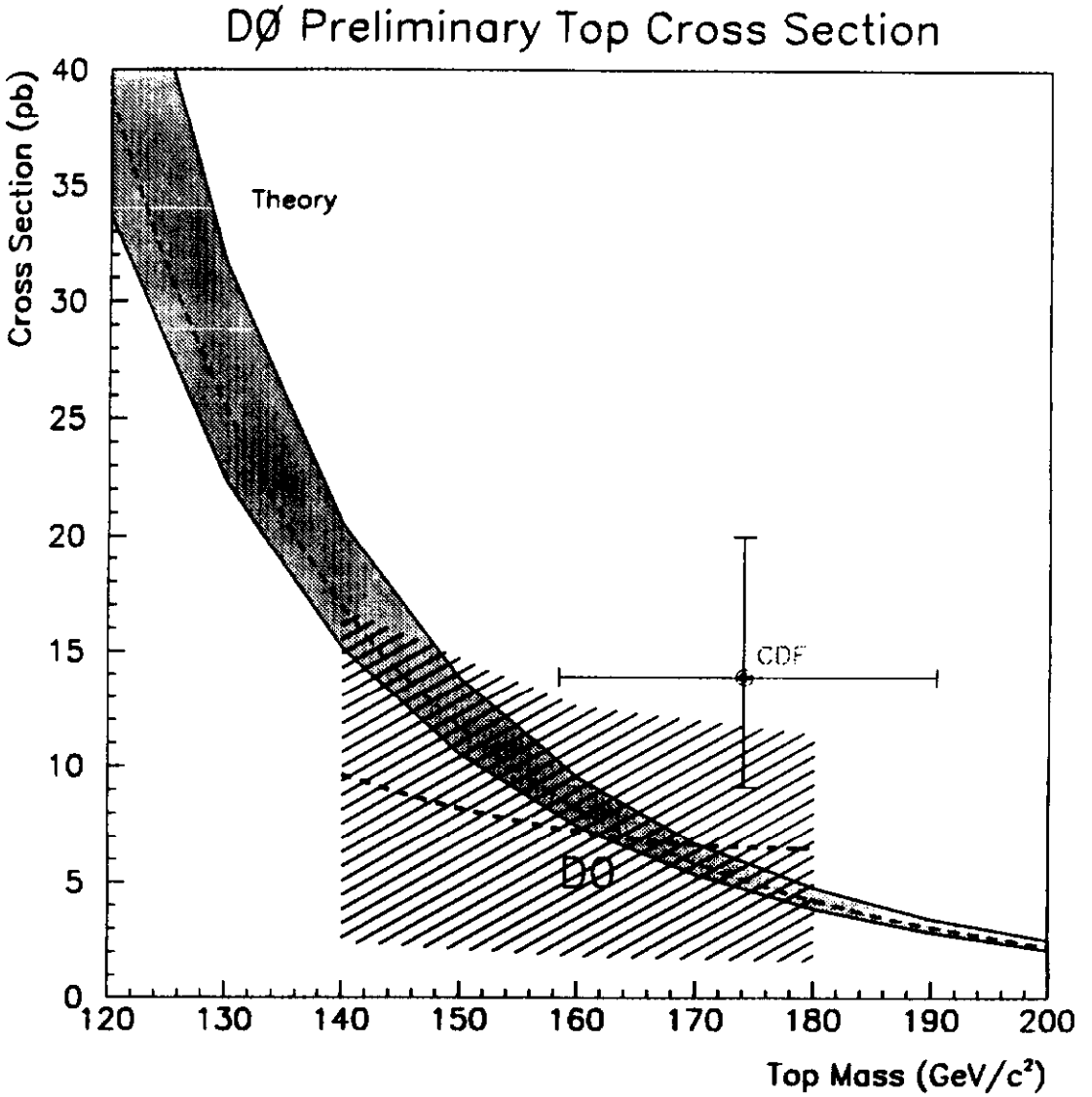

Figure 54. Cross-section vs. M_T. The dotted line and the cross-hatched area give the D0 preliminary result for the range of possible quark masses. The band is the theory curve shown in Figure 3. The cross is the CDF result.

	CDF Dilepton search	D0 Dilepton search	D0 e+jets Topology	D0 μ+jets Topology	D0 e+μ tag soft lepton	CDF e,μ + jets SVX	CDF e,μ + jets SLT
Acceptance	.78%	.67%	1.6%	1.1%	0.9%	1.69%	1.2%
Background per pb^{-1}	.028	.066	.089	.061	.044	.119	.16

Figure 55. Table showing the published acceptances of the CDF and D0 experiments. The last line shows the background events per pb^{-1} for each channel.

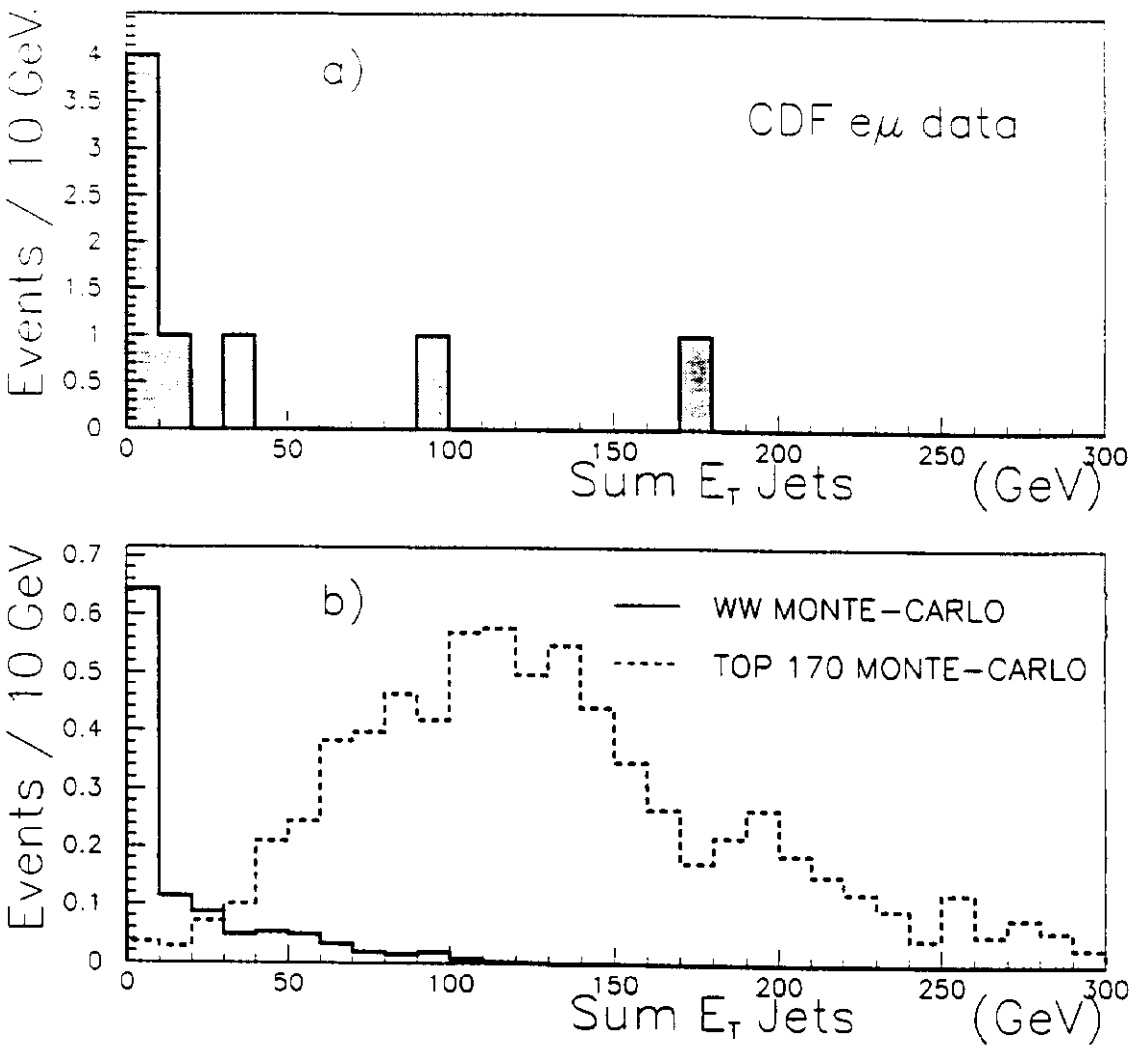

Figure 56: (a) The sum of ET(jet) for the 8 e mu events passing the pt > 20 GeV/c requirement on each lepton. Only jets with ET > 10 GeV and abs(eta) < 2.4 are included in the sum. The two events in the signal region of the dilepton analysis are the two events with the highest sum ET(jets). The 6 events at low sum ET fail both the two-jet cut and the MET cut. (b) Monte Carlo sum ET(jets) for t tbar, and for electroweak WW production, which is one of the backgrounds to the top search. The WW histogram is normalized to 19.3 pb^{-1}, while the t tbar is shown for 150 pb^{-1}. Note that the six events at low sum ET in (a) are unlikely to be mostly WW since they have low MET.

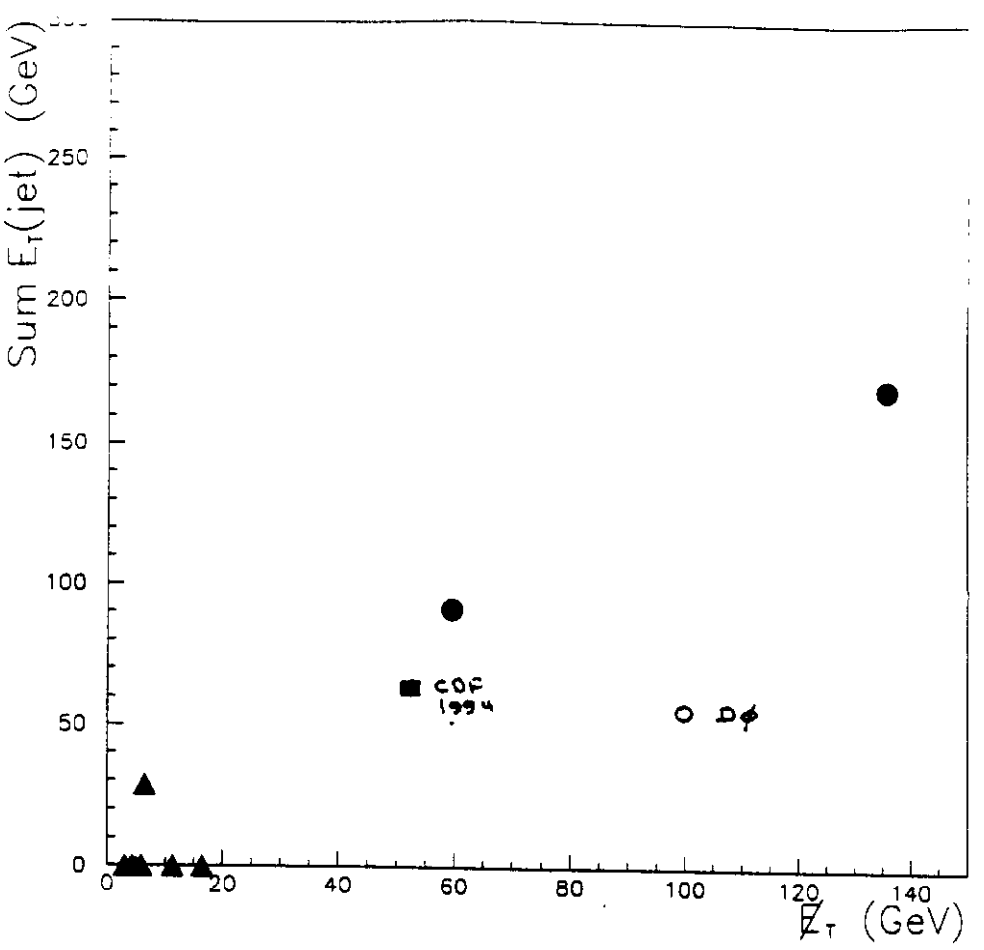

Figure 57. The published dilepton events shown in the Sum E_T (jets) vs the missing E_T plane. The solid symbols are for the events shown in Figure 56 from CDF and the open symbol is the DO event. The square is an event from CDF in the 1994 run.